Experimental hydrothermal alteration of carbonaceous chondrites and their meaning for Ceres' brine composition

DISSERTATION

zur Erlangung des Doktorgrades
der Naturwissenschaften

vorgelegt von
Dipl.-Geol. Tanja Schäfer
geb. Szymaniak
aus Freiburg im Breisgau

genehmigt von der
Fakultät für Energie– und Wirtschaftswissenschaften
der Technischen Universität Clausthal

Tag der mündlichen Prüfung
5. September 2018

Tanja Schäfer

Dissertation, TU Clausthal, 2019

74 pages, 39 figures., 13 tables, 41 references.

Mitglieder der Promotionskommission:

Univ.-Prof. Dr.-Ing. Wolfgang Busch (Vorsitzender)

Univ.-Prof. Dr. Kurt Mengel (Hauptberichterstatter)

Univ.-Prof. Dr. Hans-Jürgen Gursky (Ko-Berichterstatter)

Abstract

This work arose in the framework of the Dawn mission to dwarf planet Ceres. This body is supposed to have undergone a certain degree of ice-rock differentiation as indicated by its gravity and shape data. The existence of interior brines on Ceres is evidenced by the occurrence of bright spots, so called faculae, on the overall dark surface being clearly related to endogenic processes.

In this work laboratory hydrothermal alteration on undifferentiated chondritic meteorites (ordinary and carbonaceous chondrites) was carried out to provide brine compositions that might serve as analogues to the interior of Ceres. The leaching experiments were carried out for 2, 5, 12, 50, 100 and 200 days with a water to rock ratio of ~100 and a temperature of 90 °C. The brine composition derived from the experiments was analysed by IC and ICP-MS resulting in sulphate as the dominant anion over chloride in both carbonaceous and ordinary chondrites. Main cations occur in the order Mg > Ca > Na > K in the Murchison carbonaceous chondrite leachate and Ca > Mg > Na > K in the Jbilet carbonaceous chondrite leachate showing the main increase up to day 50 of reaction. The ordinary chondrites contain Na as the main cation and minor K, Cl, Ca and Mg.

The detection of mineralogical changes in the XRD pattern of the residual meteorite powders was very limited due to low signals of minor phases such as calcite and anhydrite caused by the small amounts of sample at hand. The same problem counts for the reflectance spectra of the carbonaceous chondrites which suggest a slight increase in those absorptions being assigned to phyllosilicates near 0.370, 0.405, 0.480, 0.950 and 1.13 μm and a decrease of the absorption near 0.73 μm.

In a second step the evolution of the derived brines during freezing and subsequent evaporation was explored applying the FREZCHEM model regarding two scenarios: a *water scenario* and a *NH_4-CO_2 scenario*. In the *water scenario* the brine is mostly enriched in Na, K and Cl compared to the initial leachate with the precipitating phases Ca-, Mg-, Na-, as well as K-Mg- and Na-Mg-sulphates (gypsum, anhydrite, epsomite, meridianiite, kieserite, mirabilite, picromerite, bloedite) and Na-, K-, Mg- and K-Mg-chlorides (halite, sylvite, carnallite, bischofite). In the *NH_4-CO_2 scenario* the brine is mostly enriched in NH_4, Cl, CO_3, Na and K, the precipitating phases being Ca-, Mg-, Na-, K-Mg-, Na-Mg- and NH_4-sulphates (gypsum, meridianiite, epsomite, mirabilite,

picromerite, bloedite, ammonium sulphate), as well as ammonium chloride and magnesite.

The present work experimentally confirms the conservative models for the evolution of chondritic brines as they exist, e.g., for Jupiter's icy satellites. Comparing to the recent Dawn VIR spectrometer data the *NH_4-CO_2 scenario* in this work is consistent with the findings of Ca-Mg-carbonates on Ceres' surface, as well as NH_4Cl as a possible ammonium bearing phase. The sodium carbonate (natrite) detected by VIR is not traceable by the simulations in this work. Concerning the sulphates on Ceres remote spectral analysis are ambiguous so far. Therefore the connection between Ceres and chondritic brines produced from terrestrial meteorite samples is still elusive.

Kurzfassung

Die vorliegende Arbeit ist im Rahmen der Raumfahrtmission Dawn zum Zwergplaneten Ceres entstanden. Angezeigt durch seine Gestalt und Schweredaten wird vermutet, dass auf diesem Körper eine Differentiation zwischen Eis und Gesteinsmaterial stattgefunden hat. Durch das Auftreten von hellen Flecken, sog. Faculae, an der insgesamt extrem dunklen Oberfläche von Ceres, konnte die Existenz von salinaren Lösungen nachgewiesen werden, die eindeutig mit endogenen Prozessen in Verbindung stehen.

In dieser Arbeit wurden hydrothermale Alterationsversuche an undifferenziertem meteoritischen Material (gewöhnlichen und kohligen Chondriten) durchgeführt, um die Zusammensetzung von salinaren Lösungen zu bestimmen, die als Analogon zu denen im Inneren von Ceres dienen können. Die Experimente wurden bei einem Wasser-/Gesteinsverhältnis von ca. 100 und einer Temperatur von 90 °C für die Dauer von 2, 5, 12, 50, 100 und 200 Tagen durchgeführt. Die Lösungszusammensetzung wurde mit IC und ICP-MS analysiert und ergab, dass sowohl in kohligen wie auch gewöhnlichen Chondriten das Sulfat- über das Chlorid-Anion dominiert. Die Hauptkationen in den Lösungen der kohligen Chondrite (Murchison und Jbilet) treten in der abnehmenden Reihenfolge Mg > Ca > Na > K bei Murchison bzw. Ca > Mg > Na > K bei Jbilet auf und zeigen ihren Hauptanstieg bis zum Tag 50. Die gewöhnlichen Chondrite enthalten Na als Hauptkation und in geringeren Konzentration K, Cl, Ca und Mg.

Der Nachweis von durch die Experimente verursachter mineralogischer Veränderungen in den residualen Probenpulvern mittels RDA war sehr eingeschränkt möglich aufgrund der schwachen Signale von Calcit und Anhydrit, verursacht durch die geringe Probenmenge. Das gleiche gilt für die Reflexionsspektren der kohligen Chondrite, in denen sich eine leichte Zunahme in den durch Schichtsilikate verursachten Absorptionsbanden nahe 0.370, 0.405, 0.480, 0.950 und 1.13 µm und eine Abnahme der Absorption bei 0.73 µm andeutet.

In einem zweiten Schritt wird die Entwicklung der experimentellen Lösungen während des Gefrierens und der anschließenden Evaporation unter Anwendung des FREZCHEM Modells für zwei unterschiedliche Szenarien untersucht: Erstens für ein *Wasser Szenario* und zweitens für ein *NH_4-CO_2 Szenario*. Im ersteren Fall ist die Lösung hauptsächlich in Na, K und Cl angereichert und die ausfallenden Phasen sind Ca-,

Mg-, Na-, K-Mg- und Na-Mg-Sulfate (Gips, Anhydrit, Meridianit, Epsomit, Kieserit, Mirabilit, Picromerit, Blödit) und Na-, K-, Mg- und K-Mg-Chloride (Halit, Sylvinit, Carnallit, Bischofit). Im *NH_4-CO_2 Szenario* ist die Lösung hauptsächlich in NH_4, Cl, CO_3, Na und K angereichert und die ausfallenden Phasen sind Ca-, Mg-, Na-, K-Mg-, Na-Mg- und NH_4-Sulfate (Gips, Meridianit, Epsomit, Mirabilit, Picromerit, Blödit, Ammoniumsulfat), sowie Ammoniumchlorid und Magnesit.

Die vorliegende Arbeit bestätigt auf der Basis experimentell erhobener Daten die konservativen Modelle zur Entwicklung chondritischer Eluate wie sie beispielsweise für Jupiters Eismonde existieren. Verglichen mit den aktuellen Daten des Dawn VIR Spektrometers stimmen die Ergebnisse des *NH_4-CO_2 Szenarios* in der vorliegenden Arbeit mit den auf Ceres detektierten Ca-Mg-Karbonaten überein, so wie auch mit Ammoniumchlorid als möglicher ammoniumhaltiger Phase. Das Natriumkarbonat (Natrit), welches von VIR auf Ceres detektiert wurde, ist in den hier durchgeführten geochemischen Modellierungen nicht rekonstruierbar. Die fernerkundliche Analyse von Sulfaten auf Ceres ist noch mehrdeutig. Daher ist Ceres‘ Verbindung zu chondritischen Lösungen wie sie aus terrestrischen Meteoritenproben erzeugt wurden schwer zu beurteilen.

Contents

1 Introduction

The collection of solar system planets, ranging from the rocky planets, over the gas giants to the outer icy planets is accompanied by smaller bodies such as the icy moons of the giant planets and the dwarf planets in the Kuiper belt. These objects are commonly placed beyond the solar system's frost line near 3 AU. They are supposed to have accreted ices and rock in varying proportions, as indicated by their low density of ~2 g/cm^3. In contrary to asteroids and comets these bodies are gravitationally rounded, indicating differentiation. Observations by the Voyager, Galileo and Cassini missions to the icy satellites of Jupiter (Europa, Ganymede and Callisto) triggered the idea that those bodies may have undergone differentiation into an outer icy shell, an interior ocean or warm ice shell and an inner rocky core as indicated by magnetic properties (Kivelson et al. 2000) and tectonic features (e.g., Pappalardo et al. 1999; Kattenhorn & Prockter, 2014).

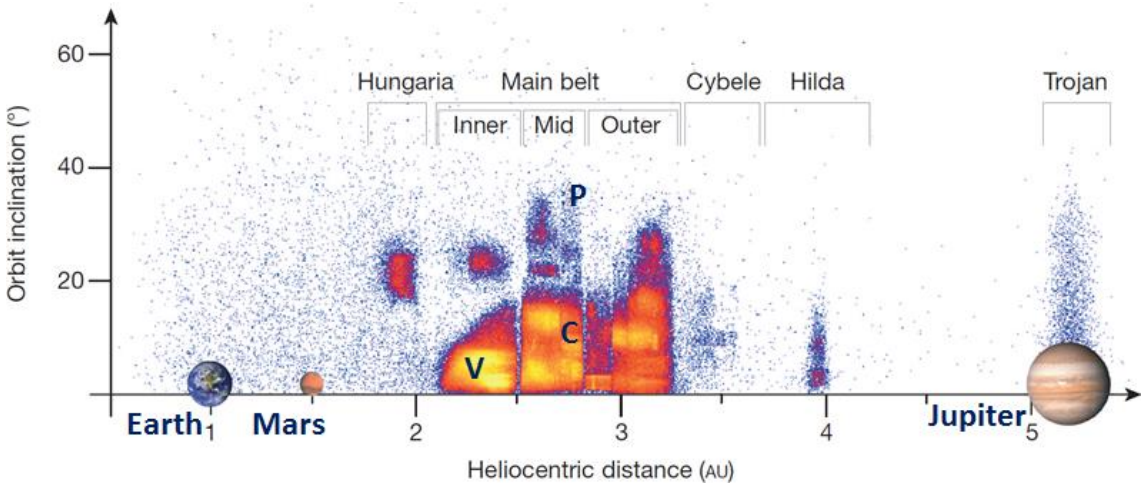

Fig. 1: Distribution of objects in the asteroid belt in context to the planets modified after DeMeo & Carry (2014). Yellow marks the highest object density, blue lowest. Letters indicate the position of the three largest ojects (1) Ceres (C), (4) Vesta (V) and (2) Pallas (P).

The dwarf planet Ceres, focussed on in this work, is the largest object in the asteroid belt with a volumetric radius of ~470 km (Park et al. 2016), beside the asteroids Vesta and Pallas, which are about half the size of Ceres. With its semi-major axis at 2.767 AU (AstDyS 2011) it is also the largest body between the terrestrial planets and the gas giants (Fig. 1), positioned near 3 AU where the frost line of water ice in our solar system is supposed. This actually makes it the candidate for ice-water-rock differentiation closest to the sun.

Ceres is currently target of the Dawn Mission being orbited since March 2015. The Dawn spacecraft is collecting data with the Framing Camera (FC), the Visible and Infrared Spectrometer (VIR) and the Gamma Ray and Neutron Detector (GRaND). These instruments reveal geologic surface features by imagery, as well as mineralogical and chemical composition. The recent shape model produced by Dawn data indicates differentiation into a rocky core and a volatile-rich mantle (Park et al. 2016). While Ceres' dark surface is consistent with highly aqueous altered carbonaceous chondrites (Schäfer et al. 2018) and ammoniated clays (De Sanctis et al. 2015), bright geologic surface features on Ceres indicate brine evaporation (De Sanctis et al. 2016, Nathues et al. 2017) and cryovolcanism (Ruesch et al. 2016).

The nature and the origin of hydrothermal alteration products including brines, evaporate minerals, and low temperature sheet silicates are not well understood to date. Short-term leaching experiments on carbonaceous chondrites have been conducted by Fanale et al. (2001) and Izawa et al. (2010). These authors tried to collect the most readily soluble chemical components which may contribute to the compositional evolution of a brine. To contribute to the understanding of Ceres' brine composition, long-term leaching experiments (200 days) on carbonaceous and ordinary chondrites were carried out in this work. Additionally freezing and evaporation of the derived leachate was simulated applying the thermodynamic code FREeZing CHEMistry (FREZCHEM) developed by Marion et al. (2010). The residual meteorite powders were investigated for mineralogical changes by XRD and by reflectance spectroscopy.

1.1 Surface mineralogy

Pre-Dawn observations

Early astronomical observations in the visible wavelength show Ceres' spectral affinity to carbonaceous chondrites (Lebofsky et al. 1978; Larson et al. 1979). Later this was established as taxonomical link, with Ceres' being classified as C-type asteroid (Bus & Binzel 2002a; 2002b; DeMeo et al. 2009). Several other authors could not confirm this link (Chapman & Salisbury 1973), but found similarities to CC

constituents such as mixtures of phyllosilicates and opaques (e.g., Johnson & Fanale 1973; Milliken & Rivkin 2009).

Ground based observations in the mid infrared detected an absorption feature between 3.0 and 3.1 μm that was first assigned to structural OH-groups and interlayer water or water ice in clay minerals (Lebofsky et al. 1981). Later, spectrally higher resolved observations of this feature gave explanations for either brucite (Milliken & Rivkin 2009), ammoniated clays (King et al. 1992), or carboxylic acids (Applin et al. 2016). Spatially resolved data from ground based observations in the near infrared by Carry et al. (2008) show dark and bright spots on the surface; the latter were attributed to the presence of Ca-, Mg- and Fe-carbonate minerals and montmorillonite.

Dawn observations

Recent multispectral image data from the Dawn VIR instrument confirm Ceres' affinity to CI/CM meteorites by their phyllosilicate absorption at 2.7 μm and spectral admixtures of carbonates and a dark component (De Sanctis et al. 2015). The phyllosilicate absorption centered between 2.72 and 2.73 μm is ubiquitously across Ceres (Ammanito et al. 2016) and is indicative for Mg-dominated sheet silicates in highly aqueously altered CMs or in CIs (Takir et al. 2013; McSween et al. 2017). Detailed comparisons covering both the visible slopes and the 2.7 μm absorption of Ceres' to the suite of CCs spectrally investigated so far, give a more exact match to the highly aqueous altered CM1 meteorites than to CM2s or CIs (Schäfer et al. 2018).

The carbonates ubiquitously found on Ceres' surface are of Ca-Mg composition, which is consistent with CI/CM mineralogy. They seem to be enriched on Ceres relative to terrestrial CIs and CM1s, as shown by comparisons to laboratory spectra (McSween et al. 2017; Schäfer et al. 2018).

The 3.0 and 3.1 μm absorption in Ceres' spectra is interpreted as NH_4-smectites (De Sanctis et al. 2015). This phase was not found in any meteorite yet, but was also not specifically searched for. Brucite was ruled out, because of the lack of other characteristic absorptions between 1.0 and 3.0 μm.

The bright spots in Occator were first identified as hexahydrite by VIS/NIR slopes (Nathues et al. 2015). Subsequent investigations of carbonate bands at 3.4 μm and 3.9 μm gave evidence for the sodium carbonate natrite and ruled out hydrated sulphates due to lack of water absorptions (De Sanctis et al. 2016). An enrichment of natrite is also seen on the cryovolcanic feature Ahuna Mons (Zambon et al. 2017).

Water hydration bands have been observed at higher latitudes in the bright areas in crater Oxo, showing the best spectral match by water ice and second best by sodium carbonate and magnesium sulphate (Combe et al. 2016).

1.2 Shaping and Differentiation

Earlier ground based observations of Ceres' shape allow a range of scenarios from a porous undifferentiated (McCord & Sotin 2005; Zolotov 2009) to a highly differentiated body with a silicate core and an outer hydrosphere (McCord & Sotin 2005; Castillo-Rogez & McCord 2010), as well as a differentiated, initially molten interior with a retained chondritic crust (Elkins-Tanton et al. 2011). A new more precise value of Ceres' moment of inertia (0.37) indicates that Ceres is less differentiated than assumed before, setting constraints on a denser rocky core allowing the range from low density CIs and CMs to ordinary chondrites of typical rock density overlain by a less dense volatile-rich shell (Park et al. 2016). Possible scenarios assuming chondritic materials for the core in a two layer model given by Park et al. (2016) are diagrammed in Fig. 2. This is consistent with Ceres' crater morphology indicating a transition between a pure rocky and pure icy crust (Hiesinger et al. 2016; Russell et al. 2016).

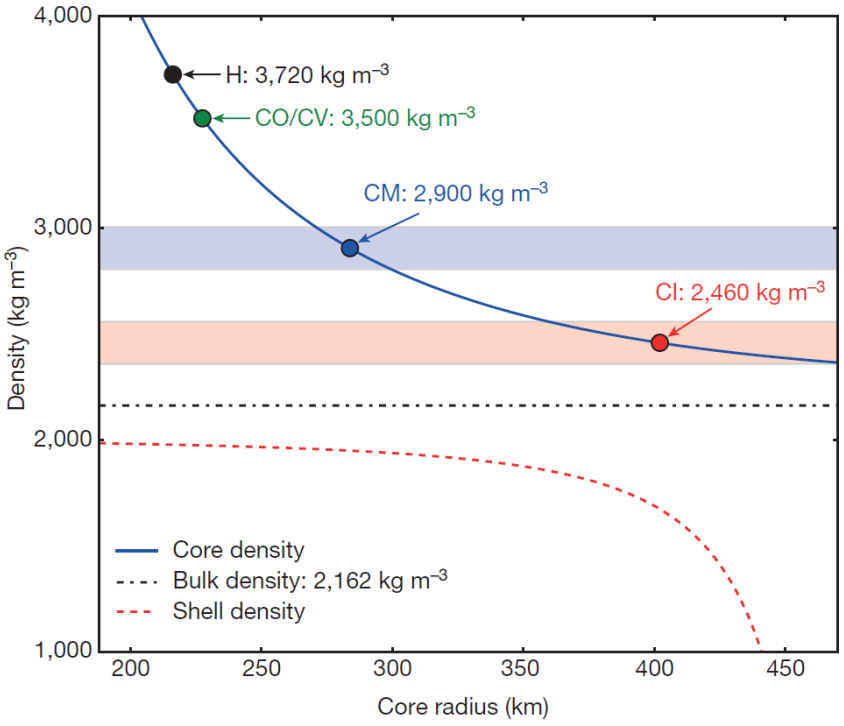

Fig. 2: Varying combinations of core and shell densities in a two layer model from Park et al. (2016). A reasonable scenario indicated by Ceres' mineralogy is given for a core density of CM materials (2.9 g cm^{-3}) resulting in a shell density of 1.95 g cm^{-3}. But also anhydrous CCs in the core result in a shell density near 2 g cm^{-3}.

The occurrence of bright spots on Ceres being several times brighter than the dark background (Nathues et al. 2015) give evidence for salt precipitates from interior brines. From these observations a more enhanced model for the differentiation of

Ceres shell is reasonable. The prominent surface features Occator and Ahuna Mons are fed by interior brines, which are evidently overlain by an ice-rich outer shell and a dark, CI/CM-like lag deposit, from which ice is completely sublimated in most parts of Ceres (Fig. 3). This indicates that Ceres differentiation at least in the shell is possibly more diverse than indicated by its gravity and shape data, due to the low difference in density of the components.

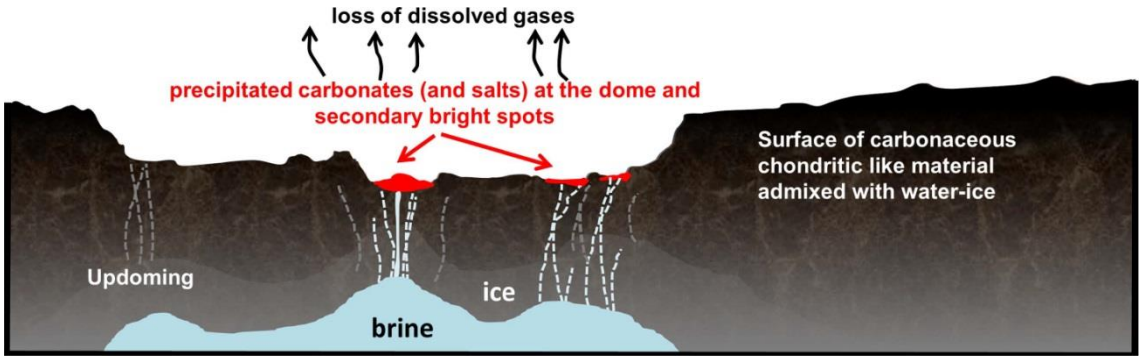

Fig. 3: Bright spots in Occator indicate a more detailed differentiation of Ceres outer shell in a brine reservoir overlain by an icy outer shell gradually merging in a CC-like lag deposit from sublimating ice (Nathues et al. 2017).

2 Experimental Design

2.1 Samples

For the experiments in this work two carbonaceous chondrites (CM2) and three ordinary chondrites were chosen (H3, L3, H3-6) (see Tab.1). Apart from Murchison all of the specimens are saw-cut slices purchased from Meteorite Market containing only small amounts of fusion crust. The Murchison sample consists of several tiny pieces (< 1gr.) purchased from the same source.

Tab. 1: Meteorite samples used in this work. This information is taken from Meteoricial Bulletin Database of the Meteoritical Society (http://www.lpi.usra.edu/meteor/metbull.php)

Official name	Abbreviation	Classification	Find/Fall	Year	Mass (pieces)
Murchison	-	Carbonaceous chondrite (CM2)	Fall	1969	100 kg (meteorite shower)
Jbilet Winselwan	Jbilet	Carbonaceous chondrite (CM2)	Find	2013	6 kg (several 3 - > 200 g)
Northwest Africa 8039	NWA 8039	Ordinary chondrite (H3)	Find	2013	99 g (40)
Northwest Africa 7936	NWA 7936	Ordinary chondrite (L3)	Find	2012	1300 g (2)
Zag	-	Ordinary chondrite (H3-6)	Fall	1998	175 kg (several)

Carbonaceous chondrites of CM2-type are, like other chondrites, primarily considered to be a condensate of the solar nebular, as indicated by their texture characterised by olivine/pyroxene chondrules and CAIs embedded in a dark fine grained phyllosilicate-rich matrix (Fig. 4a). Meanwhile a secondary post accretionary parent body aqueous alteration of the CMs is commonly accepted as indicated by numerous textural and mineralogical characteristics summarized in Brearley (1997, 2006). CM2s are dominated by a volatile-rich mineralogy containing 2-16% of water and ~70-80% phyllosilicates including tochilinite (e.g., Brearley 2006). The dry silicates olivine and

pyroxene, which are mainly allocated in chondrules, make up ~15-30% (Howard et al. 2009; 2011). The olivine and pyroxene composition in CMs is dominated by their Mg-endmembers forsterite and enstatite. Minor components described in CMs are carbonates, sulphates, sulphides (Troilite, Pentlandite), Ni-Fe, magnetite and halite (as reviewed in Brearley 1998; 2006; Hutchison 2004). The bulk mineralogy of Murchison, which is a typical CM2 specimen, from XRD analysis conducted by Bland et al. (2004) is given in Table 2. A similar bulk mineralogical composition is identified by Howard et al. (2009).

The CMs cover an aqueous alteration sequence from CM2 to CM1, the latter ones being most altered. In this sequence advanced aqueous alteration is expressed by an increasing amount of phyllosilicates at the expense of olivine/pyroxene, as seen by alteration of chondrules (Zolensky et al. 1997, Rubin et al. 2007) and XRD analysis (Howard et al. 2009). Concomitantly observations of CM matrices by electron beam (McSween 1979; Browning et al. 1996) and bulk XRD analysis (Howard et al. 2011) indicate a higher content of Mg-rich phyllosilicates with increasing alteration.

As Ceres' surface is widely covered by Mg-dominated sheet silicates (De Sanctis et al. 2015; Ammanito et al. 2016) and shows spectral similarity to CM1 material (Schäfer et al. 2018), CM2s are a reasonable starting material for the leaching experiments. Furthermore their low density (<3 g cm^{-3}, Britt & Consolmagno 2003) suits well in the models for Ceres' differentiation (Park et al. 2016).

Ordinary chondrites mainly consist of dry silicates (olivine, pyroxene, plagioclase), troilite and Ni-Fe (taenite, kamacite) (e.g., Menzies et al. 2005; Dunn et al. 2010). In contrary to carbonaceous chondrites they are of minor relevance for Ceres, regarding their mineralogy, spectral properties and their higher density (>3.5 g cm^{-3}, Britt & Consolmagno 2003). But although they are not likely to appear on Ceres' surface presently, they cannot be ruled out as a reactant to hydrothermal fluids in the interior of Ceres (see Fig. 2) or of other solar system bodies accreting rock and ice, e.g., Jupiter's icy moons (Kuskov & Kronrod 2005). Therefore these samples were include to acquire data for future geochemical modelling, but do not discuss it further in the context of Ceres.

Although unlikely for Ceres, because of its high metal content and hence high density, the Zag regolith breccia is included in this study, because halite and sylvite grains including fluid inclusions (Rubin et al. 2002), as well as dark CC-like inclusions (Zolensky et al. 2013) are described in the unaltered matrix of this meteorite. These are discussed to possibly stem from a CC-bearing body like Ceres and could have been delivered to the unaltered regolith on a Zag parent body by cryovolcanism (Fries et al. 2013). But in this work Zag will not be discussed as a leaching educt from Ceres.

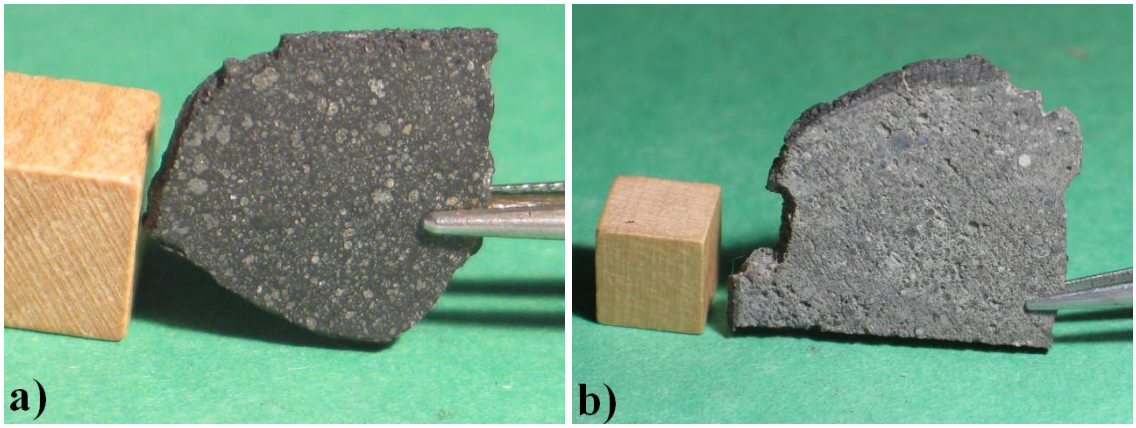

Fig. 4: a) Slice of Murchison CM2 carbonaceous chondrite and b) slice of NWA 8039 ordinary chondrite type H3.4 (photos provided by E. Twelker from www.meteoritemarket.com)

2.2 Experimental procedure

Sample preparation

Saw cut pieces of the meteorite slices were wrapped in foil and crushed into millimetre-sized pieces by hammer. Then the samples were ground by an achate mortar and dry sieved to grain size < 63 µm through a nylon sieve. The mortar was cleaned with aceton and silica sand after each sample. The ZAG sample had a high metal content which formed ductile chips during grinding. These were removed magnetically.

Hydrothermal leaching

The leaching experiments were carried out for 2, 5, 12, 50, 100 and 200 days, to observe the most readily soluble elements, as well as advanced brine composition.

For each experiment an aliquot of ~0.11 g meteorite powder and ~11 g of 18 MΩ deionized, degassed water was filled in a 15 ml PFA standard vessel from Savillex and sealed with a PFA closure. The water was degassed before by stirring it in a bottle connected with a vacuum pump for ~20 minutes until bubbling stopped.

The vessels were put in an oven and temperature was constantly held around 90 °C. This is a reasonable value, because this temperature is modeled for radii between 250 and 350 km (Fig. 5), which is the region where the core shell boundary in case of a CM core is supposed and hydrothermal leaching may have taken place (see Fig. 2).

For the water/rock ratio (W/R) of ~100 in the experiments a tradeoff was made, because at least 10 ml of leachate were necessary for analytics. This W/R is possibly too high as Ceres should yield only one third of water ice, when the rocky material is assumed to be CMs. But it is possibly not to unrealistic for local brine accumulates.

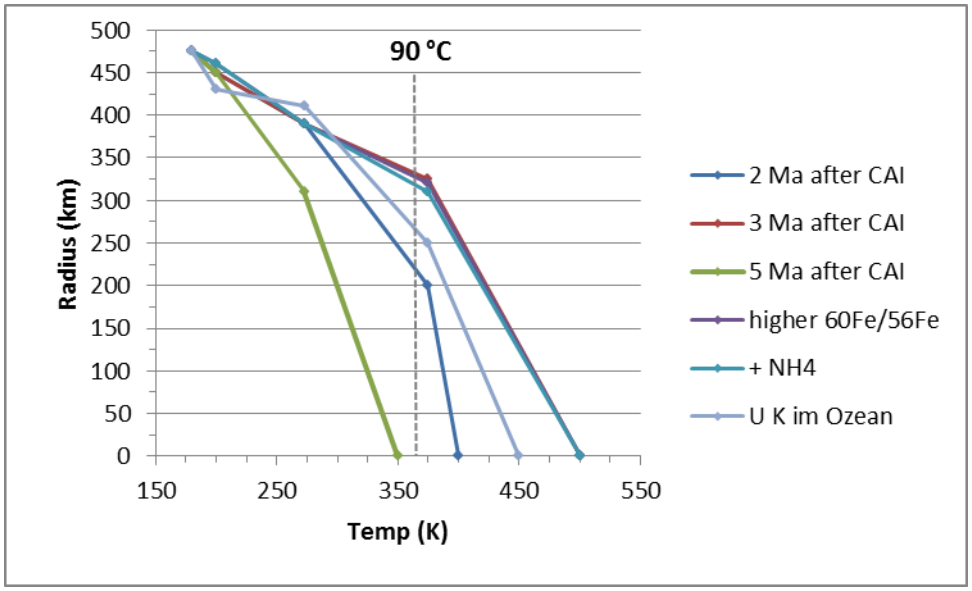

Fig. 5: Present day temperature profiles on Ceres, depending on time of accretion and radiogenic components or NH_4 (modified from Castillo-Rogez & McCord 2011).

Preparation for analytics

The vessels were opened after cooling to room temperature and leachates were extracted from the vessels using a syringe equipped with a filter to avoid extracting the fines in suspension. This was especially necessary for the finely dispersed CM material. The leachates were diluted by factor 2, filling them up to a volume of 20 ml. A 15 ml aliquot was separated for ion chromatography (IC) analysis and 1% of 1 mol HNO_3 was added directly before analytics. A 5 ml aliquot was separated for inductively-coupled-plasma mass-spectrometry (ICP-MS) analysis and 50 µl of HCl 30%, Suprapur for trace analytics was added immediately.

The residual meteorite powders were freeze-dried in a Christ ALPHA 1-2 LDplus freeze-dryer. The powders were cooled to -20 °C for 1:30 hour and dried at low pressure of 0.370 mbar for 4.45 hours until samples approximated the shelf temperature of +30 °C.

2.3 Prognosis of leachate composition

For an approximate prognosis of leachate composition balance was made up from modal mineralogy and bulk chemical composition of Murchison (Tab. 2), presuming that some of the elements in the balance column in Table 2 are contained in leachable phases. Murchison was the sole of our samples for which both XRD data (Bland et al. 2004) and chemical composition (Jarosewich 1971) was available. In Tab. 3 contents of water soluble species in Murchison are given.

Tab. 2: Balance from modal mineralogy (Bland et al. 2004) and chemical composition (Jarosewich 1971) of Murchison. All values are given in weight%. The composition of olivine, enstatite, serpentine and calcite is taken from Deer, Howie & Zussman (1992). Sulphides, magnetite and cronstedtite were calculated theoretically.

	Olivine ($Fo_{100, 80, 50}$)	Enstatite (En_{98})	Sulphides	Magnetite	Serpentine	Cron-stedtite	Calcite	Σ	Chemical analysis	Balance
Modal mineralogy	**11.6**	**2.2**	**3.4**	**0.4**	**22.8**	**58.5**	**1.1**	100		
SiO_2	41.85	57.1	-	-	43.60	15	-	24.83	**29.07**	4.24
TiO_2	0.07	0.17	-	-	0.01	-	-	0.03	**0.13**	0.1
Al_2O_3	0.00	0.7	-	-	1.03	-	-	0.25	**2.15**	1.9
Cr_2O_3	-	0.27	-	-	0.02	-	-	0.02	**0.48**	0.46
NiO	-	-	+	-	0.16	-	-	>0.04	**1.75**	<1.71
FeO	2.05	5.75	-	93	0.89	72	0.00	43.06	**22.39**	-20.67
MnO	0.21	0.17	-	-	0.04	-	0.04	0.04	**0.20**	0.16
MgO	56.17	34.52	-	-	41.00	-	-	16.62	**19.94**	3.32
CaO	0.00	0.62	-	-	0.05	-	55.92	0.64	**1.89**	1.25
Na_2O	-	0.07	-	-	0.01	-	-	0.004	**0.24**	0.24
K_2O	-	0.03	-	-	0.03	-	-	0.008	**0.04**	0.03
P_2O_5	-	-	-	-	-	-	-	-	**0.23**	0.23
H_2O	-	0.70	-	-	12.26	13	-	10.41	**10.09**	0.33
SO_3	-	-	-	-	-	-	-	-	**0.90**	0.90
FeS	-	-	3.4	-	-	-	-	3.4	**7.24**	-3.16
C	-	-	-	-	-	-	-	-	**1.85**	1.85
CO_2	-	-	-	-	-	-	43.95	0.48	**1.00**	0.52
Total	100.35	100.20	-	-	99.92	100	99.91	99.83	**99.55**	
Total Fe	-	-	-	-	-	-	-	-	**22.13**	
Total S	-	-	-	-	-	-	-	-	**3.00**	
Total C	-	-	-	-	-	-	-	-	**2.18**	

As can be seen in Table 2, the Fe and Mg are not balanced between the bulk mineralogy and the bulk chemistry. This is attributed to the fact that the phyllosilicates in CMs are structurally different from terrestrial ones and reveal a complicated stoichiometry of Mg, Fe^{2+}, and Fe^{3+}, which is in fact similar to cronstedtite (Müller & Kurat 1979), but may not be exactly represented by this mineral. The complexity of phyllosilicates in CCs is demonstrated by numerous studies (as reviewed in Tomeoka 1989; Brearley 1998; 2006) and may not have been completely resolved by electronbeam techniques so far, least of all their bulk content in the meteorites.

Tab. 3: Water soluble species in Murchison.

Cl (ppm)	Br (ppm)	SO_4 (%)
231[a)]	971[a)]	1.77[c)]
180[b)]	0.61[b)]	1.68, 1.80 [d)]

[a)] Clay et al. (2017), [b)] Dreibus et al. (1979), [c)] Labidi et al. (2017), [d)] Gao & Thiemens (1993)

Estimate of FeS oxidation

Although degassed water was used in the experiments, a small amount of oxygen in the vessel has to be taken into account possibly causing oxidation of FeS contained in the meteorites. In the following the amount of SO_4 is calculated, which is being produced by a maximum volume of 4 ml filled with air (≙ 1ml oxygen) left in the 15 ml vessels. Troilite oxidation during the experiment is described by the reaction:

(1) $FeS + H_2O + 2\ O_2 \rightarrow FeSO_4 * H_2O$

The amount of oxygen $n(O_2)$ in mol contained in a volume V_{O_2}= 0.001 L is calculated by assuming an ideal gas, a temperature of *T*=295,15 K (22 °C) and a pressure of *P*=101.3 kPa:

$$V_m = \frac{R\ T}{P} = \frac{V_{O_2}}{n(O_2)} \leftrightarrow n(O_2) = \frac{V}{V_m}$$

$$V_m = \frac{8.3144598\ \frac{kg\ m^2}{s^2\ mol\ K}}{101.3\ kPa} = 24.47\ L\ mol^{-1}$$

$$n(O_2) = \frac{0.001\ L}{24.23\ L\ mol^{-1}} = 4.13\ \cdot 10^{-5} mol$$

V_m*: molar volume*

R: ideal gas constant

In the following the masses $m(X)$ in g of the species, which are produced or consumed by $n(O_2) = 4.13 \cdot 10^{-5} mol$ following reaction (1) are calculated:

$$m(X) = \frac{1}{2}\, n(O_2) \cdot \mathrm{M(X)}$$

M(X): molar mass in g mol^{-1}

$$m(FeS) = 1.81 \cdot 10^{-3} g \rightarrow 165 \frac{mg}{L}$$

$$m(Fe^{2+}) = 1.16 \cdot 10^{-3} g \rightarrow 105 \frac{mg}{L}$$

$$m(S^{2-}) = 0.66 \cdot 10^{-3} g \rightarrow 66 \frac{mg}{L}$$

$$m(FeSO_4) = 3.14 \cdot 10^{-3} g \rightarrow 285 \frac{mg}{L}$$

$$m(SO_4^{2-}) = 1.98 \cdot 10^{-3} g \rightarrow 180 \frac{mg}{L}$$

These results show that around 180 ppm SO_4^{2-} and 105 ppm Fe^{2+} can be expected by troilite oxidation from residual oxygen in the vessel.

2.4 Analytical procedure

2.4.1 Leachates

Ion Chromatography

Ion chromatography was applied to analyse Na^+, NH_4^+, K^+, Ca^{2+}, Mg^{2+}, Cl^-, Br^- and SO_4^{2} in the leachates. The carbonate anion could not be analysed.

For the analysis a Metrohm 761 Compact IC was utilized. Cations were separated in a Metrosep C4-150/4.0 IC column consisting of silicagel with carboxyl-groups as ion exchange material. As eluent for the cations 1.7 mmol HNO_3/L plus 0.7 mmol/L 2.6-pyridine-dipicolinic acid was used. Anions were separated in a Metrosep A Supp 5 column consisting of polyvinyl alcohol with quaternary ammonia groups, utilizing 3.2 mmol/L Na_2CO_3 plus 1.0 mmol/L $NaHCO_3$ as anion eluent with chemical suppression. Detection of ions was done by measuring electric conductivity and evaluating peak areas applying an external multipoint calibration (see App. B).

ICP-MS

The leachates were analysed for Li, Al, P, Fe, Mn, Cu, Rb, Sr, Cd and Cs utilizing a Thermo Scientific iCAP ICP-MS. The instrument is equipped with a dynode and analogue working detector. The choice between signal registration by either detector depends on the concentration of trace elements. The contents of all elements analysed here was low enough for ion counting detection. The usage of internal standards (10 ppb of each Be, Rh and Re) guaranties stable signals over time, because every mass counting rate is divided by Be, Rh or Re counting rates. Detected blanks are exclusively material blanks (water, nitric acid) and are not due to handling. Precision and accuracy are in the range of ± 1 ppb for Li, Mn, Rb, Sr, Cd and Cs and of ± 5 ppb for Al, P, Cu and Fe.

2.4.2 Residual meteorite powders

X-ray Diffraction Analysis

The original and the residual powders of each meteorite were measured as stray preparation, because of the small amount of sample. For this ~10 mg of the sample were spread on a silica plate fixed in a sample holder. The original meteorite powders (~1-2 g) were additionally measured as a backload preparation, because this preparation technique yields higher intensity and better accuracy of the position of the diffraction lines. As can be seen in Appendix C, Figs. C1-C5, the diffraction patterns based on stray preparation are shifted slightly compared to those based on backload preparation technique. Therefore the mineralogy was analysed done on the latter ones.

The X-ray diffraction analysis (XRD) was performed using a Pan Analytical Expert Pro instrument equipped with a Cobalt X-ray tube (Empyrean Co LFF). The samples were scanned between 5 and 100 °2θ with a step size of 0.0131303 °2θ. The diffraction patterns were processed using the X'pert Highscore Software Vers. 2.2b produced by PANalytical. Phase analysis was performed manually using the software included powder diffraction files (PDF) released from the International Center of Diffraction Data for reference. Preferably PDF files of S, I and C quality were used.

Reflectance spectroscopy

Reflectance spectra of the residual meteorite powders in the visible and infrared wavelength region (0.35–2.6 μm) were taken with an ASD Fieldspec with a spectral resolution of 1 in the laboratory at the Planetary Spectrophotometer Facility at the Universitiy of Winnipeg. The spectra were continuum removed to check for changes in main absorptions from phyllosilicates, olivine and pyroxene, as well as to check for additional phases by using the ENVI software package.

3 Results of experimental liquids and solids

The chemical and mineralogical procedures described above were employed to each liquid collected from the experiments after 1, 2, 5, 12, 50, 100 and 200 days of duration. The solids were taken from the respective experiments and were analysed with XRD and reflectance spectroscopy. The results are given below.

3.1 Leachates

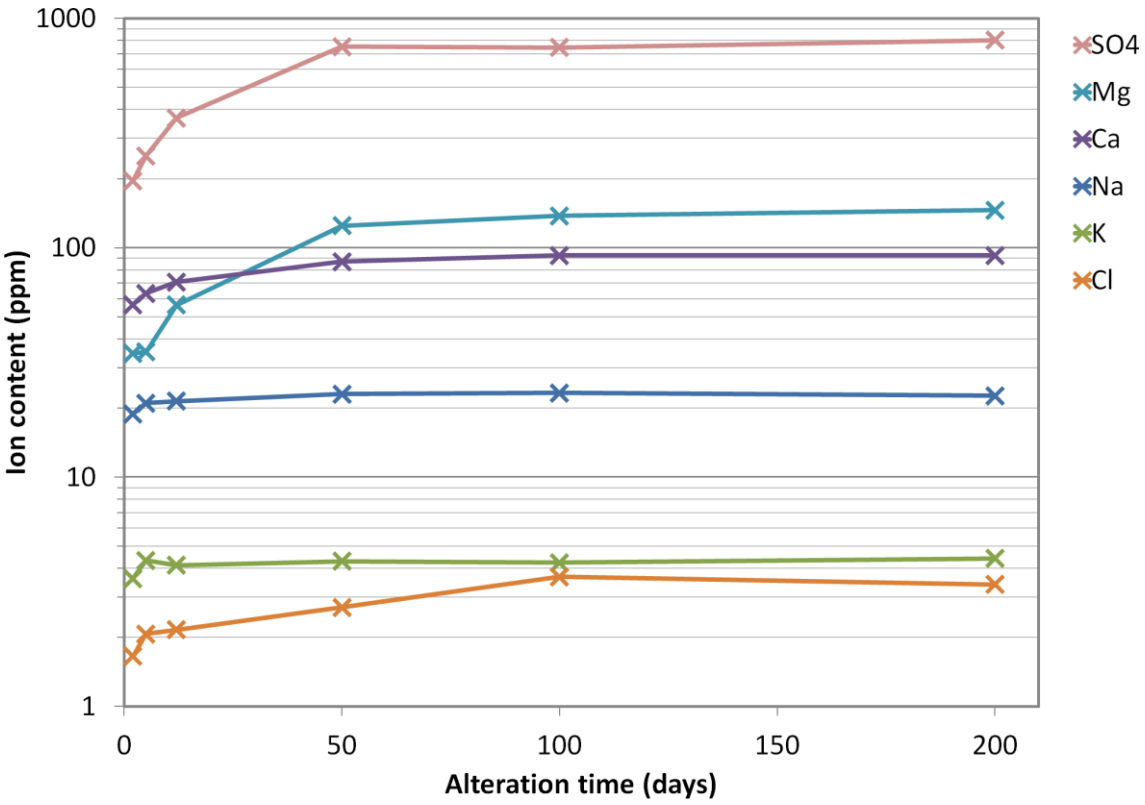

Fig. 6: Murchison leachate (brine) after reaction times of 2, 5, 12, 50, 100, 200 days.

An inspection of Fig. 6 reveals that sulphate is the major anion with low additional contents of Cl in the leachate derived from Murchison. Major cations are Mg, Ca and Na plus minor contents of K. A systematic increase of all major elements is visible until 50 days of reaction. At longer times concentrations increase only slightly. Although chemical equilibrium conditions cannot be proven, it seems that the leaching of extractable material has come to a near steady state.

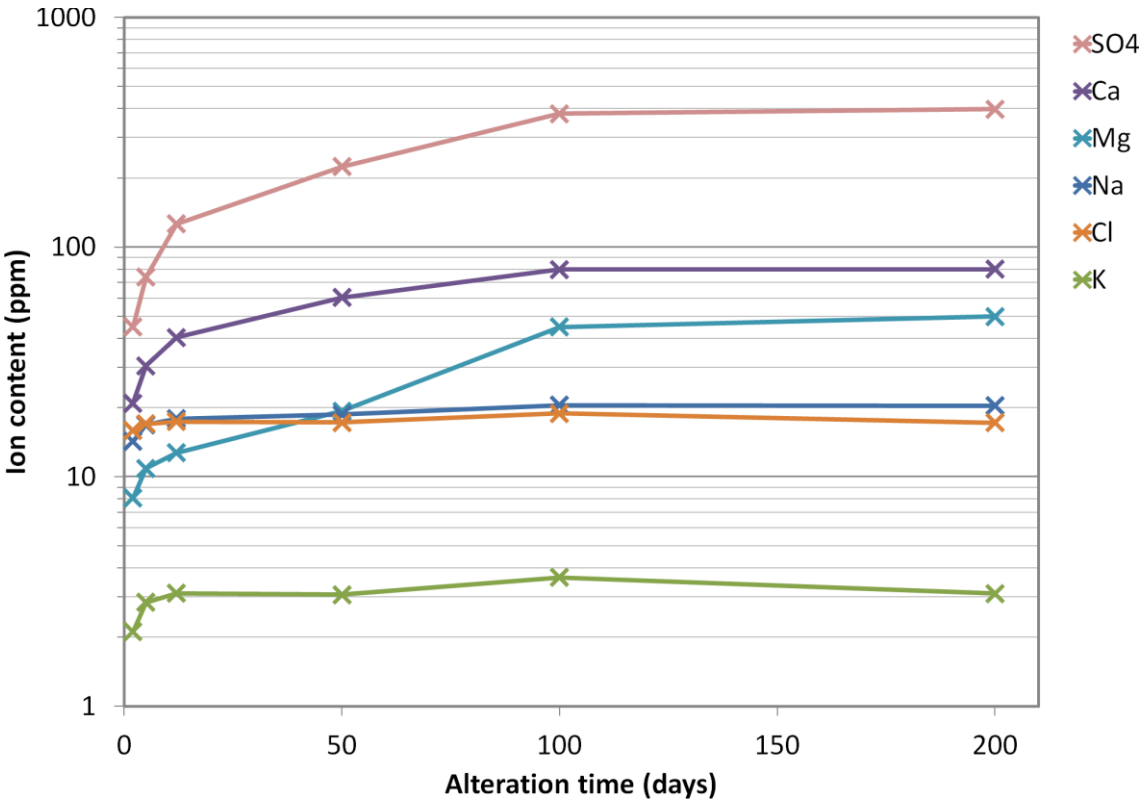

Fig. 7: Jbilet leachate (brine) after reaction times of 2, 5, 12, 50, 100, 200 days.

The observations made for Murchison leachates are nearly the same for Jbilet (Fig. 7). A slight exception is the increase of Mg until 100 days of reaction time. Absolute concentrations of the major solutes Mg are three times higher and SO_4 is twice as high in Murchison compared to Jbilet. Cl is approximately five times higher in Jbilet leachates.

In both the carbonaceous and the ordinary chondrites SO_4 is the prevailing anion. Whereas the major cations in Murchison and Jbilet are Mg and Ca, while in the ordinary chondrites Na is the dominating cation (see Tab. 4 and App. A, Figs. A3, A4 and A5). In leachates of all three ordinary chondrites Mg and Ca contents are peaking at day 2 of reaction time and decrease until 200 days. The total content of solutes in the leachates of ordinary chondrites NWA 7936 and NWA 8039 is around 1/7 to 1/14 the order of magnitude compared to the carbonaceous chondrites Murchison and Jbilet. Zag is the specimen with the lowest content of solutes in its leachate.

Tab. 4: Main anions and cations of Murchison, Jbilet and Zag after 200 days of alteration time.

Leachate composition (ppm)	Murchison	Jbilet	Zag	NWA 7936	NWA 8039
Cl	2.80	16.59	0.84	1.52	3.31
SO_4	802.01	398.04	8.64	44.44	36.48
Na	22.65	20.34	11.05	26.80	28.19
K	4.41	3.10	1.38	2.63	3.97
Ca	92.49	80.00	0.28	0.76	2.64
Mg	145.61	49.79	< 0.5	< 0.5	< 0.5
Σ	1069.97	567.86	22.19	76.15	75.191

3.2 Residual meteorite powders

3.2.1 X-ray Diffraction Analysis

X-ray diffraction of fresh and hydrothermally treated solids was employed in order to attain an overview on the mineral phases occurring in the meteorites and to detect changes in the residual meteorite powders over alteration time, e.g. the possible decomposition of troilite by oxidation or the dissolution of water soluble minerals such as sulphates and carbonates. These have been reported for CCs and could serve as a plausible source for the solute composition detected by ion chromatography. A mass balance calculation of total extracted solutes (SO_4, Cl, Na, K, Ca, Mg) from the sample (~111 mg) after 200 days reveals a chemical conversion of 11% and of 6% for Murchison and Jbilet, respectively. This observation allows the prediction that only minor components have reacted or of the major components only a small fraction has taken part in the hydrothermal reactions.

For the silicate minerals diffraction patterns are dominated by lines of olivine and enstatite. Furthermore the CCs consist of a very unusual mineral mixture including the so called Poorly Characterized Phase (PCP). The presence of poorly known mineral species makes it difficult to uniquely identify minor phases such as carbonates, sulphates or magnetite in the CC matrix. A comparison between diffraction patterns of altered and unaltered samples shows that most of the diffraction lines remain in position and intensity regardless of experimental conversion (see App. C, Figs. C1-C5). Exceptions are: two weak unidentified lines at 17.096 °2θ (d=6.018 Å) and 19.034 °2θ (d=5.4100 Å) in Murchison and the calcite line in Jbilet.

Murchison

For the Murchison original sample the following mineral phases were detected by their main diffraction lines (flagged in Fig. 8): olivine, orthopyroxene, troilite and kamacite. The characteristic line at 14.338 °2θ (d=7.1667 Å) is closely flanked by the lines of greenalite, antigorite and cronstedtite. This gives evidence for an Mg-Fe-serpentine phase. Magnetite is not uniquely identifiable in Murchison, because its main diffraction line at 41.378 °2θ (2.5302 Å) is overlain by a pyroxene line. The second strongest magnetite line at 67.229 °2θ (1.4845 Å) does not appear.

Additionally there are weak main diffraction lines of calcite (3.035, 2.095, 2.285 Å) and gypsum (7.63, 4.28, 3.07 Å), which are seen only in the diffraction pattern from the backload preparation; therefore the presence of calcite and gypsum cannot be checked for changes with alteration time because the material was insufficient for the use in back-loading XRD preparation. The check for aragonite, anhydrite and epsomite is negative. The only changes detectable with alteration time is the disappearance of a diffraction line at 19.034 °2θ (d=5.4100 Å) after 2 days (Fig. 9) and the disappearance of an unidentified line (marked with n. i. in Fig. 8) at 17.096 °2θ (d=6.018 Å) also after 2 days (App. C, Fig. C1). The former one is consistent with the main diffraction line of tochilinite, but the other two main lines of tochilinite (2.320 and 1.860 Å) are not significant in the pattern. The diffraction lines of troilite at 50.56 °2θ (d=2.0947 Å) and kamacite at 52.347 °2θ (d=2.0280 Å) remain stable during alteration time (Fig. 10).

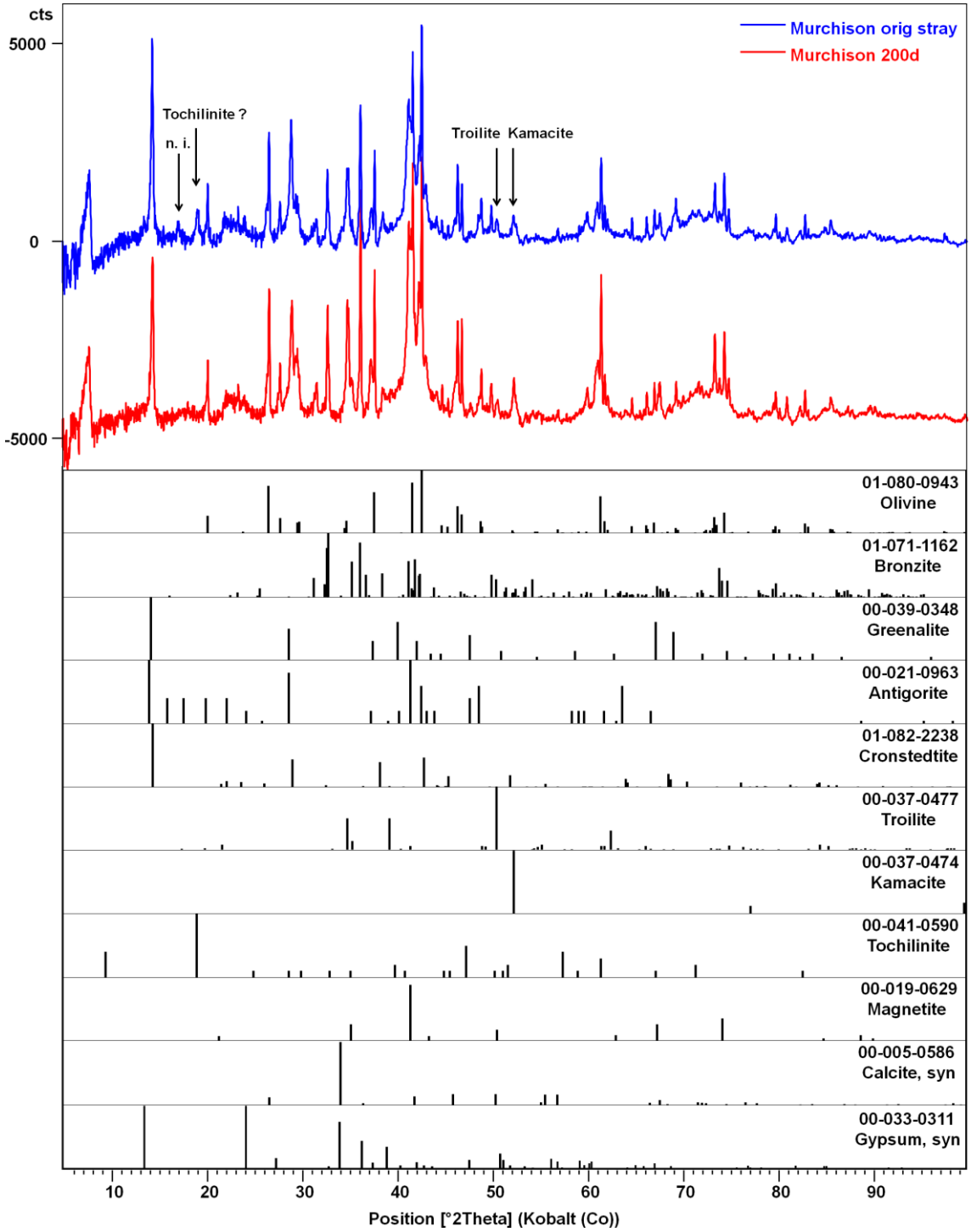

Fig. 8: Diffraction pattern of original Murchison and powder after 200 days alteration with diffraction lines of best matching minerals from PDF files.

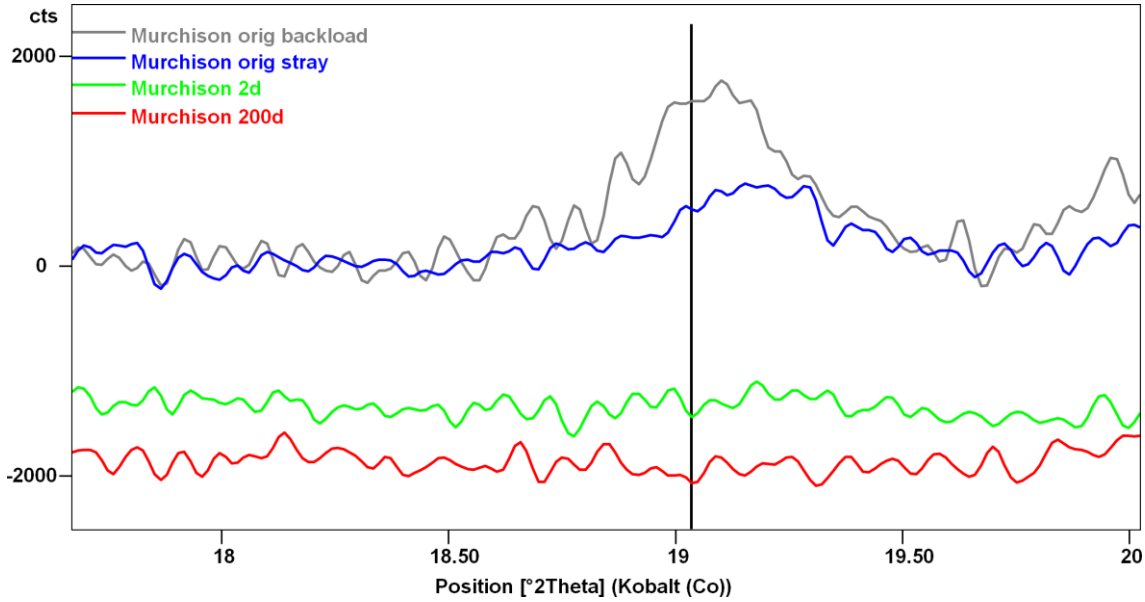

Fig. 9: Subset of the tochilinite line at 19.034 °2θ (5.4100 Å) in diffraction pattern of Murchison original powders in stray- and backload preparation, Murchison 2 days and 200 days alteration time. The diffractrograms of Murchison 2 days and 200 days are shifted by -1500 and -2000 cts for clarity.

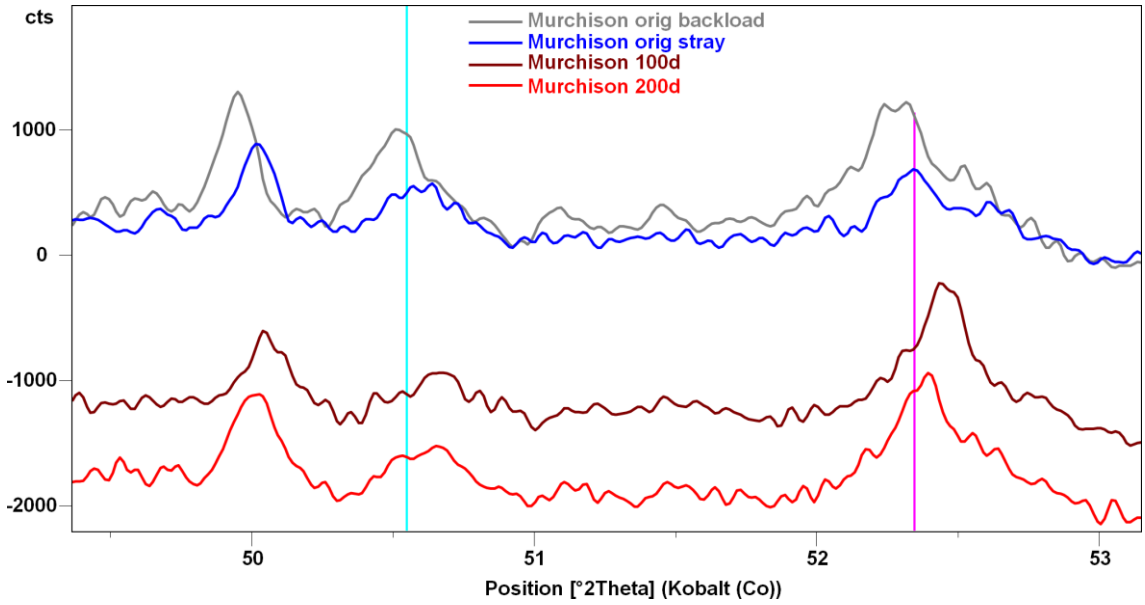

Fig. 10: Subset of the troilite line at 50.56 °2θ (2.0947 Å) in diffraction pattern of Murchison pure, 100 and 200 days with lines from PDF file troilite (light blue) and kamacite (pink). The diffractrograms of Murchison 100 days and 200 days are shifted by -1500 and -2000 cts for clarity.

Jbilet

For the Jbilet original sample the following mineral phases were detected by their main diffraction lines (flagged in Fig. 11): Forsteritic olivine, enstatite, troilite, kamacite and most probably calcite. Magnetite is not uniquely identifiable in Jbilet,

because its main diffraction line at 41.378 °2θ (2.5302 Å) is overlain by a pyroxene line. The second strongest magnetite line at 67.229 °2θ (1.4845 Å) is embedded in a broader shoulder.

Calcite is identified relatively certain by the presence of a diffraction line at 34,305 2θ (d=3.0330 Å) and a weak line at around 46.088 (d=2.2849 Å). The calcite line weakens after 12 days of alteration time and is vanished completely in the diffraction pattern after 50 days (Fig. 12). The second strongest line at 50.56 °2θ (d=2.0947 Å) is identic with the main troilite line. The weakening of this line as can be observed in Figure 13 is consistent with the weakening of the calcite line rather than the weakening of the troilite line due to iron oxidation, because the kamacite line remains stable.

Anhydrite cannot uniquely be identified because the main lines are very weak and overlain by lines of olivine. The check for the other water soluble phases aragonite, gypsum and epsomite is negative.

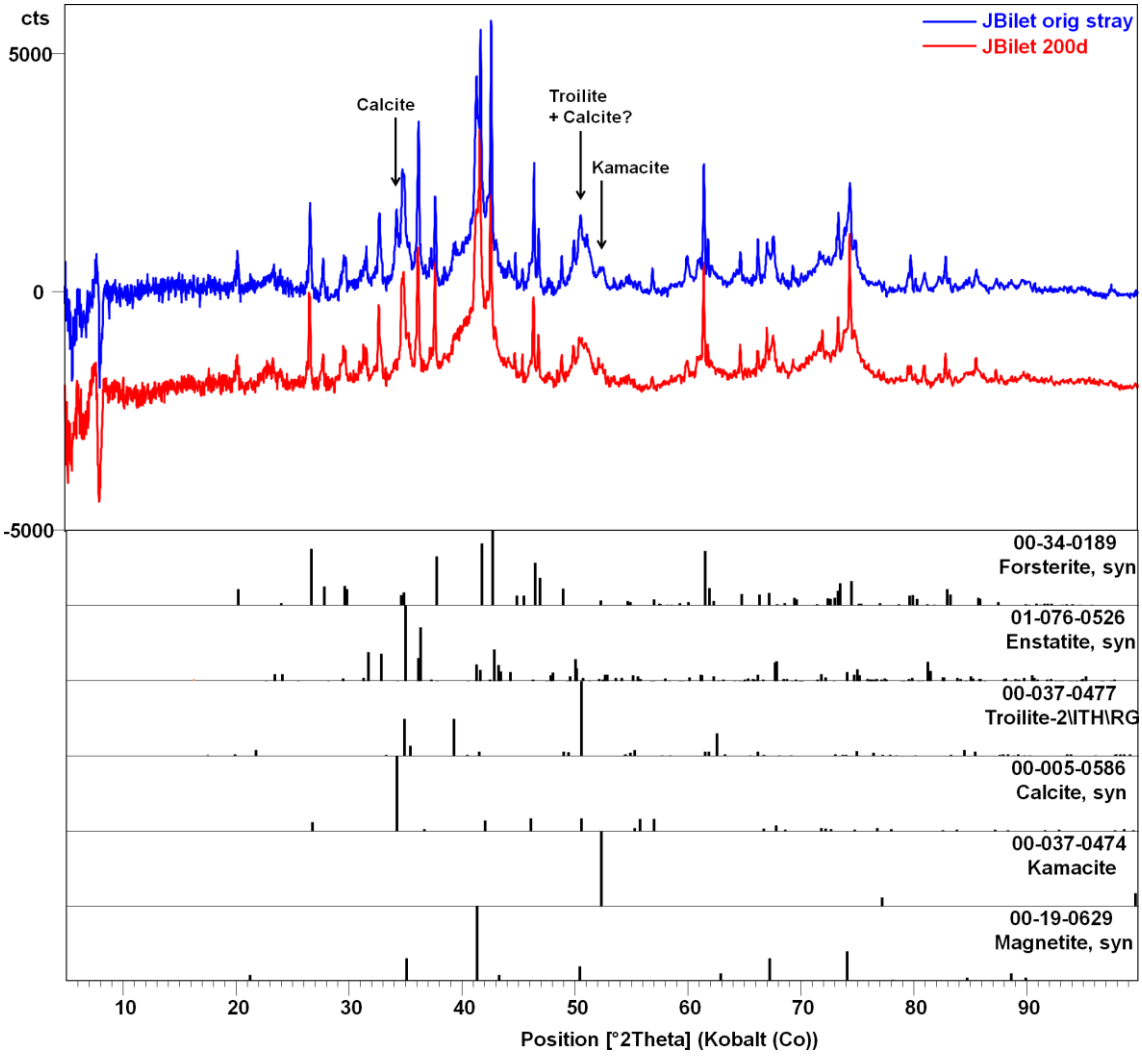

Fig. 11: Diffraction pattern of Jbilet pure and 200 days with diffraction lines of best matching minerals from PDF files.

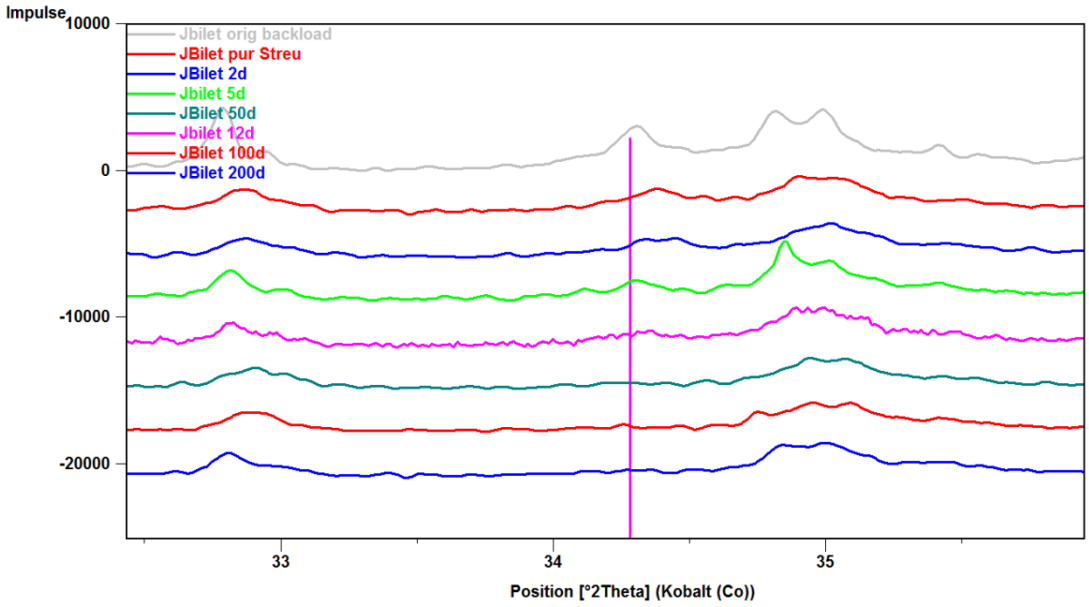

Fig. 12: Subset of the calcite line at 34,305 2θ (d=3.0330 Å) in diffraction patterns of Jbilet alteration time series with vanishing of the calcite line between day 12 and 50.

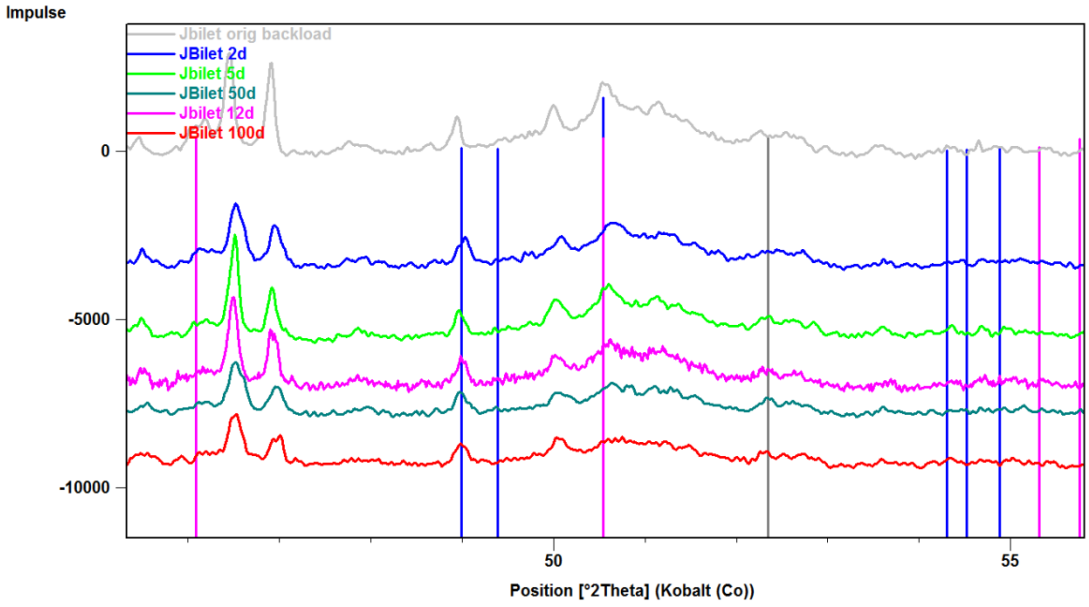

Fig. 13: Subset of the troilite line at 50.56 °2θ (2.0947 Å) in diffraction pattern of the Jbilet alteration time series with lines from PDF file troilite (blue), kamacite (grey) and calcite (pink).

Ordinary chondrites

The ordinary chondrites NWA 8039, NWA 7936 and Zag show the diffraction lines for olivine, pyroxene, troilite and kamacite (see Appendix C, Figs. C3, C4, and C5). In these specimens no mineralogical changes during alteration time can be observed.

3.2.2 Reflectance spectroscopy

Carbonaceous chondrites

The spectra shown in Figure 14 indicate that the spectra of Murchison and Jbilet become brighter with increasing alteration time. The spectra normalized to 0.650 µm show that the Murchison spectra get redder with increasing alteration (reflectance increases towards longer wavelengths), while those of Jbilet do not change in slope during the experiment.

Figure 15a shows the Murchison spectra continuum removed between 0.60 and 0.83 µm and between 0.83 and 1.75 µm. An inspection of the absorption bands indicates that the absorptions at ~0.95 µm and ~1.13 µm strengthen with experimental duration, while the absorption at 0.73 µm weakens and moves to longer wavelengths up to a position at 0.75 µm. The olivine absorption seen on the longer wavelength shoulder at 1.25 µm remains constant (Fig. 15a).

The inspection of the same wavelength region in Jbilet spectra (Fig. 15b) shows a broad absorption between ~0.7 and ~1.75 µm. Absorptions of phyllosilicates near 0.7, 0.9 and 1.1 µm, as well as absorptions of dry silicates such as olivine and pyroxene near 0.95, 1.05 and 1.25 µm cannot be resolved, but a very weak absorption around 0.75 µm is suggested in the unaltered and for 2 days altered Jbilet.

Additional absorption features in Murchison and Jbilet are detected near 0.370, 0.405 and 0.480 µm (Fig. 16a and b). Further inspection shows that all three absorption increase with increasing experimental duration.

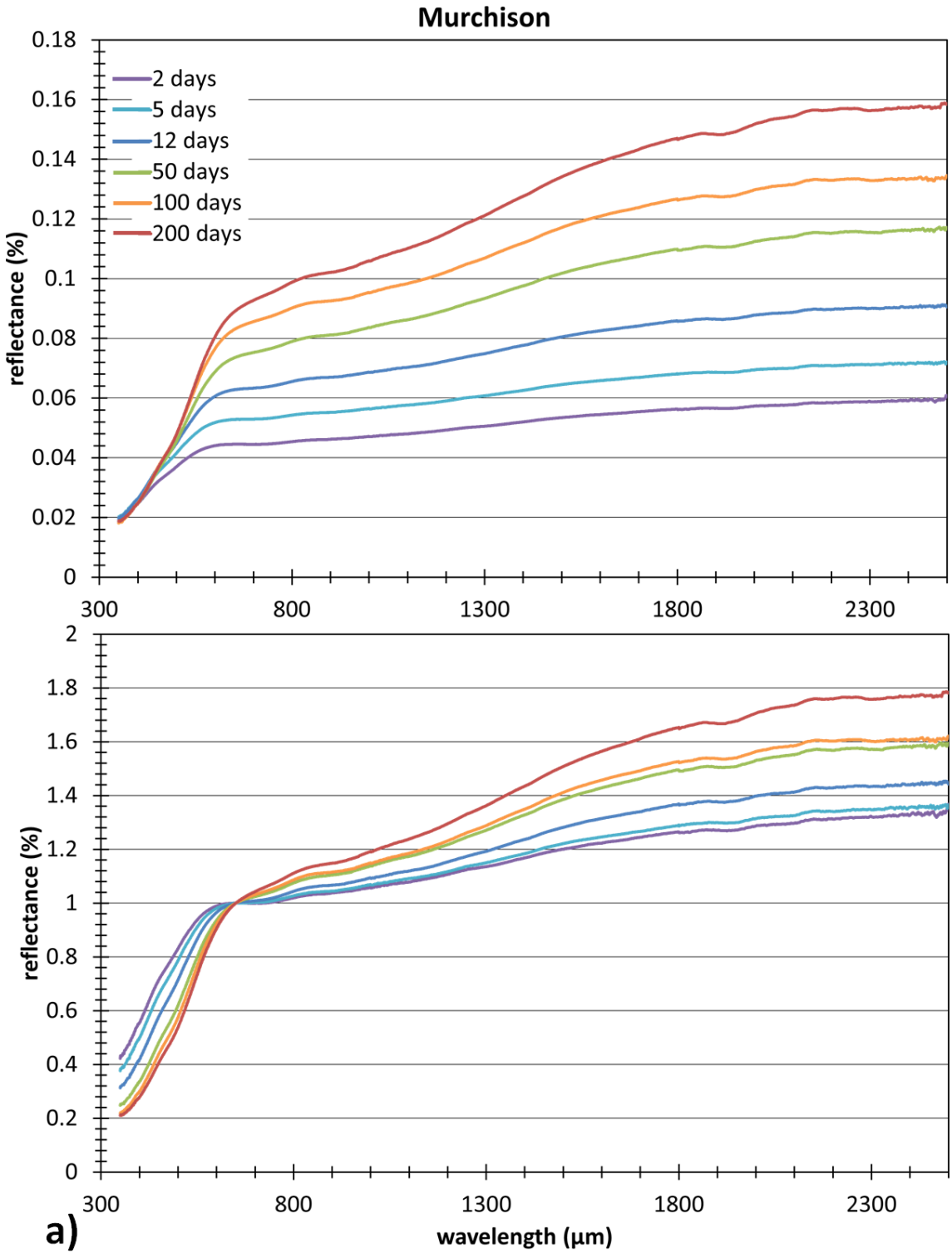

Fig. 14: Reflectance spectra of a) Murchison not normalized (top) and normalized to 0.650 µm (bottom).

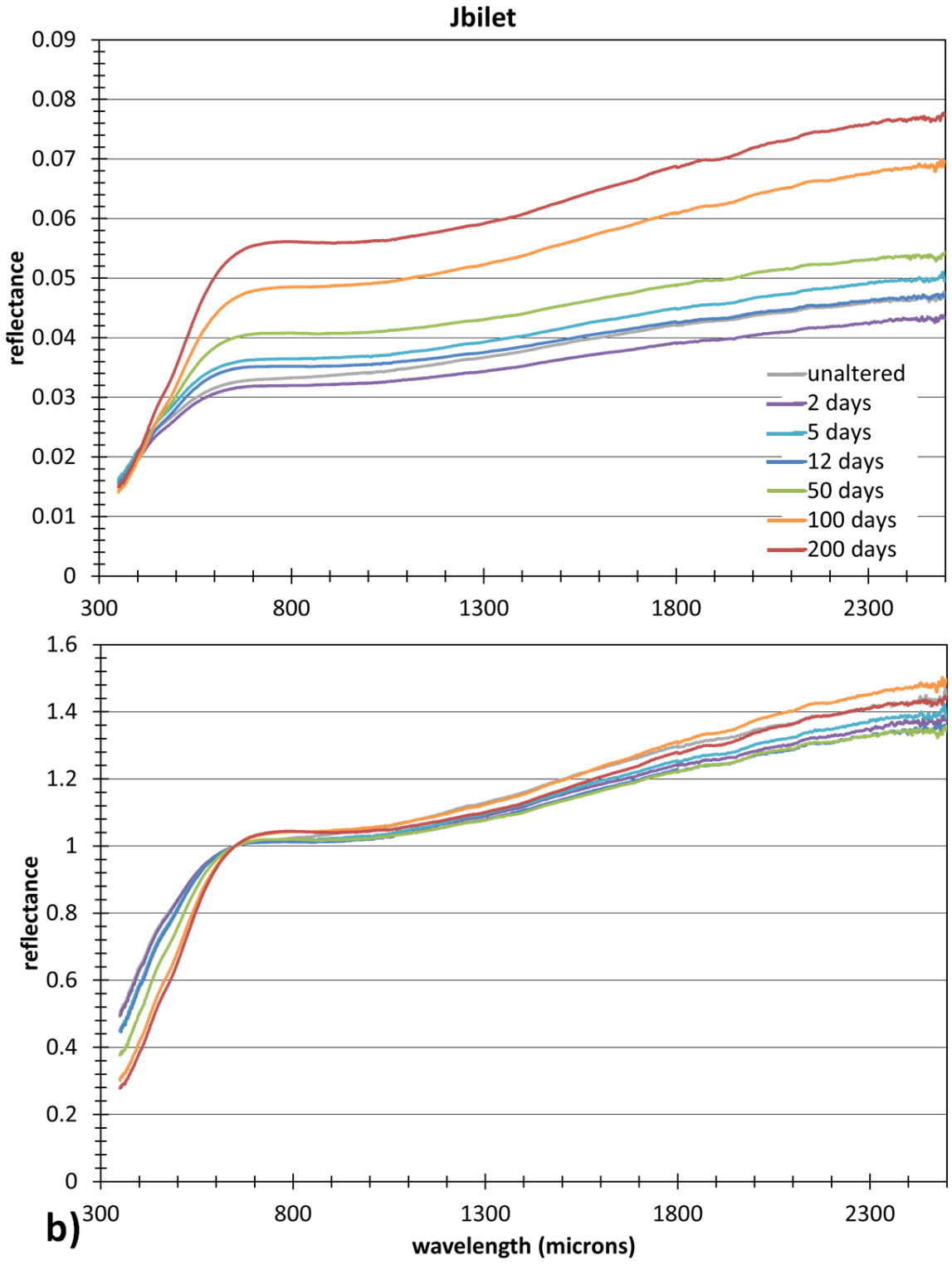

Fig. 14 (cont.): Reflectance spectra of b) Jbilet not normalized (top) and normalized to 0.650 µm (bottom).

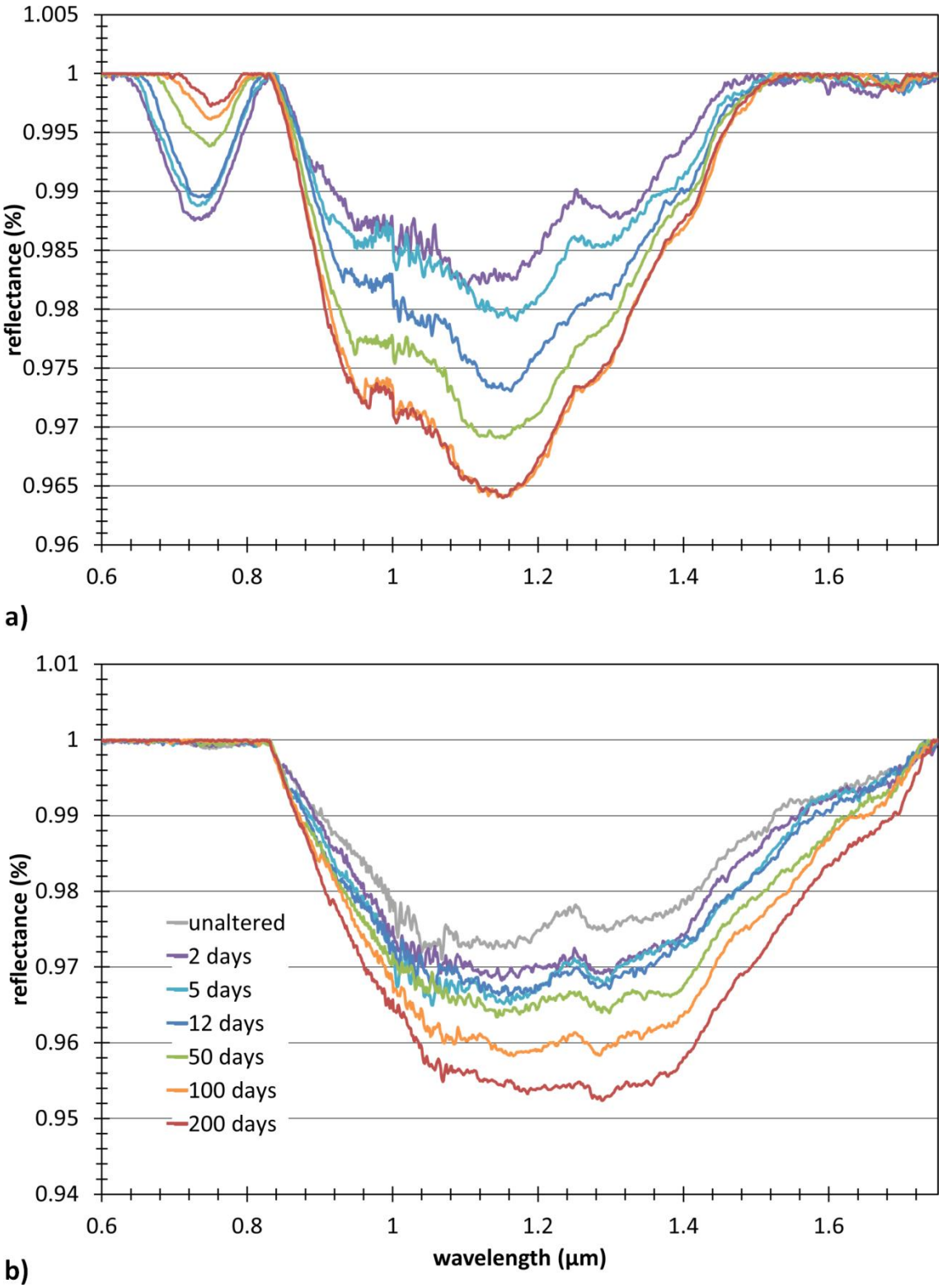

Fig. 15: Spectra continuum removed between 0.60 and 0.83 µm and 0.83 and 1.75 µm of a) Murchison and b) Jbilet.

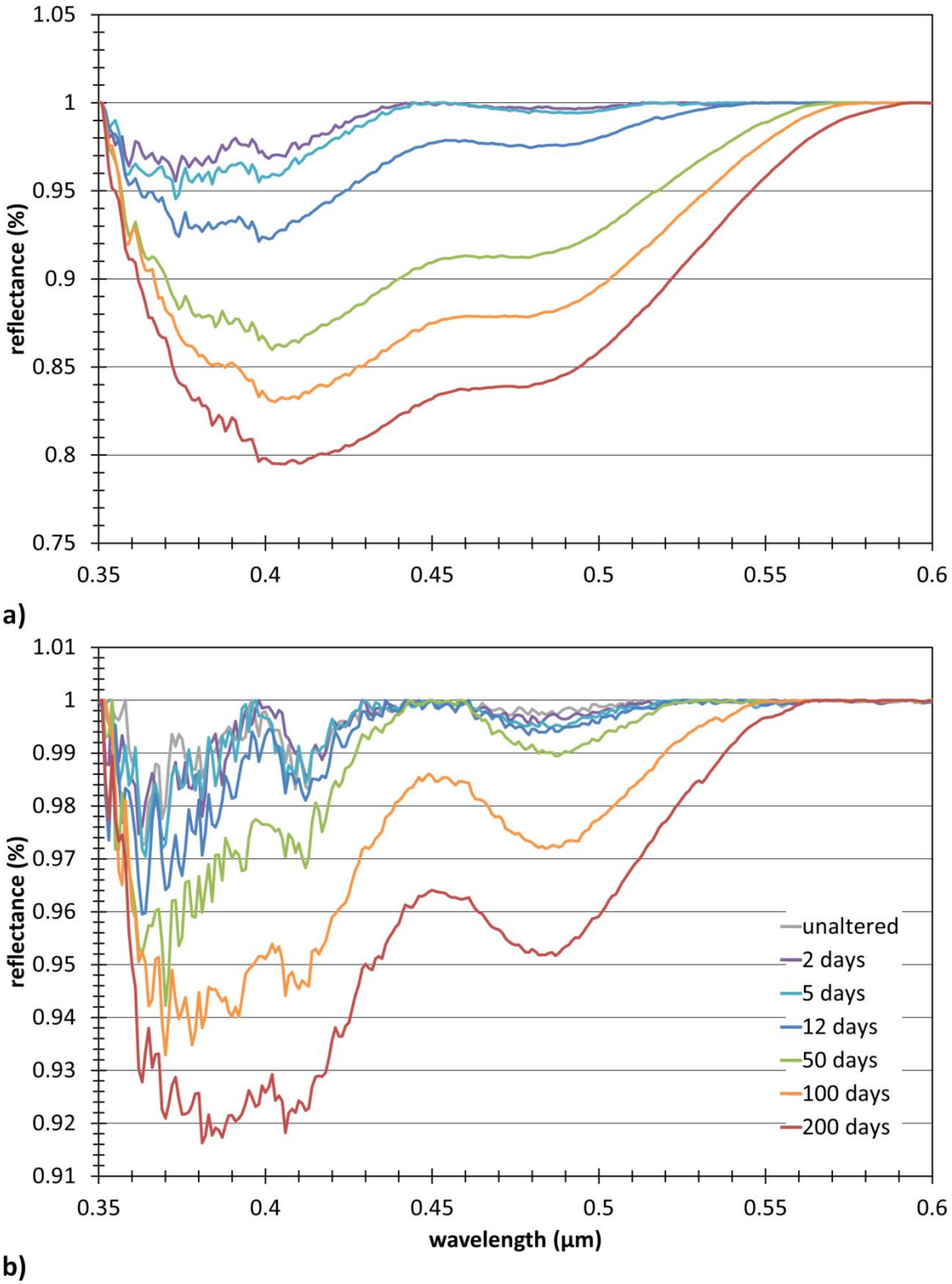

Fig. 16: Spectra continuum removed between 0.35 and 0.60 µm of a) Murchison and b) Jbilet.

Ordinary chondrites

NWA 8039, NWA 7936 and Zag do not show any significant changes in brightness or slope during the experiments (see App. D, Figs. D3, D4, and D5). An inspection of their spectra continuum removed between 0.6 and 2.5 µm shows the main absorption lines

for dry silicates olivine and pyroxene near 0.9, 1.05 and 1.25 µm and between 1.9 and 2.1 µm (Figs. 17a, b, c). These absorption signatures remain stable over alteration time.

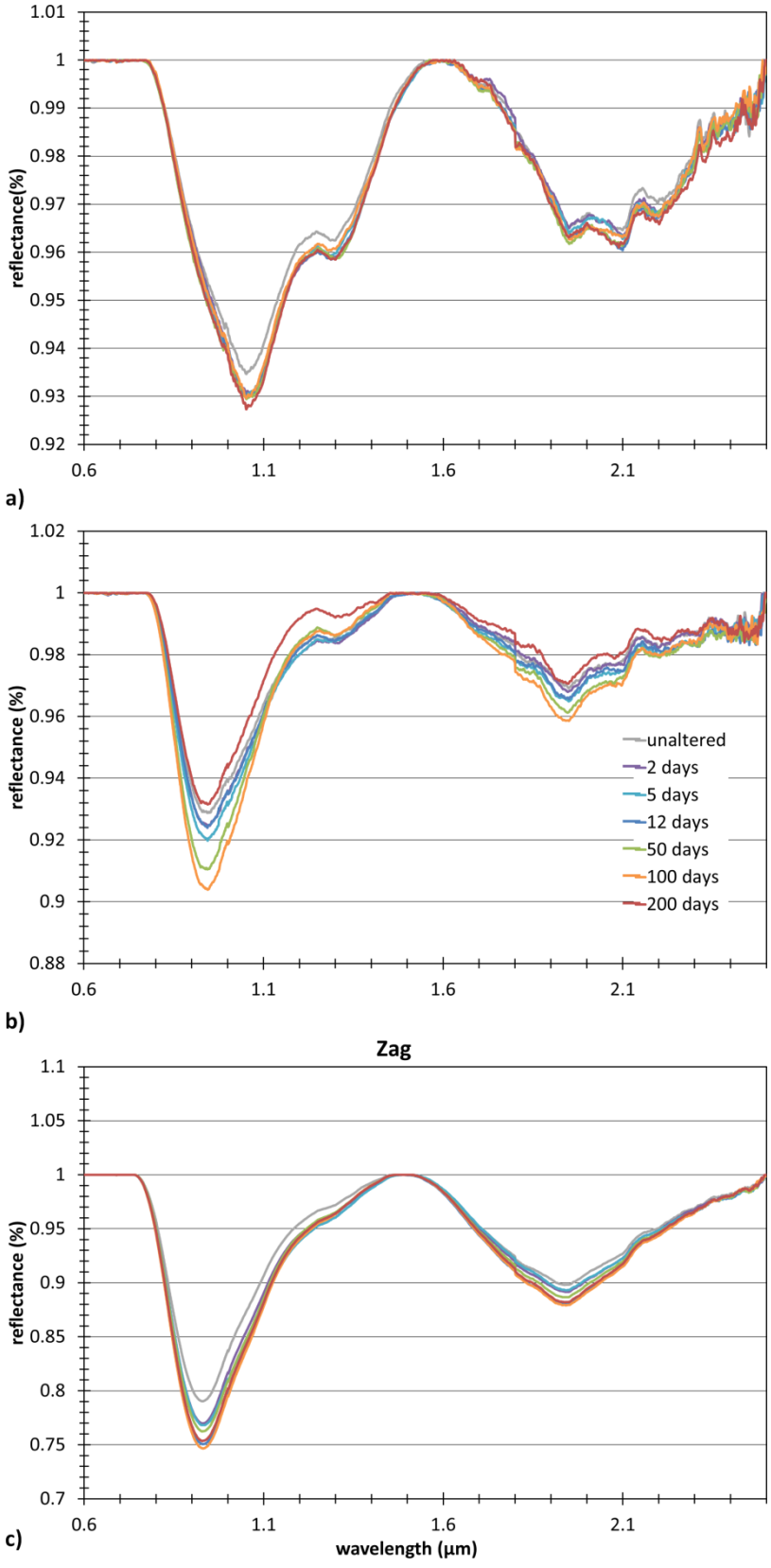

Fig. 17: Continuum removed 0.6 to 2.5 µm wavelength region of ordinary chondrites a) NWA 8039, b) NWA 7936 and c) Zag

4 Discussion

4.1 Leachate composition

With respect to the anions, leachate compositions of CCs after 200 days are dominated by SO_4 with low Cl contents. Main cations occur in the liquids in the order Mg > Ca > Na > K for Murchison and Ca > Mg > Na > K for Jbilet. These findings are in principal agreement with poorly controlled short leaching experiments on CC Tagish Lake (C2 meteorite, ungrouped) by Izawa et al. (2010). Short duration leaching on Murchison by Fanale et al. (2000) also shows SO_4 as main anion. Sulphate as the major anion is compatible to bulk SO_4 content dominating over bulk Cl (see Tab. 4). The analytical setup of the Murchison and Jbilet experiments presented here did not allow the detection of $HCO3^{2-}$ and/or $CO3^{2-}$. However, since the ion balance (total cation vs. anion charges) is nearly equal, it can be assumed that carbonate play a minor role in the anion composition of the leachates.

Troilite oxidation can potentially account for 180 ppm SO_4 in the leachate (~1.8% of the sample, see section 2.3), which is nearly one quarter of the amount of SO_4 in the Murchison leachate (802 ppm) and nearly half of that in the Jbilet leachate (398 ppm) after 200 days. The SO_4 values in the ordinary chondrite leachates ranging from ~9 to 44 ppm indicate that the calculated value of 180 ppm is not realistic during the 200 days, because troilite oxidation should not produce significant higher values than that of the ordinary chondrites. Furthermore XRD data show that troilite and kamacite is not significantly consumed during the experiments.

The values of bulk sulphur in Murchison range from 3.0 to 3.38% (Jarosewich 1971, Burgess et al. 1991, Fuchs et al. 1973) and the amount of pyrrhotite from XRD is 1.2-2.9% (Bland et al. 2004, Howard et al. 2009), which does account for ~0.4 to 1% of sulphur. Adding up the sulphate sulphur from the leachate (2.7%) and the sulphide sulphur from the XRD results in a plausible amount of bulk sulphur between 3.1 and 3.7%.

Gao and Thiemens (1993) and Labidi et al. (2017) report low $\Delta^{34}S$ values in the extracted sulphate, clearly indicating an extraterrestrial origin. Therefore a terrestrial contamination of the sulphate in the leachates is unlikely, but cannot be ruled on the specific sample.

As expected, the ordinary chondrites containing mainly dry silicates, possessing a well crystalline habit are more resistant against leaching. Their total amount of solutes leached is less than 1%, which is minor in contrary to Murchison (10.59%) and Jbilet (5.56%). Although water soluble minerals are not described in ordinary chondrites, their leachates contain around 40 ppm SO_4. As all the used specimens are desert finds, a terrestrial origin of the sulphate cannot be ruled out.

Among the ordinary chondrites leached in this project, Zag is the only specimen for which soluble minerals have been described (Rubin et al. 2002). Although halite grains have been observed, this sample (see Appendix A) contains much lower Cl than the CM samples and shows the lowest content of leachable ions among the five chondrite samples used in this work. Given the large lithological heterogeneity of regolith breccia Zag it is not clear whether halite grains were present in the very specimen fragment used here or the halite grains may contribute very little to bulk Cl content. The description of apatite in Zag (Jones et al. 2016) explains the detection of P (ICP-MS) and PO_4 (IC) in the leachates.

4.2 Composition of experimental solids

XRD results

The XRD patterns of untreated Murchison is mainly in accordance with what is known from former XRD data of CMs (Bland et al. 2004, Howard et al. 2009). Exceptions are 1) the presence of magnetite described by other authors is not confirmed here and 2) the presence of anhydrite which appears as weak diffraction lines in our work has not been found by Bland et al. 2004). The contents of water soluble minerals such as carbonates and sulphates which have been reported in CMs from electron beam investigations (e.g., Fuchs et al. 1973, Barber 1981, Johnson & Prinz 1993) are too low to be detected by XRD using the applied stray preparation technique. Therefore systematic changes of these minerals with alteration time are not possible. The only changes with alteration time are the disappearance of one tochilinite line and an unidentified line at 17.096 °2θ (d=6.018 Å). This unidentified line could be identical to a line described by Fuchs et al. (1973) near 6.1 Å, which has been reported as an unidentified acid soluble phase. In the analytical program set up and outlined here, it is generally assumed that the unequivocal detection of a mineral requires the presence of the three major diffraction lines. The presence of just one diffraction line is not valid to quote the presence of a mineral. This statement is in

strong contrast to many laboratories working on the mineralogy of meteorites but is common and good practice in XRD laboratories elsewhere. An exception is the presence of the base reflex of some sheet silicate such as smectites; here the d(001) signal of diffraction can often be interpreted unequivocally as the base reflex. As a consequence and as an example for Murchison and Jbilet it is stated, that the presence of one diffraction line of e.g. tochilinite merely means that the presence of this mineral cannot be ruled out.

While Murchison is a typical, well investigated CM2-type specimen which belongs to the least aqueously altered CMs (Rubin et al. 2007, Howard et al. 2011), contradicting knowledge circulates on Jbilet. The XRD patterns taken in this work differ from that of typical CMs, mainly because it completely lacks any sign of phyllosilicates and of tochilinite. Whereas Hewins & Garvie (2013) report a typical CM composition, containing serpentine, smectite and tochilinite from XRD and Sievert et al. (2018) detected tochilinite along with Mg-Fe-sheet-silicates (probably nontronite) by recent electron microprobe analysis. However Russell et al. (2014) found an unusual XRD pattern similar to our work, lacking Fe-serpentine and tochilinite. Apart from that there are several hints indicating that Jbilet is an impact breccia consisting of typical CM2 material and thermally metamorphosed regions (Russell et al. 2014, Zolensky et al. 2016, Bischoff et al. 2017). This would also explain the composition of Jbilet's leachates which are indeed qualitatively similar to that of Murchison, but its total amount of solutes is much lesser (see section before). Nevertheless water soluble minerals such as anhydrite (Russell et al. 2014) and calcite (this work) have been detected in the XRD pattern of Jbilet. The calcite is slowly being dissolved until day 50 during the experiment.

The XRD pattern of ordinary chondrites in this work, showing lines of pyroxene, olivine and metal Fe work are mainly consistent with the comprehensive study of Dunn et al. (2010). The only exception is that plagioclase could not uniquely be identified because it was overlain by other phases.

Reflectance spectroscopy

The reflectance spectra of Murchison powders are consistent with typical CM spectral properties. The major absorptions near 0.7, 0.9 and 1.1 μm have been assigned to mixed valence Fe-bearing serpentine group phyllosilicates in CM spectra along with absorptions centered at 0.370, 0.405 and 0.480 μm (Cloutis et al. 2011). The observed increase in intensity of almost all phyllosilicate absorptions combined with the decrease of the 0.7 μm absorption accompanied by a shift to longer wavelength with increasing alteration time (Fig. 15a), reveals significant changes in the Fe distribution within the phyllosilicates and possibly a slight change of their structure.

Another remaining question is on the fate of iron during the experiments. Ferrihydrite cannot be detected in the XRD data, because it probably takes a long time to crystallize from a gel to a mineral structure; in addition, its main lines at 2.45 and 2.25 ° 2θ (Co-K_a) are overlain by olivine. An inspection of the reflectance spectra of altered Murchison and Jbilet does not show any obvious contribution from Fe oxyhydroxides, such as the characteristic absorption between 0.95 and 1.0 µm.

The brightening of the Murchison spectra with increasing alteration may be caused by the decomposition of tochilinite (as suggested in Cloutis et al. 2010). Furthermore the destruction of other opaques such as organics may contribute to the brightening. This supported by the observation that the vessels containing Murchison powder and leachate smelled characteristically when opened after the experiment, which stopped at day 100.

The reflectance spectra of Jbilet substantiate its nature of a partial thermally metamorphosed breccia, showing a broad absorption between ~0.7 and ~1.7 µm most probably caused by the superposition of phyllosilicate absorptions and absorption of dry silicates (olivine and pyroxene). These spectral properties resemble very much that of the aqueously altered and thermally metamorphosed CCs described by Cloutis et al. (2012).

The ordinary chondrites remain stable in their spectral properties during alteration, indicating that their dry silicates are not substantially affected.

5 Geochemical modelling of brines

In a next step the evolution of the experimentally obtained leachate from Murchison 200 days alteration will be explored under freezing conditions and subsequent evaporation applying the thermodynamic model FREZCHEM (FREeZing CHEMistry) by Marion et al. (2010).

5.1 Model assumptions

Freezing

Input parameters were set for freezing at 500 bars which corresponds approximately 100 km depth on Ceres calculated by

$$p = h \cdot \rho \cdot g$$

where p is pressure, ρ=1.950 g cm^{-3} density of Ceres' outer shell (Park et al. 2016) and gravity g=0.28 m/s^2 (Russel et al. 2016).

As Ceres might be an interloper from the outer solar system concluded from dynamical considerations (McKinnon et al. 2008) or at least might have accreted material from outer regions (De Sanctis et al. 2015), unknown amounts of CO_2 and NH_4 may contribute to the system. For this reason two different compositional cases are explored. One scenario comprises freezing of the brine without additional volatiles in the following denoted as *water scenario*, the other scenario incorporates carbonate chemistry (alkalinity and pCO_2) as well as ammonium denoted as *NH_4-CO_2 scenario*.

Since there is no information on the concentration range of carbonate/bicarbonate/CO_2 a value for carbonate alkalinity was chosen arbitrarily as 0.002 mol/kg HCO_3^-, which is comparable to that of Earth's seawater (e.g., Bockmon & Dickson 2015). The value for partial pressure of CO_2 was set to pCO_2=0.02 bars. The concentration of NH_4=0.0001 mol/kg was chosen equally to that of potassium. The input data files for FREZCHEM are given in Appendix E.

During freezing a fractional crystallization process is assumed. Due to the different density the ice is floating on the brine enclosing intercrystalline salt minerals and brine pockets as described for sea ice (e.g., Koslowski 1986).

Evaporation

As input for the evaporation runs the compositions of the residual brines after freezing were given for both the *water scenario* and the *NH_4-CO_2 scenario*. The residual amounts of 0.11 g and 0.13 g were expanded to 1000 g in order to allow successful evaporation runs. The evaporation process is problematic to model, because thermodynamic data realistic for temperatures at Ceres equatorial region fluctuating between ~110 and 240 K (Hayne & Aharonson 2015) and vacuum conditions are not available. Therefore to simulate the brine evolution during evaporation a temperature of 293 K and a pressure of 0.1 bars was chosen.

5.2 Results

Freezing output

The brine evolution and precipitating salts of the freezing run are presented in Fig. 18 for the *water scenario* and in Fig. 19 for the *NH_4-CO_2 scenario*. The model is running out of water (leaving ~0.1 g residual brine) at 263 K and at 261 K, respectively. In both scenarios the initial low mineralized leachates with a total salinity of ~1 g/kg (see also Tab. 4) evolves to brines with a salinity of about 200 g/kg. Like the initial leachate, the brines are still dominated by SO_4 as the major anion, but the Cl to SO_4 ratio increases from 0.01 up to 0.7. Cations in the brines occur in the order Mg > Na > K > Ca in the water scenario and Mg > NH_4 > Na > K > HCO_3 > Ca > CO_3 in the NH_4-CO_2 scenario. Ca is enriched by a factor of 10 and starts being consumed at 268 K with the precipitation of gypsum. Further precipitating salts are Mg-sulphate (meridianiite), Na-sulphate (mirabilite) and Mg-K-sulphate (picromerite) (see Figs. 18b, c and 19b, c). In the NH_4 and CO_2 containing brine Ca-carbonate (magnesite) occurs as additional early phase.

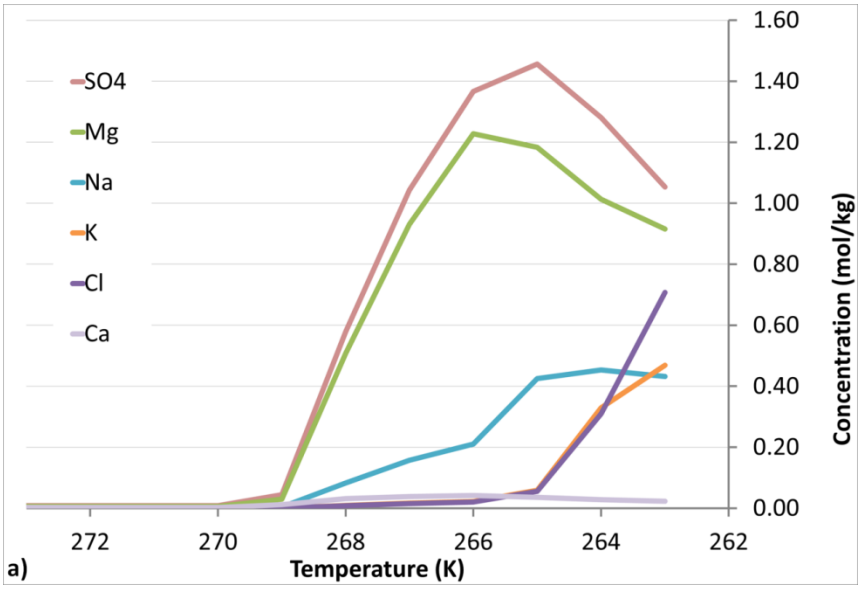

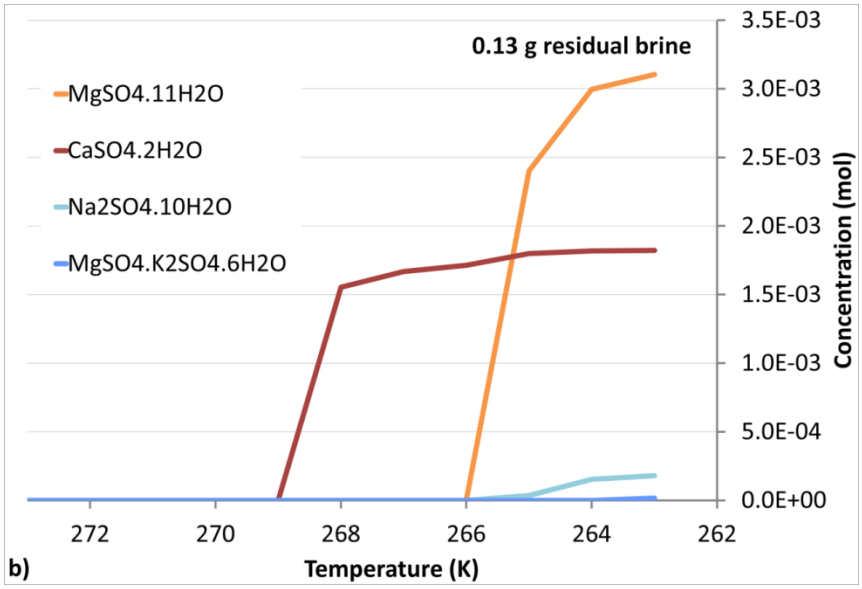

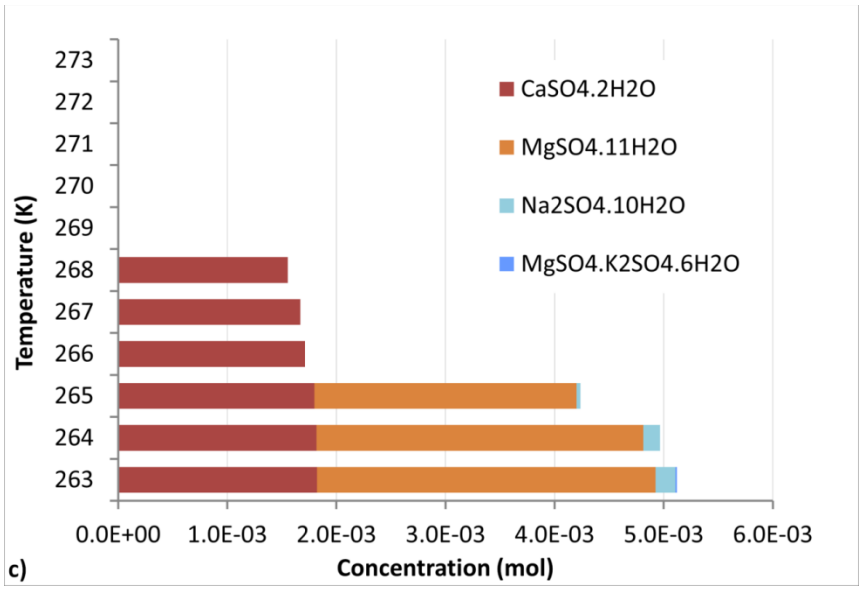

Fig. 18: Simulated brine evolution a) and precipitating salts b) and c) for the *water scenario* during freezing at 500 bars.

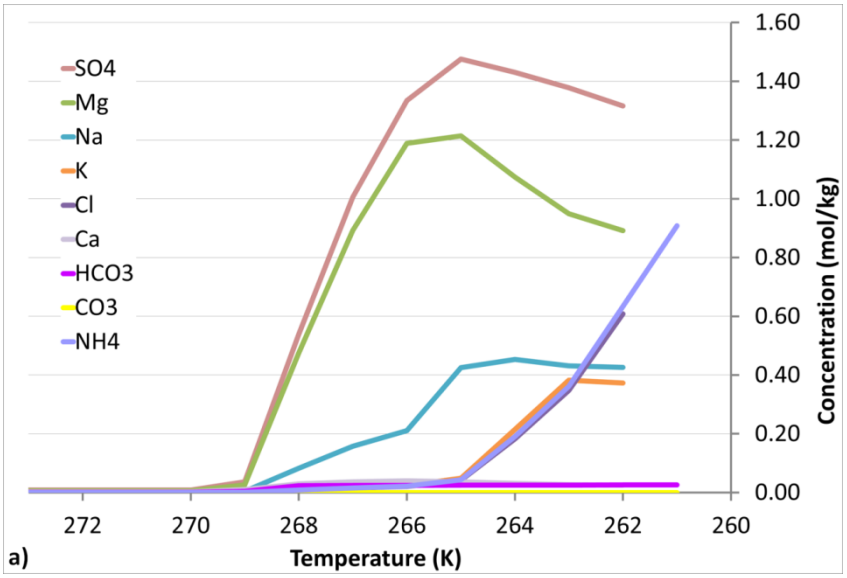

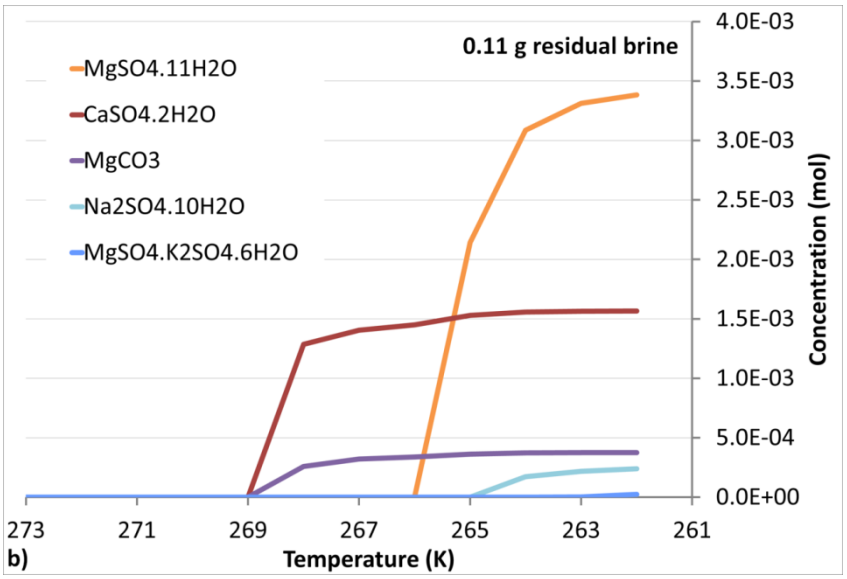

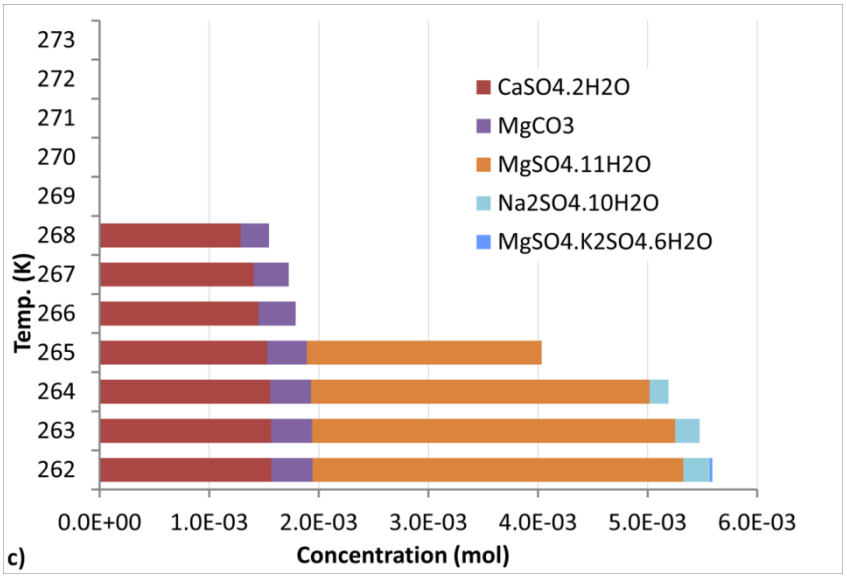

Fig. 19: Simulated brine evolution a) and precipitating salts b) and c) for the *NH_4-CO_2 scenario* during freezing at 500 bars with NH4=0.0001 mol/kg, pCO2=0.02 and carbon alkalinity=0.002.

Evaporation output

The advanced brine evolution during evaporation is diagrammed in Fig. 20 for the water scenario and in Fig. 21 for the NH_4-CO_2 scenario. During evaporation the salinity of the brines raises to 554 g/kg for the water scenario and 758 g/kg for the NH_4-CO_2 scenario. Both scenarios differ significantly in brine evolution and precipitating salts.

The residual brine in the water scenario is highly dominated by Cl as the major anion and Mg as the major cation. While the freezing run results in the enrichment of all ions, the evaporation leads to a depletion of the brine in Na, K, Ca and SO_4, accompanied by the precipitation of Ca-, Mg-, Na- and K-Mg-sulphates (gypsum, picromerite, epsomite, bloedite, anhydrite), as well as Na-, K-, Mg- and K-Mg-chlorides (halite, sylvite, carnallite, kieserite, bischofite) (see Figs. 20b and c).

The residual brine in the NH_4-CO_2 scenario is dominated by the highly enriched NH_4 cation, followed by moderate concentrations of Mg > Na > K, which are only minor enriched during the evaporation process. Calcium is depleted by the early starting precipitation of gypsum. The Cl to SO_4 ratio is at 0.7 over a wide range with Cl exceeding temporarily, but subsequently being consumed by late precipitating NH_4Cl so that SO_4 is the dominating anion in the residual brine (Fig. 21a). The sequence of precipitating sulphates (gypsum, picromerite, epsomite, bloedite) is comparable to the water scenario (Fig. 21b and c). Differences induced by the addition of ammonium and carbonate occur in the precipitation of ammonium chloride instead of Na-, K- and Mg-chlorides and in the additional phases ammonium sulphate and magnesite.

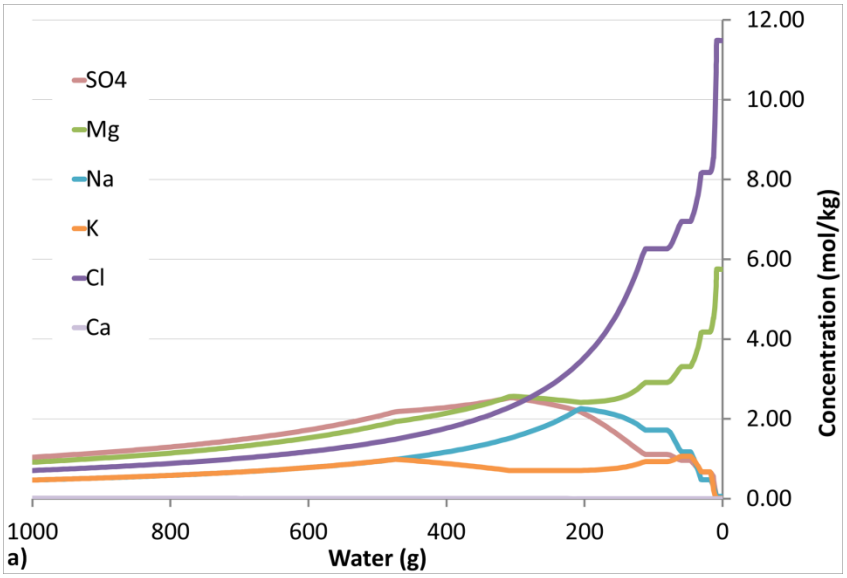

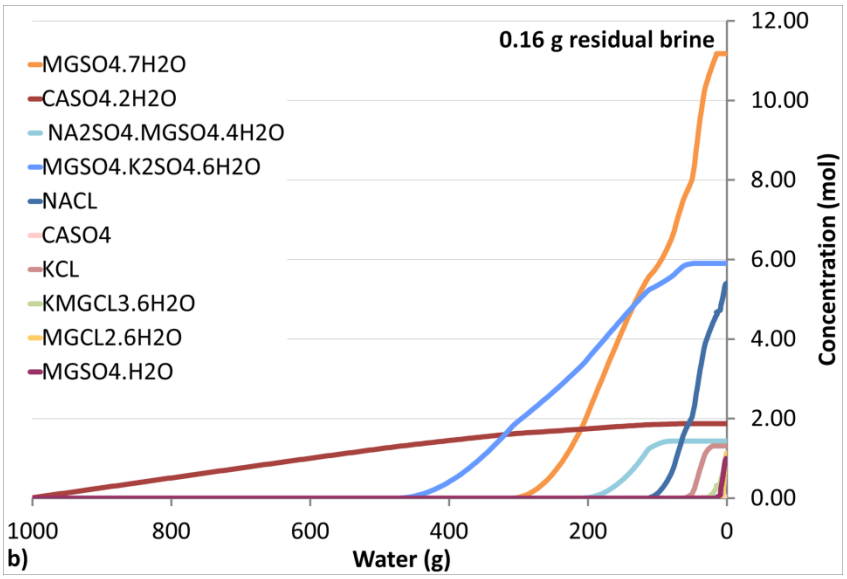

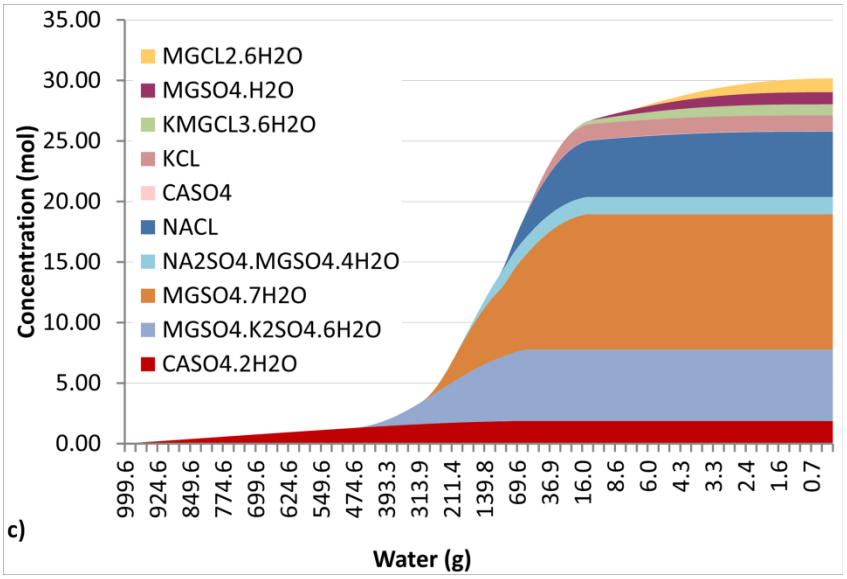

Fig. 20: Simulated brine evolution a) and precipitating salts b) and c) for the water scenario during evaporation at 0.1 bars and 293 K. The x-axis in Fig. c) is scaled non-linear in order to emphasize the preciptating phases near dryness.

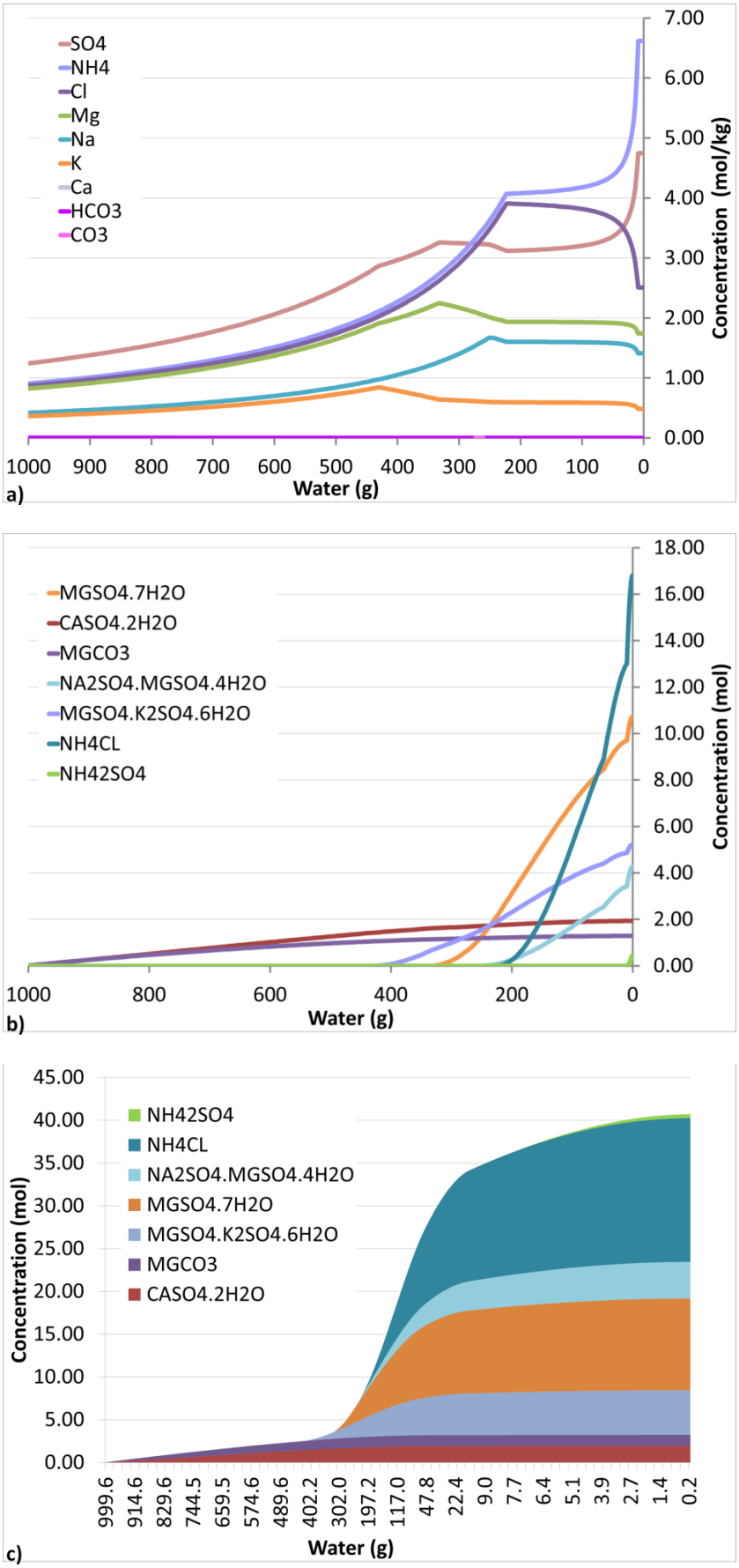

Fig. 21: Simulated brine evolution a) and precipitating salts b) and c) for the NH_4-CO_2 scenario during evaporation at 0.1 bars and 293 K. The x-axis in Fig. c) is scaled non-linear in order to emphasize the preciptating phases near dryness.

6 Implications for Ceres and icy bodies

The experiments and modelling in this work assume that Ceres was warm enough to drive internal hydrothermal leaching of a rocky CM core with subsequent freezing from outside as suggested by thermal evolution models by Castillo-Rogez & McCord (2010). Differentiation into rock, ice and liquid on small bodies like Ceres, which are assumed to have accreted a mixture of ice and CM carbonaceous chondrite material leads to the evolution of high salinity brines (~550–750 g/kg) in the outer shell, as explored in this work

During freezing Mg-sulphate (meridianiite), Na-sulphate (mirabilite) and Mg-K-sulphate (picromerite) precipitate, as well as magnesite if carbonate anions are present. But the fractionation process of precipitating salts in a freezing slurry ocean under low gravity conditions is not well understood. It can be assumed that some part of the salts precipitate enclosed in the ice together with brine pockets and another part stays in suspension. Depending on the viscosity of the underlying slurry ocean a layered sedimentation of the precipitated minerals or a retention within the suspension is imaginable (Fig. 22).

For the escape of the brine into space two different scenarios are imaginable: First, instantaneous sublimation of the brines reaching the surface by impact triggered processes, which forms the so called “faculae” as seen by spacecraft imagery (e.g., Nathues et al. 2015) and for which several cryoclastic depositional processes are investigated by Ruesch et al. (2018). Second, gradual evaporation through the regolith forming a sequence of caliche layers (see Fig. 23).

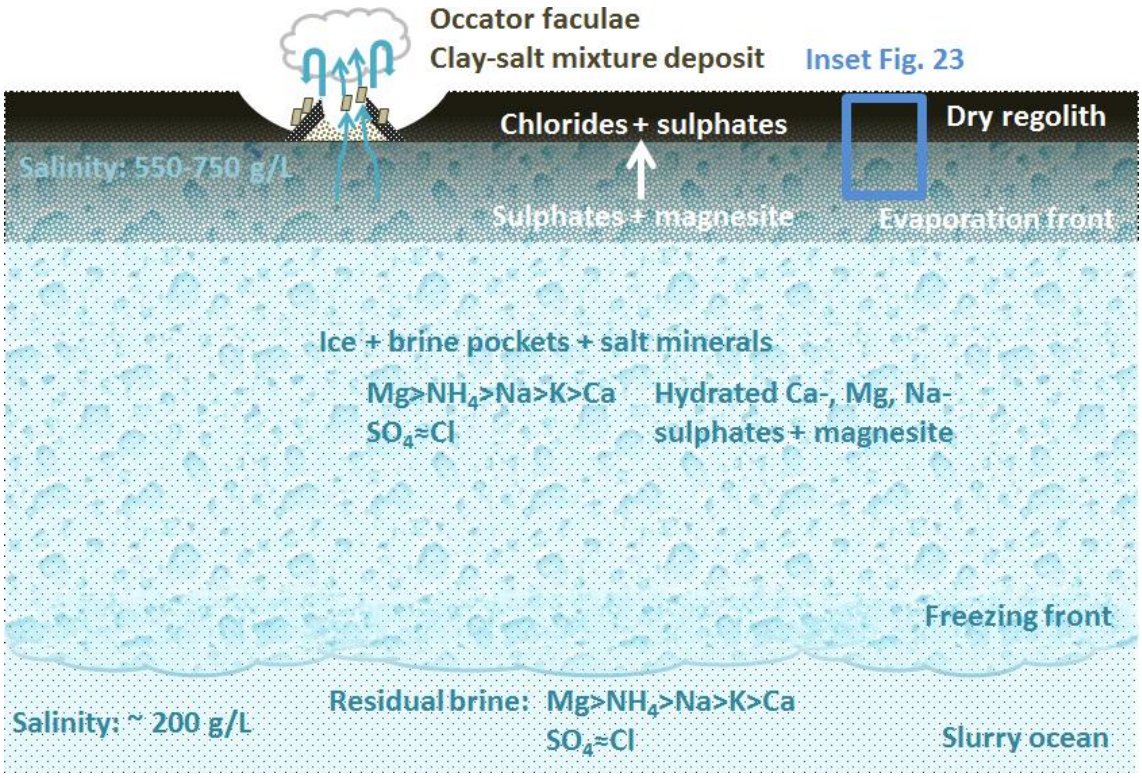

Fig. 22: Concept of the freezing slurry ocean in Ceres' interior containing brine pockets and precipitated sulphates, chlorides and carbonate. Brines and ice evaporate gradually through the regolith leaving behind caliche layers. In Occator crater instantanious sublimation of the brines forms faculae.

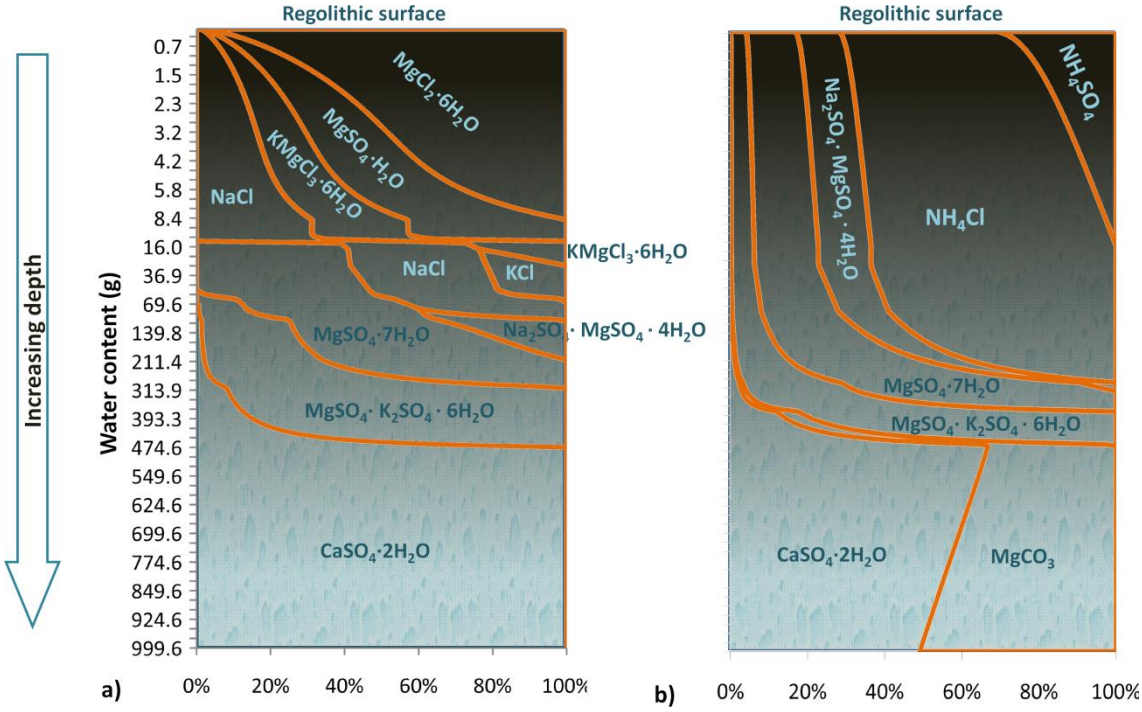

Fig. 23: Precipitating salts by gradual evaporation through the regolith for a) the water scenario and for b) the NH_4-CO_2 scenario. Both scenarios were simulated at 0.1 bar and 293 K (see section 5) due to limitations of the model.

The modelling results for the *water scenario* in this work are in principal agreement with FREZCHEM simulations for freezing of chondritic brines for Europa's ocean by Kargel et al. (2000). These simulations reach the eutectic temperature at 237 K, which is much lower than in this work, due to much higher Na and Cl concentrations assumed in the initial brine. These authors result in brines highly enriched in Cl, which finally dominates over SO_4. In the final brine composition the anions occur in the order Mg > Na > Ca (K is not regarded in this system). The precipitating salts in the work by Kargel et al. (2001) are Ca-, Mg- and Na-sulphates, as well as Na- and Mg-chlorides.

Regarding the present work and that of Kargel (1991) and Kargel et al. (2001), it is inevitable that if Ceres accreted CM material, sulphates precipitated throughout the outer shell. But they could not unambiguously be identified on Ceres' surface yet by remote sensing. Nathues et al. (2015) found indications of hydrated sulphates in Occator's bright spots based on spectral slopes in colour filter spectra, which are ambiguous. Other authors found indications of anhydrous sulphates (Bu et al. 2017) or S and SO_2 frost (Hendrix et al. 2017). VIR investigations rule out hydrated sulphates (contents above 2-3%) by the lack of H_2O absorption bands (De Sanctis et al. 2016). Although, this is not an indicator that sulphates are absent, because Bu et al. (2017) show that sulphates dehydrate under Ceres' surface conditions, which would explain the absence of their H_2O absorptions. The S-O overtones of sulphates spectrally detectable between 4 and 5 µm (Cloutis et al. 2006) are an indicator which is independent of the hydration state. However, this wavelength region was not analysed yet in the VIR data most probably because of the influence of thermal emission in this wavelength region.

While the detected Ca-Mg-carbonates on Ceres' surface, as well as NH_4Cl as a possible ammonium bearing phase (De Sanctis et al. 2016) are consistent with the precipitates during freezing and evaporation of CC leachates assuming the *NH_4-CO_2 scenario*, the formation of Na_2CO_3 (natrite) as detected on Ceres in Occator and on Ahuna Mons (De Sanctis et al. 2016, Zambon et al. 2017) cannot readily be explained by the simulations in this work. The highly NaCl concentrated residual brine may have reacted with NH_4 and CO_2 to form Na_2CO_3, which is the Solvay-Process being described on Ceres (De Sanctis et al. 2016). This process needs temperatures around 200°C, which could be generated by impact heating, but specific exploration of this scenario is needed. Alternatively Zolotov (2017) reconstructed a brine composition to precipitate natrite, which prerequisites a HCO_3 to Cl ratio above unity whereas simulations in the present work regard much lower HCO_3 contents, which may be chosen too low as sea water alkalinity was assumed. Apart from that Zolotov (2017) does not include SO_4 and Mg, K, Ca in the system as it would be realistic for a CC leachate.

Castillo-Rogez et al. (2018) reconstruct alkaline, low hydrogen fugacity conditions on Ceres mainly inferred from the presence of dolomite and ammonium bearing species as detected by Dawn VIR observations (De Sanctis et al. 2015, 2016). They derive chondritic brines by altering CM/CI material (for which the mineralogical composition is not given) simulative using PhreeqC and Geochemists Workbench, but in contrary to the present experiments they do not result in SO_4 being contained in the brine, possibly because sulphate minerals were not included in the CM/CI input assemblage. Furthermore, Castillo-Rogez et al. (2018) also simulated subsequent freezing of the brine using FREZCHEM, consequently resulting in a sulphate-free mineral assemblage of Ca-, Mg-, Na- and NH_4-carbonates, as well as KCl, NaCl and NH_4Cl. But the authors state that "if their presence [of sulphates] is confirmed on Ceres' surface, then a different set of conditions should be considered".

The other way round – if sulphates on Ceres can really be ruled out the general remaining question is on the origin of sulphates in the CM chondrites. If they condensed in the solar nebular they should be present on Ceres, but if they are a product of parent body alteration – how does this body differ from Ceres to bear oxidizing conditions?

7 Outlook

This work represents a starting point on the controlled hydrothermal leaching of chondritic meteorites and the further evolution of resulting brines as they may occur on icy bodies in the solar system and be important for cryovolcanic processes.

Next steps in this direction could be the controlled adding of CO_2, NH_4 and other cometary volatiles, as well as oxygen buffers during leaching including control of carbon alkalinity in the liquids. Furthermore a better understanding on precipitating mineral phases and brine evolution is needed during freezing and evaporation if both the carbonate and sulphate anion co-occur in the chondritic brine, especially in the case of sublimation against space environment (low temperature and vacuum conditions).

The remote search for sulphates on Ceres should be revisited using a better set of unambiguous spectral characteristics. But this may be difficult to realize due to influence of thermal emission in the wavelength region longward of 4 μm, where S-O vibrations may be characteristic.

To track mineralogical changes of the leached residual meteorite powders a more intensive investigation by advanced XRD and electron beam techniques could be useful, especially for the fate of iron, which may possibly have undergone some redistribution process causing the changes in the reflectance spectra.

8 References

AstDyS 2011. AstDyS-2 Ceres Synthetic Proper Orbital Elements. Department of Mathematics, University of Pisa, Italy. Archived from the original on 5 October 2011. Retrieved 1 October 2011.

Barber, D.J., 1981. Matrix phyllosilicates and associated minerals in C2M carbonaceous chondrites. Geochimica et Cosmochimica Acta 45, pp. 945–970. doi:10.1016/0016-7037(81)90120-4

Bockmon, E.E., Dickson, A.G., 2015. An inter-laboratory comparison assessing the quality of seawater carbon dioxide measurements. Marine Chemistry 171, pp. 36–43. doi:10.1016/j.marchem.2015.02.002

Bischoff, A., Ebert, S., Metzler, K., Lentfort, S., 2017. Breccia classification of CM chondrites. Annual meteoritical society meeting, abstract 6089.

Bland, P.A., Cressey, G., Menzies, O.N., 2004. Modal mineralogy of carbonaceous chondrites by X-ray diffraction and Mössbauer spectroscopy. Meteorit. Planet. Sci. 39 (1), pp 3–16. doi:10.1111/j.1945-5100.2004.tb00046.x

Britt, D.T., Consolmagno, S.J., 2003. Stony meteorite porosities and densities: A review of the data through 2001. Meteorit. Planet. Sci. 38 (8), pp. 1161–1180. doi:10.1111/j.1945-5100.2003.tb00305.x

Castillo-Rogez, J.C., Neveu, M., McSween, H.Y., Fu, R., Toplis, M., Prettyman, T., 2018. Insights into Ceres's Evolution from Surface Composition. Meteorit. Planet. Sci. 53 (9), pp. 1820–1843. doi:10.1111/maps.13181

Castillo-Rogez, J.C., McCord, T.B., 2010. Ceres' evolution and present state constrained by shape data. Icarus 205 (2), pp. 443–459. doi:10.1016/j.icarus.2009.04.008

Deer, W. A., Howie, R. A., Zussman, J., 1992. An introduction to the rock-forming minerals. - 2nd ed. Pearson, Harlow (England), 696 pp.

DeMeo, F.E., Carry, B., 2014. Solar System evolution from compositional mapping of the asteroid belt. Nature 505 (7485), pp. 629–634. doi:10.1038/nature12908

De Sanctis, M.C., Ammannito, E., Raponi, A., Marchi, S., McCord, T.B., McSween, H.Y., Capaccioni, F., Capria, M.T., Carrozzo, F.G., Ciarniello, M., Longobardo, A., Tosi, F., Fonte, S., Formisano, M., Frigeri, A., Giardino, M., Magni, G., Palomba, E., Turrini, D., Zambon, F., Combe, J.-P., Feldman, W., Jaumann, R., McFadden, L.A., Pieters, C.M., Prettyman, T., Toplis, M., Raymond, C.A., Russell, C.T., 2015. Ammoniated phyllosilicates with a likely outer Solar System origin on (1) Ceres. Nature 528 (7581), pp. 241–244. doi:10.1038/nature16172

De Sanctis, M.C., Raponi, A., Ammannito, E., Ciarniello, M., Toplis, M.J., McSween, H.Y., Castillo-Rogez, J.C., Ehlmann, B.L., Carrozzo, F.G., Marchi, S., Tosi, F., Zambon, F., Capaccioni, F., Capria, M.T., Fonte, S., Formisano, M., Frigeri, A., Giardino, M., Longobardo, A., Magni, G., Palomba, E., McFadden, L.A., Pieters, C.M., Jaumann, R., Schenk, P., Mugnuolo, R., Raymond, C.A., Russell, C.T., 2016. Bright carbonate deposits as evidence of aqueous alteration on (1) Ceres. Nature 536 (7614), pp. 54–57. doi:10.1038/nature18290

Dunn, T.L., Cressey, G., McSween Jr, Harry Y., McCoy, T.J., 2010. Analysis of ordinary chondrites using powder X-ray diffraction: 1. Modal mineral abundances. Meteoritics and Planetary Science. doi:10.1111/j.1945-5100.2009.01011.x

Dreibus, G., Spettel, B., Wänke, H., 1979. Halogens in meteorites and their primordial abundance. Physics and chemistry of the Earth 11, pp. 33–38. doi:10.1016/0079-1946(79)90005-3

Fries, M., Messenger, S., Steele, A., Zolensky, M.E., 2013. Do we alredy have samples of Ceres? H chondrite halites and the Ceres-Hebe Link. 76th Annual meteoritical society meeting, abstract 5266.

Hayne, P.O., Aharonson, O., 2015. Thermal stability of ice on Ceres with rough topography. J. Geophys. Res. Planets 120 (9), pp. 1567–1584. doi:10.1002/2015JE004887

Howard, K.T., Benedix, G.K., Bland, P.A., Cressey, G., 2011. Modal mineralogy of CM chondrites by X-ray diffraction (PSD-XRD): Part 2. Degree, nature and settings of

aqueous alteration. Geochimica et Cosmochimica Acta 75 (10), pp. 2735–2751. doi:10.1016/j.gca.2011.02.021

Johnson, C.A., Prinz, M., 1993. Carbonate compositions in CM and CI chondrites and implications for aqueous alteration. Geochim cosmochim acta 57 (12), pp. 2843–2852. doi:10.1016/0016-7037(93)90393-B

Jones, R.H., McCubbin, F.M., Guan, Y., 2016. Phosphate minerals in the H group of ordinary chondrites, and fluid activity recorded by apatite heterogeneity in the Zag H3-6 regolith breccia. American Mineralogist 101 (11), pp. 2452–2467. doi:10.2138/am-2016-5728

Kargel, J.S., 1991. Brine volcanism and the interior structures of asteroids and icy satellites. Icarus 94 (2), pp. 368–390. doi:10.1016/0019-1035(91)90235-L

Kargel, J., 2000. Europa's Crust and Ocean: Origin, Composition, and the Prospects for Life. Icarus 148 (1), pp. 226–265. doi:10.1006/icar.2000.6471

Koslowski, G., 1986. 8.2 Salinity of sea ice, in: Sündermann, J. (Ed.), Numerical data and functional relationships in science and technology. Group 5: Geophysics and space research, 3c. Landolt-Börnstein - Group V Geophysics. Springer, Berlin, Heidelberg, pp. 170–171.

Kattenhorn, S.A., Prockter, L.M., 2014. Evidence for subduction in the ice shell of Europa. Nature Geosci. 7 (10), pp. 762–767. doi:10.1038/ngeo2245

Kivelson, M.G., Khurana, K.K., Russell, C.T., Volwerk, M., Walker, R.J., Zimmer, C., 2000. Galileo Magnetometer Measurements: A Stronger Case for a Subsurface Ocean at EuropaGalileo Magnetometer Measurements: A Stronger Case for a Subsurface Ocean at Europa. Science 289 (5483), pp. 1340–1343. doi:10.1126/science.289.5483.1340

Kuskov, O.L., Kronrod, V.A., 2005. Internal structure of Europa and Callisto. Icarus 177 (2), pp. 550–569. doi:10.1016/j.icarus.2005.04.014

Marion, G.M., Mironenko, M.V., Roberts, M.W., 2010. FREZCHEM: A geochemical model for cold aqueous solutions. Computers & Geosciences 36 (1), pp. 10–15. doi:10.1016/j.cageo.2009.06.004

McCord, T.B., Sotin, C., 2005. Ceres: Evolution and current state. J. Geophys. Res. 110 (E5), pp. 1–14. doi:10.1029/2004JE002244

McKinnon, W.B., Prialnik, D., Stern, S.A., Coradini, A., 2008. Structure and Evolution of Kuiper Belt Objects and Dwarf Planets. The Solar System beyond Neptune. The University of Arizona Press, 30 pp.

Müller, W.F., Kurat, G., Kracher, A., 1979. Chemical and crystallographic study of cronstedtite in the matrix of the Cochabamb CM2 carbonaceous chondrite. Tschermaks Min. Petr. Mitt. 26, pp. 293–304.

R. T. Pappalardo, M. J. S. Belton, H. H. Breneman, M. H. Carr, C. R. Chapman, G. C. Collins, T. Denk, S. Fagents, P. E. Geissler, B. Giese, R. Greeley, R. Greenberg, J. W. Head, P. Helfenstein, G. Hoppa, S. D. Kadel, K. P. Klaasen, J. E. Klemaszewski, K. Magee, A. S. McEwen, J. M. Moore, W. B. Moore, G. Neukum, C. B. Phillips, L. M. Prockter, G. Schubert, D. A. Senske, R. J. Sullivan, B. R. Tufts, E. P. Turtle, R. Wagner, K. K. Williams, 1999. Does Europa have a subsurface ocean? Evaluation of the geological evidence. JGR 104 (E10), pp. 24015–24055. doi:10.1029/1998JE000628

Park, R.S., Konopliv, A.S., Bills, B.G., Rambaux, N., Castillo-Rogez, J.C., Raymond, C.A., Vaughan, A.T., Ermakov, A.I., Zuber, M.T., Fu, R.R., Toplis, M.J., Russell, C.T., Nathues, A., Preusker, F., 2016. A partially differentiated interior for (1) Ceres deduced from its gravity field and shape. Nature 537, pp. 515–517. doi:10.1038/nature18955

Rubin, A.E., Trigo-Rodríguez, J.M., Huber, H., Wasson, J.T., 2007. Progressive aqueous alteration of CM carbonaceous chondrites. Geochimica et Cosmochimica Acta 71 (9), pp. 2361–2382. doi:10.1016/j.gca.2007.02.008

Ruesch, O., Platz, T., Schenk, P., McFadden, L.A., Castillo-Rogez, J.C., Quick, L.C., Byrne, S., Preusker, F., O'Brien, D.P., Schmedemann, N., Williams, D.A., Li, J.-Y., Bland, M.T., Hiesinger, H., Kneissl, T., Neesemann, A., Schaefer, M., Pasckert, J.H., Schmidt, B.E., Buczkowski, D.L., Sykes, M.V., Nathues, A., Roatsch, T., Hoffmann, M., Raymond, C.A., Russell, C.T., 2016. Cryovolcanism on Ceres. Science 353 (6303). doi:10.1126/science.aaf4286

Ruesch, O., Quick, L.C., Landis, M.E., Sori, M.M., Čadek, O., Brož, P., Otto, K.A., Bland, M.T., Byrne, S., Castillo-Rogez, J.C., Hiesinger, H., Jaumann, R., Krohn, K., McFadden, L.A., Nathues, A., Neesemann, A., Preusker, F., Roatsch, T., Schenk, P.M., Scully, J.E.C., Sykes, M.V., Williams, D.A., Raymond, C.A., Russell, C.T., 2018. Bright carbonate surfaces on Ceres as remnants of salt-rich water fountains. Icarus. doi:10.1016/j.icarus.2018.01.022

Russell, C.T., Raymond, C.A., Ammannito, E., Buczkowski, D.L., Sanctis, M.C. de, Hiesinger, H., Jaumann, R., Konopliv, A.S., McSween, H.Y., Nathues, A., Park, R.S., Pieters, C.M., Prettyman, T.H., McCord, T.B., McFadden, L.A., Mottola, S., Zuber, M.T., Joy, S.P., Polanskey, C., Rayman, M.D., Castillo-Rogez, J.C., Chi, P.J., Combe, J.P., Ermakov, A., Fu, R.R., Hoffmann, M., Jia, Y.D., King, S.D., Lawrence, D.J., Li, J.-Y., Marchi, S., Preusker, F., Roatsch, T., Ruesch, O., Schenk, P., Villarreal, M.N., Yamashita, N., 2016. Dawn arrives at Ceres: Exploration of a small, volatile-rich world. Science 353 (6303), pp. 1008–1010. doi:10.1126/science.aaf4219

Russell, S.S., King, A.J., Schofield, P.F., Verchovsky, A.B., Abernethy, F., Grady, M.M. The Jbilet Winselwan carbonaceous chondrite 1. mineralogy and petrology: strengthening the link between CM and CO meteorites? Annual meteoritical society meeting, abstract 5253.

Schäfer, M., Schäfer, T., Izawa, M.R.M., Cloutis, E.A., Schröder, S.E., Roatsch, T., Preusker, F., Stephan, K., Matz, K.-D., Raymond, C.A., Russell, C.T., 2018. Ceres' spectral link to carbonaceous chondrites – Analysis of the dark background materials. Meteorit. Planet. Sci. 53 (9), pp. 1925–1945. doi:10.1111/maps.13079

Sievert, M., 2018. Mineralogie und Geochemie des kohligen Chondriten Jbilet. BSc thesis, TU Clausthal, in preparation.

Tosi, F., De Sanctis, M. C., Ammannito, E., Capaccioni, F., Zambon, F., Raponi, A., Russell, C.T., 2015. Surface Temperature of Dwarf planet Ceres: Preliminary results from Dawn. Lunar and Planetary Sci. Conf., abstract 1745.

Zolensky, M. E., Fries, M., Bodnar, Robert, J., Yurimoto, H., Itoh, S., Steele, A., Mikouchi, T., Hagiya, K. Ohsumi, K., Le, L. Rahman, Z., 2013. Early Solar System Cryovolcanics in the Laboratory. 76th Annual meteoritical society meeting, abstract 5200.

Zolensky, M. E., Mikouchi, T., Hagiya, K., Ohsumi, K., Komatsu, M., Chan, Q. H. S., Le, L., Kring, D., Cato, M., Fagan, A. L., Gross, J., Tanaka, A., Takegawa, D., Hoshikawa, T., Yoshida, T., Sawa, N., 2016. Unique view of C asteroid regolith from the Jbilet Winselwan CM chondrite. Lunar and Planetary Sci. Conf., abstract 2148.

9 Appendix

Appendix A: Leachate composition

Appendix B: Blanks and replicability

Appendix C: X-ray diffractograms

Appendix D: Visible and infrared reflectance spectra

Appendix E: Input parameter files for the FREZCHEM model

Appendix A: Leachate composition

Tab. A1: Leachate composition of Murchison

Murchison						
Alteration time (days)	2	5	12	50	100	200
Rock R (g)	0.111	0.112	0.112	0.0725	0.111	0.111
Water W (g)	10.977	10.971	11.042	7.205	10.981	10.961
W/R	98.712	97.776	98.767	99.372	98.929	98.657
Loss of water W_L [1] (g)	0.013	0.085	0.083	0.313	0.590	1.904
Kations in ppm						
Na	18.89	21.03	21.45	23.00	23.24	22.65
NH_4	< 0.05	< 0.05	< 0.05	< 0.05	< 0.05	1.51
K	3.61	4.33	4.13	4.29	4.23	4.41
Ca	56.52	63.22	70.88	86.97	92.50	92.49
Mg	34.60	35.13	56.35	124.77	137.53	145.61
Li	< 0.1	< 0.1	< 0.1	< 0.1	< 0.1	< 0.1
Al	< 0.5	< 0.5	< 0.5	< 0.5	< 0.5	< 0.5
P	< 5	< 5	< 5	< 5	< 5	< 5
Fe	< 5	< 5	< 5	< 5	< 5	< 5
Mn	< 0.05	< 0.05	0.12	0.61	0.51	0.58
Cu	0.027	< 0.01	0.013	< 0.01	< 0.01	< 0.01
Rb	< 0.01	0.012	0.014	0.015	0.016	0.017
Sr	0.039	0.044	0.054	0.78	0.76	0.86
Cd	< 0.001	< 0.001	< 0.001	< 0.001	< 0.001	< 0.001
Cs	< 0.002	< 0.002	< 0.002	< 0.002	< 0.002	< 0.002
Anions in ppm						
Cl	1.05	1.47	1.56	2.11	3.08	2.80
Br	< 0.025	< 0.025	< 0.025	< 0.025	< 0.025	< 0.025
SO_4	195.74	251.63	367.28	752.27	745.60	802.01
Σ	310.48	376.87	521.85	994.82	1007.47	1072.94
% of initial rock mass	3.07	3.69	5.14	9.89	9.96	10.59

[1] All final anion and cation concentrations are corrected for loss of water by multiplying with $W_L = \frac{W - \Delta W}{W}$.

Tab. A2: Leachate composition of Jbilet

Jbilet						
Alteration time (days)	2	5	12	50	100	200
Rock R (g)	0.111	0.113	0.112	0.112	0.113	0.112
Water W (g)	11.282	11.039	11.050	10.962	10.967	10.953
W/R	101.911	97.950	98.573	98.136	96.796	97.968
Loss of water W_L (g)	0.029	0.052	0.098	0.266	0.973	1.071
Kations in ppm						
Na	14.24	16.85	17.87	18.63	20.47	20.34
NH_4	< 0.05	< 0.05	< 0.05	< 0.05	< 0.05	< 0.05
K	2.11	2.84	3.11	3.07	3.65	3.10
Ca	20.91	30.43	40.36	60.32	79.78	80.00
Mg	8.06	10.87	12.71	19.31	44.81	49.79
Li	< 0.1	< 0.1	< 0.1	< 0.1	< 0.1	< 0.1
Al	< 0.5	< 0.5	< 0.5	< 0.5	< 0.5	< 0.5
P	< 5	< 5	< 5	< 5	< 5	< 5
Fe	< 5	< 5	< 5	< 5	< 5	< 5
Mn	< 0.05	< 0.05	< 0.05	< 0.05	< 0.05	< 0.05
Cu	< 0.01	< 0.01	< 0.01	< 0.01	< 0.01	< 0.01
Rb	< 0.01	< 0.01	< 0.01	< 0.01	< 0.01	< 0.01
Sr	0.13	0.19	0.22	0.28	0.39	0.42
Cd	< 0.001	< 0.001	< 0.001	< 0.001	< 0.001	< 0.001
Cs	< 0.002	< 0.002	< 0.002	< 0.002	< 0.002	< 0.002
Anions in ppm						
Cl	15.33	16.38	16.76	16.65	18.28	16.59
Br	0.27	0.27	0.28	0.28	0.29	0.30
SO_4	44.91	73.95	126.03	223.74	380.52	398.04
Σ	105.96	151.78	217.34	342.28	548.19	568.49
% of initial rock mass	1.08	1.49	2.14	3.35	5.32	5.56

Tab. A3: Leachate composition of Zag

Zag						
Alteration time (days)	2	5	12	50	100	200
Rock R (g)	0.110	0.112	0.112	0.113	0.113	0.111
Water W (g)	11.067	11.026	11.031	10.953	10.975	10.965
W/R	100.242	98.186	98.668	97.356	96.777	98.961
Loss of water W_L (g)	0.026	0.076	0.328	0.322	0.627	1.075
Kations in ppm						
Na	5.22	6.91	7.88	10.13	10.35	11.05
NH_4	< 0.05	< 0.05	< 0.05	< 0.05	< 0.05	< 0.05
K	0.59	0.76	0.96	1.18	1.21	1.38
Ca	0.95	1.09	0.81	0.42	0.35	0.28
Mg	2.51	1.70	0.95	0.63	0.60	< 0.5
Li	< 0.1	< 0.1	< 0.1	< 0.1	< 0.1	< 0.1
Al	1.46	1.81	1.77	1.28	0.98	0.87
P	8.41	8.21	8.41	6.85	6.54	7.10
Fe	< 5	< 5	< 5	< 5	< 5	< 5
Mn	< 0.05	< 0.05	< 0.05	< 0.05	< 0.05	< 0.05
Cu	< 0.01	< 0.01	< 0.01	< 0.01	< 0.01	< 0.01
Rb	< 0.01	< 0.01	< 0.01	< 0.01	< 0.01	< 0.01
Sr	< 0.005	< 0.005	< 0.005	< 0.005	< 0.005	< 0.005
Cd	< 0.001	< 0.001	< 0.001	< 0.001	< 0.001	< 0.001
Cs	< 0.002	< 0.002	< 0.002	< 0.002	< 0.002	< 0.002
Anions in ppm						
Cl	0.83	0.85	0.86	0.95	0.90	0.84
Br	< 0.025	< 0.025	< 0.025	< 0.025	0.026	0.022
SO_4	4.11	4.62	5.68	6.23	7.47	8.64
PO_4	*	*	*	*	*	*
Σ	24.08	25.95	27.32	27.67	28.43	30.18
% of initial rock mass	0.25	0.26	0.27	0.27	0.27	0.30

*PO_4 peak visible, but not calibrated.

Tab. A4: Leachate composition of NWA 7936

NWA 7936						
Alteration time (days)	2	5	12	50	100	200
Rock R (g)	0.111	0.111	0.111	0.112	0.112	0.114
Water W (g)	10.967	10.997	11.087	10.983	10.976	10.922
W/R	98.444	98.895	99.887	98.410	98.351	96.147
Loss of water W_L (g)	0.027	0.158	0.163	0.280	0.659	1.040
Kations in ppm						
Na	8.44	10.99	12.94	18.66	22.26	26.80
NH_4	< 0.05	< 0.05	< 0.05	< 0.05	< 0.05	< 0.05
K	0.83	0.95	1.22	1.71	1.92	2.63
Ca	2.59	2.05	1.89	1.79	1.20	0.76
Mg	1.37	0.51	< 0.5	< 0.5	< 0.5	< 0.5
Li	< 0.1	< 0.1	< 0.1	< 0.1	< 0.1	< 0.1
Al	1.84	1.89	1.39	1.07	1.04	0.86
P	< 5	< 5	< 5	< 5	< 5	< 5
Fe	< 5	< 5	< 5	< 5	< 5	< 5
Mn	< 0.05	< 0.05	< 0.05	< 0.05	< 0.05	< 0.05
Cu	< 0.01	< 0.01	< 0.01	< 0.01	< 0.01	< 0.01
Rb	< 0.01	< 0.01	< 0.01	< 0.01	< 0.01	< 0.01
Sr	< 0.005	< 0.005	< 0.005	< 0.005	< 0.005	< 0.005
Cd	< 0.001	< 0.001	< 0.001	< 0.001	< 0.001	< 0.001
Cs	< 0.002	< 0.002	< 0.002	< 0.002	< 0.002	< 0.002
Anions in ppm						
Cl	1.05	1.06	1.11	1.39	1.77	1.52
Br	< 0.025	< 0.025	< 0.025	< 0.025	< 0.025	< 0.025
SO_4	14.13	18.24	22.45	29.84	35.18	44.44
Σ	30.25	35.69	41.00	54.46	63.37	77.01
% of initial rock mass	0.30	0.35	0.40	0.54	0.63	0.74

Tab. A5: Leachate composition of NWA 8039

NWA 8039						
Alteration time (days)	2	5	12	50	100	200
Rock R (g)	0.112	0.112	0.111	0.112	0.111	0.110
Water W (g)	11.001	11.093	11.061	10.981	10.996	10.905
W/R	98.219	98.778	99.829	97.692	98.796	99.136
Loss of water W_L (g)	0.012	0.082	0.162	0.280	0.694	1.110
Kations in ppm						
Na	7.22	9.57	10.69	16.45	22.49	28.19
NH_4	< 0.05	< 0.05	< 0.05	"+" not cal.	0.24	"+" not cal.
K	1.01	1.17	1.45	2.29	3.12	3.97
Ca	8.96	8.04	7.76	6.53	4.85	2.64
Mg	1.39	< 0.5	< 0.5	< 0.5	< 0.5	< 0.5
Li	< 0.1	< 0.1	< 0.1	< 0.1	< 0.1	< 0.1
Al	3.41	3.63	3.63	2.67	2.47	3.48
P	< 5	< 5	< 5	< 5	< 5	< 5
Fe	< 5	< 5	< 5	< 5	< 5	< 5
Mn	< 0.05	< 0.05	< 0.05	< 0.05	< 0.05	< 0.05
Cu	< 0.01	< 0.01	< 0.01	< 0.01	< 0.01	< 0.01
Rb	< 0.01	< 0.01	< 0.01	< 0.01	< 0.01	0.011
Sr	0.058	0.054	0.043	0.025	0.013	0.007
Cd	< 0.001	< 0.001	< 0.001	< 0.001	< 0.001	< 0.001
Cs	< 0.002	< 0.002	< 0.002	< 0.002	< 0.002	< 0.002
Anions in ppm						
Cl	2.41	2.89	3.05	2.81	3.32	3.31
Br	< 0.025	< 0.025	< 0.025	< 0.025	< 0.025	0.027
SO_4	14.95	16.44	21.97	33.09	37.35	36.48
Σ	39.41	41.79	48.59	63.84	73.85	78.12
% of initial rock mass	0.38	0.41	0.49	0.63	0.73	0.77

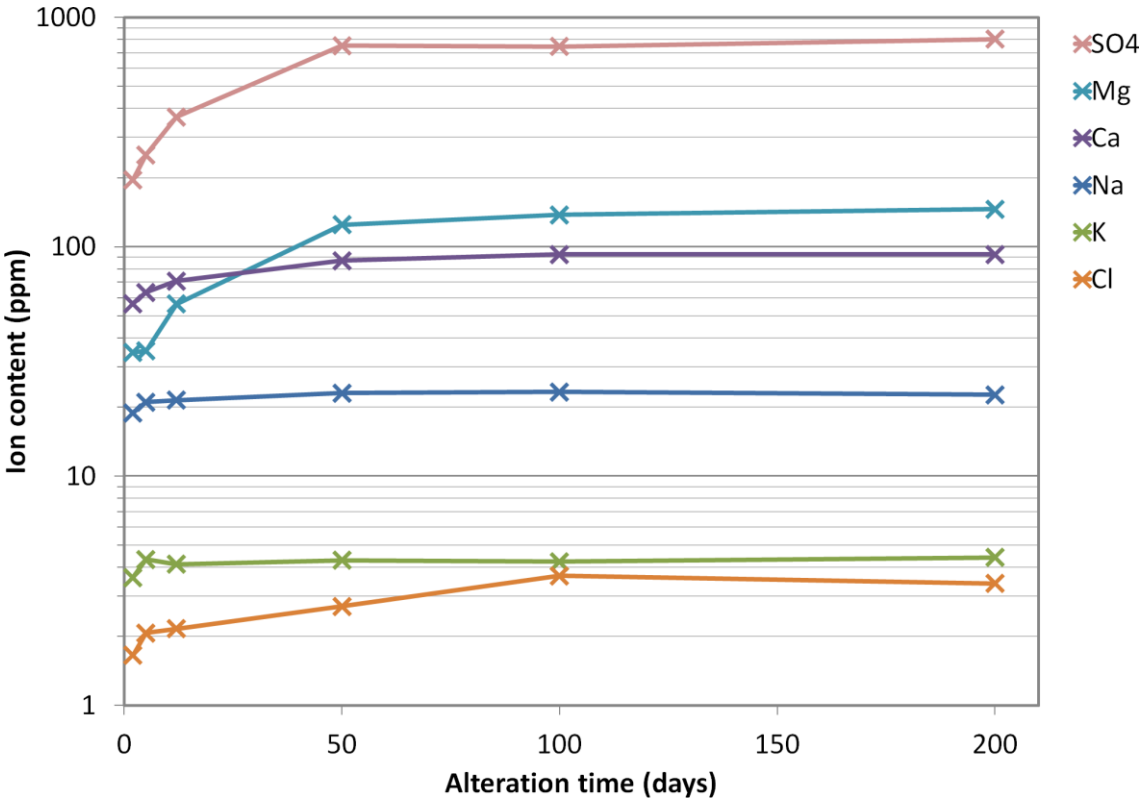

Fig. A1: Ion content of Murchison leachate with alteration time (2, 5, 12, 50, 100, 200 days).

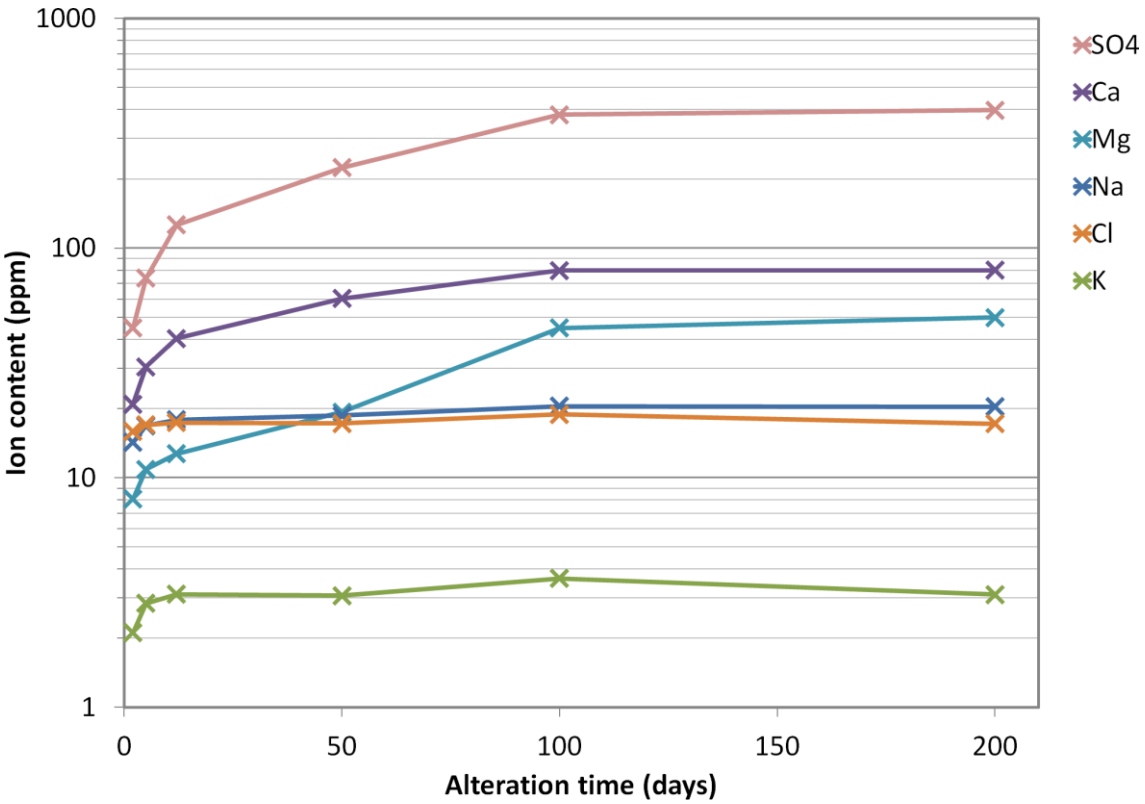

Fig. A2: Ion content of Jbilet leachate with alteration time (2, 5, 12, 50, 100, 200 days).

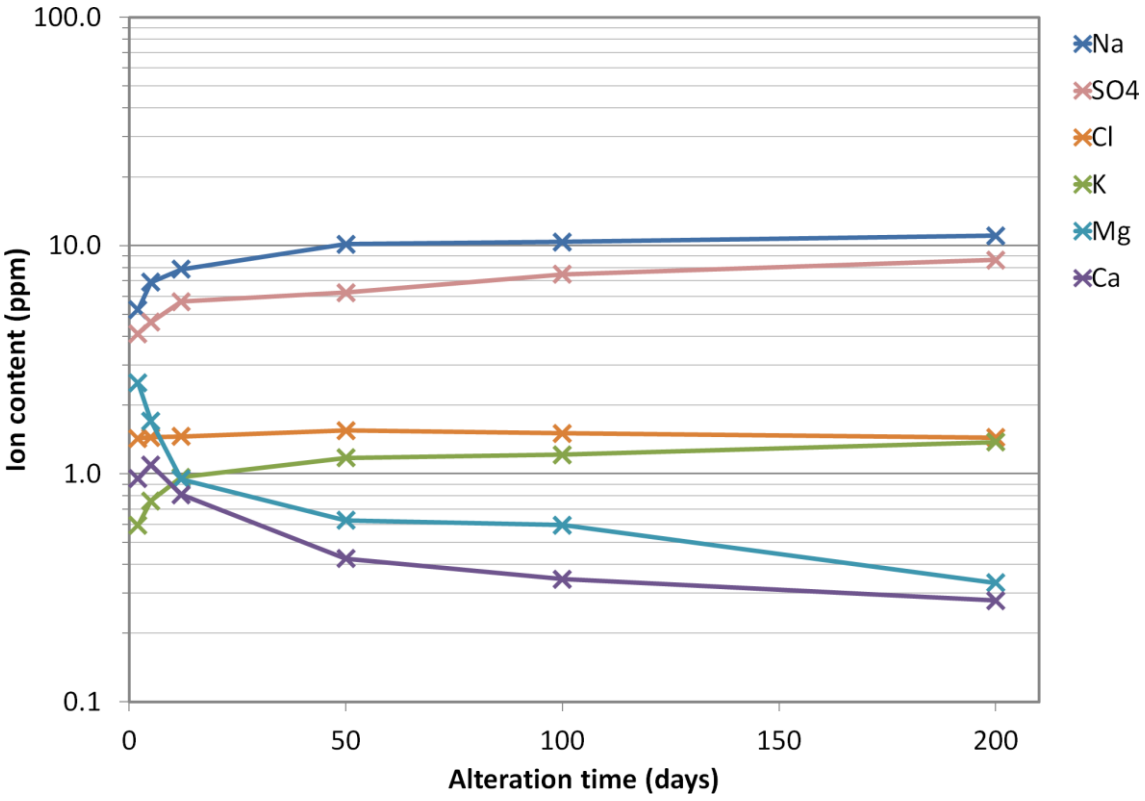

Fig. A3: Ion content of Zag leachate with alteration time (2, 5, 12, 50, 100, 200 days).

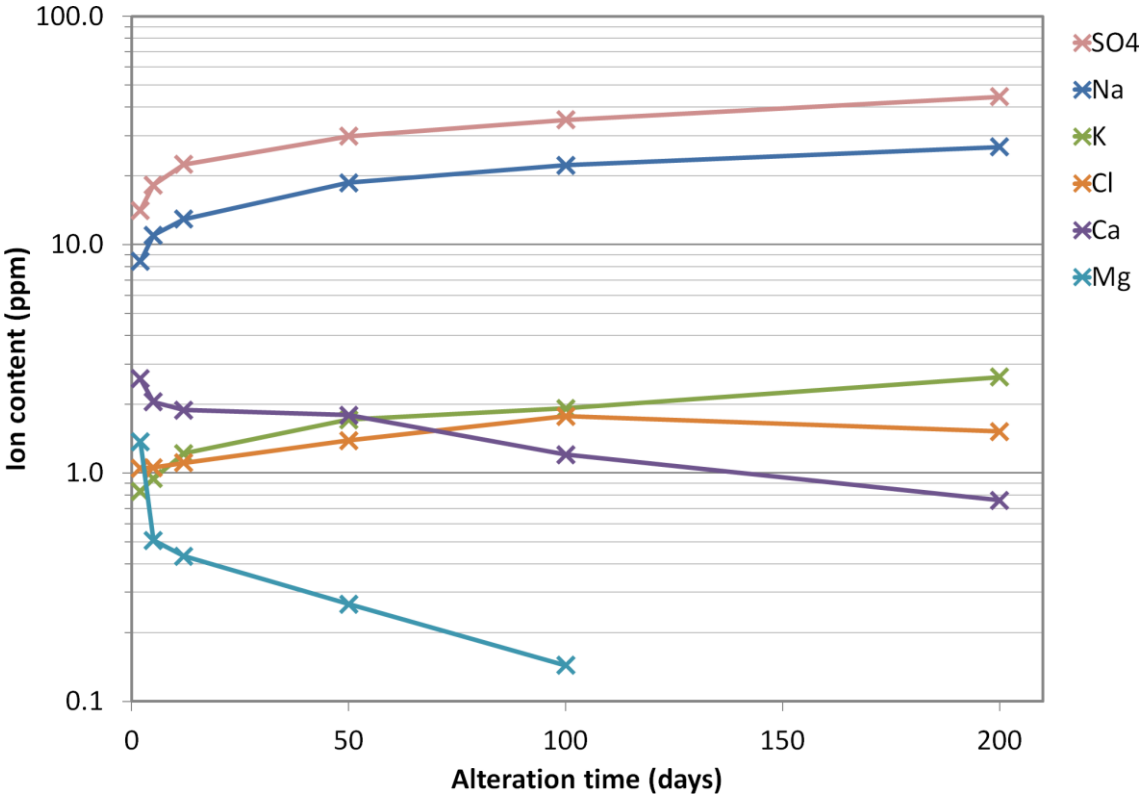

Fig. A4: Ion content of NWA 7936 leachate with alteration time (2, 5, 12, 50, 100, 200 days). Mg content for 200 days is below detection limit.

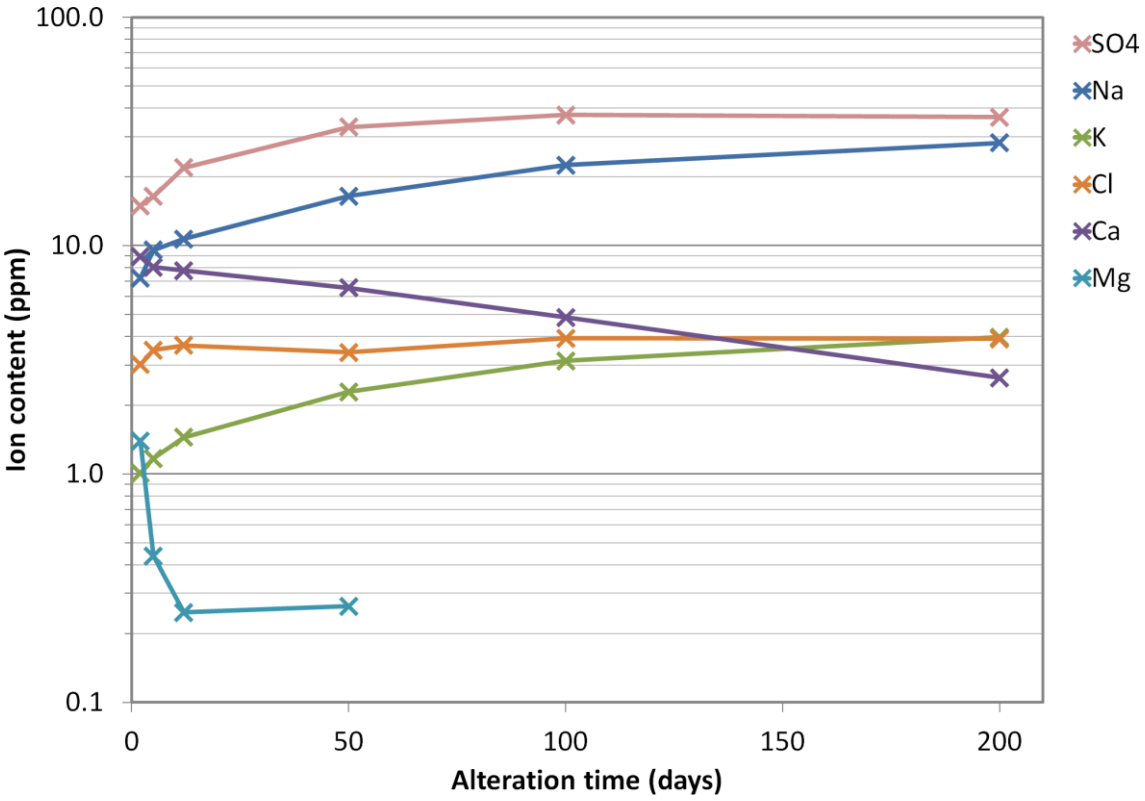

Fig. A5: Ion content of NWA 8039 leachate with alteration time (2, 5, 12, 50, 100, 200 days). Mg content for 100 and 200 days is below detection limit.

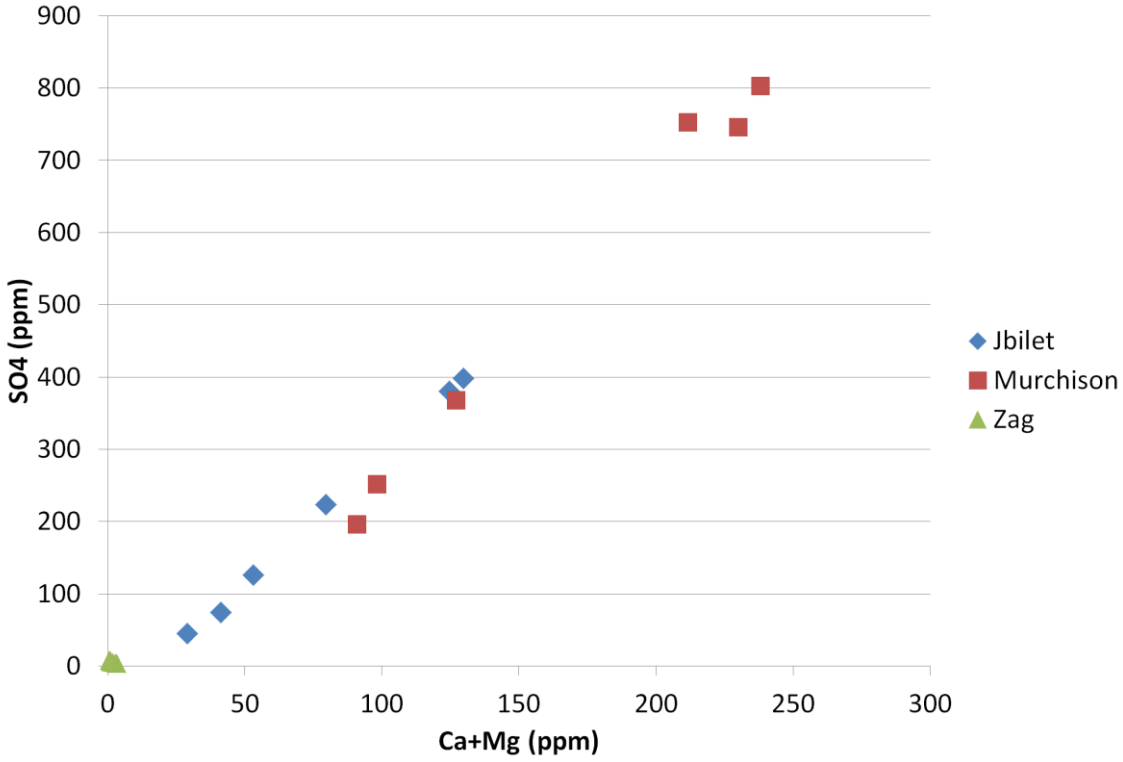

Fig. A6: Ca plus Mg content against SO_4 content of Murchison, Jbilet and Zag with alteration time 2, 5, 12, 50, 100 and 200 days.

Appendix B: Calibration, Blanks and Replicability

Tab. B1: IC analysis of blank solutions heated parallel to experiments. Ion contents are given in ppm.

Blank (days in oven)	Na	NH_4	K	Ca	Mg	Cl	Br	SO_4
0	< 0.25	< 0.05	< 0.05	< 0.025	< 0.5	< 0.5	< 0.025	0.273
2	0.125	< 0.05	0.036	0.048	< 0.5	0.717	< 0.025	0.688
5	0.058	< 0.05	< 0.05	0.030	< 0.5	0.594	< 0.025	0.604
12	0.060	< 0.05	< 0.05	< 0.025	< 0.5	0.596	< 0.025	0.620
50	0.089	< 0.05	< 0.05	0.050	< 0.5	0.615	< 0.025	0.668
100	0.092	< 0.05	< 0.05	0.042	< 0.5	0.618	< 0.025	0.878
200	0.076	< 0.05	< 0.05	< 0.025	< 0.5	0.578	< 0.025	0.606

Tab. B2: ICP-MS analysis of blank solutions heated parallel to experiments. Ion contents are given in ppm.

Blank (days in oven)	Li	Al	P	Fe	Mn	Cu	Rb	Sr	Cd	Cs
0	< 0.1	< 0.5	< 5	< 5	< 0.05	0.024	< 0.01	0.008	0.001	< 0.002
2	< 0.1	< 0.5	< 5	< 5	< 0.05	< 0.01	< 0.01	0.005	< 0.001	< 0.002
5	< 0.1	< 0.5	< 5	< 5	< 0.05	< 0.01	< 0.01	0.006	< 0.001	< 0.002
12	< 0.1	< 0.5	< 5	< 5	< 0.05	< 0.01	< 0.01	0.005	< 0.001	< 0.002
50	< 0.1	< 0.5	< 5	< 5	< 0.05	< 0.01	< 0.01	0.005	< 0.001	< 0.002
100	< 0.1	< 0.5	< 5	< 5	< 0.05	< 0.01	< 0.01	0.005	< 0.001	< 0.002
200	< 0.1	< 0.5	< 5	< 5	< 0.05	< 0.01	< 0.01	0.006	< 0.001	< 0.002

Tab. B3: IC leachate analysis with of 10 replicate samples of NWA 8039 leached for 5 days. Ion contents are given in ppm.

NWA 8039 5d	Na	NH_4	K	Ca	Mg	Cl	Br	SO_4
#1	8.45	< 0.05	1.08	8.19	0.89	3.18	< 0.025	15.44
#2	8.33	< 0.05	1.04	8.39	1.26	3.21	< 0.025	18.46
#3	7.80	< 0.05	1.10	8.05	1.35	3.11	< 0.025	18.36
#4	7.91	< 0.05	1.01	7.82	1.35	3.08	< 0.025	17.73
#5	8.77	< 0.05	1.07	7.81	0.69	3.34	< 0.025	14.38
#6	8.23	< 0.05	1.05	8.25	1.26	3.17	< 0.025	20.22
#7	8.51	< 0.05	1.05	7.63	0.70	3.19	< 0.025	17.18
#8	8.59	< 0.05	1.07	7.51	0.84	3.22	< 0.025	18.44
#9	8.86	< 0.05	1.28	7.85	0.72	3.26	< 0.025	17.52
#10	8.29	< 0.05	1.03	8.15	1.35	3.22	< 0.025	20.20
$\overline{x}$	**8.74**		**1.08**	**7.97**	**1.04**	**3.20**		**17.79**
σ	0.34		0.08	0.29	0.29	0.07		1.84
σ (%)	**4.06**		**7.00**	**3.58**	**28.43**	**2.28**		**10.35**

Tab. B4: ICP-MS leachate analysis with of 5 replicate samples of NWA 8039 leached for 5 days. Ion contents are given in ppm.

NWA 8039 5d	Li	Al	P	Fe	Mn	Cu	Rb	Sr	Cd	Cs
#6	< 0.1	3.46	< 5	< 5	< 0.05	< 0.01	< 0.01	0.056	< 0.001	< 0.002
#7	< 0.1	3.67	< 5	< 5	< 0.05	< 0.01	< 0.01	0.053	< 0.001	< 0.002
#8	< 0.1	3.41	< 5	< 5	< 0.05	< 0.01	< 0.01	0.055	< 0.001	< 0.002
#9	< 0.1	3.61	< 5	< 5	< 0.05	< 0.01	< 0.01	0.056	< 0.001	< 0.002
#10	< 0.1	3.57	< 5	< 5	< 0.05	< 0.01	< 0.01	0.057	< 0.001	< 0.002
$\overline{x}$		**3.54**						**0.055**		
σ		0.11						0.001		
σ (%)		**3.02**						**2.26**		

Appendix C: X-ray diffractograms

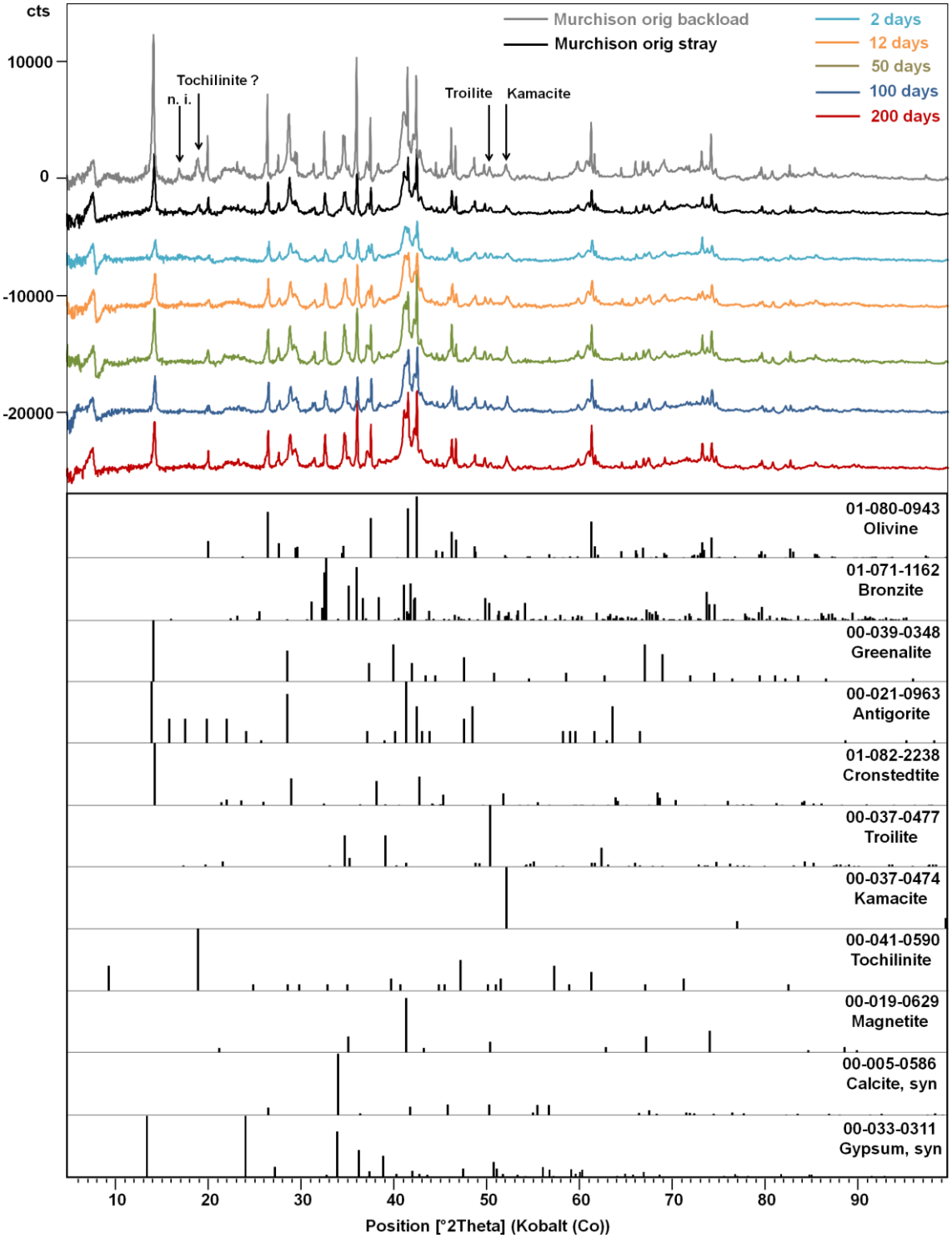

Fig. C1: Diffractograms of Murchison powders with increasing alteration time and diffraction lines of matching minerals from PDF files. The diffractograms are shifted for clarity. The 5 days diffractogram is not used, because of low quality.

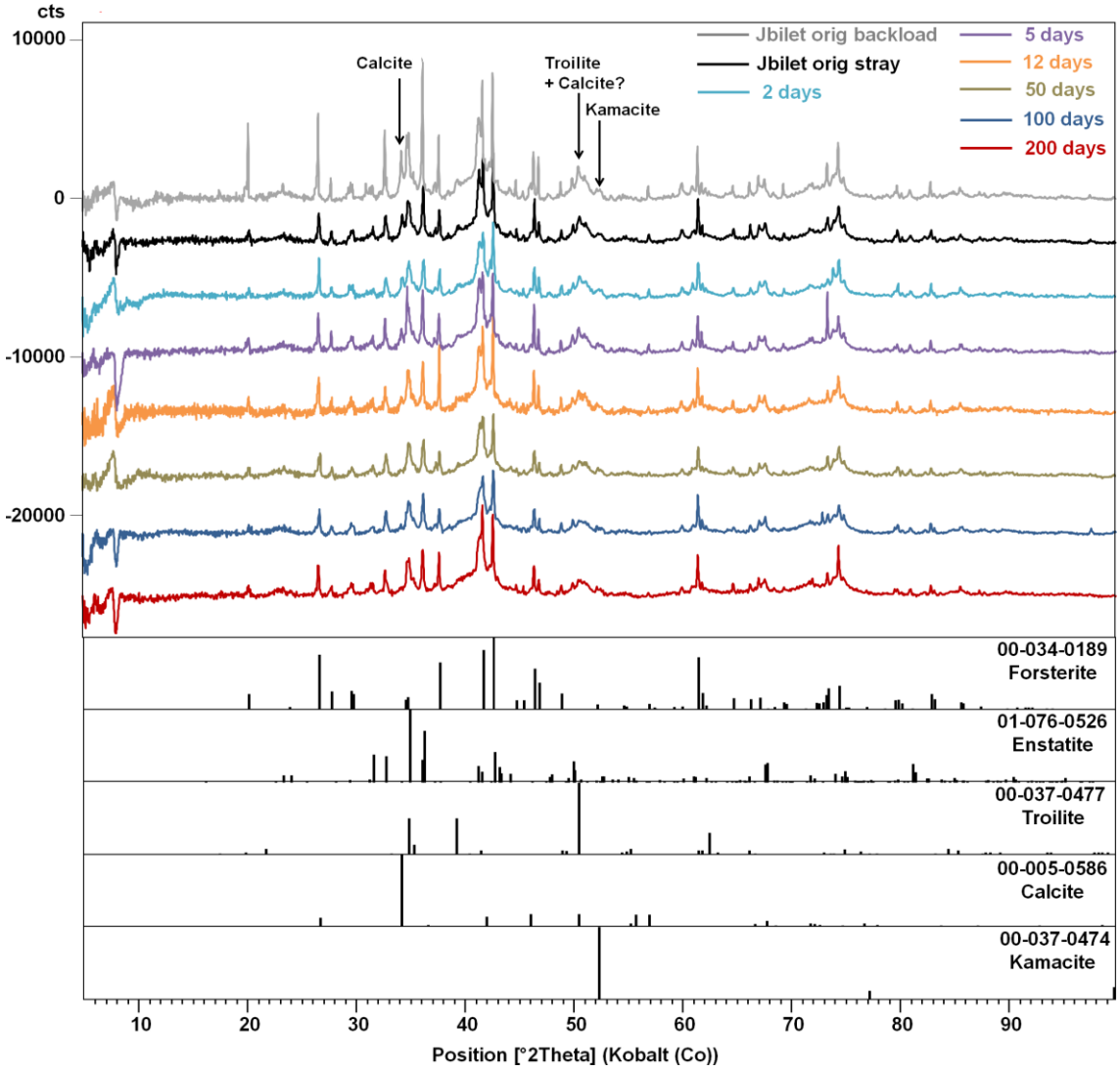

Fig. C2: Diffractograms of Jbilet powders with increasing alteration time and diffraction lines of matching minerals from PDF files. The diffractograms are shifted for clarity.

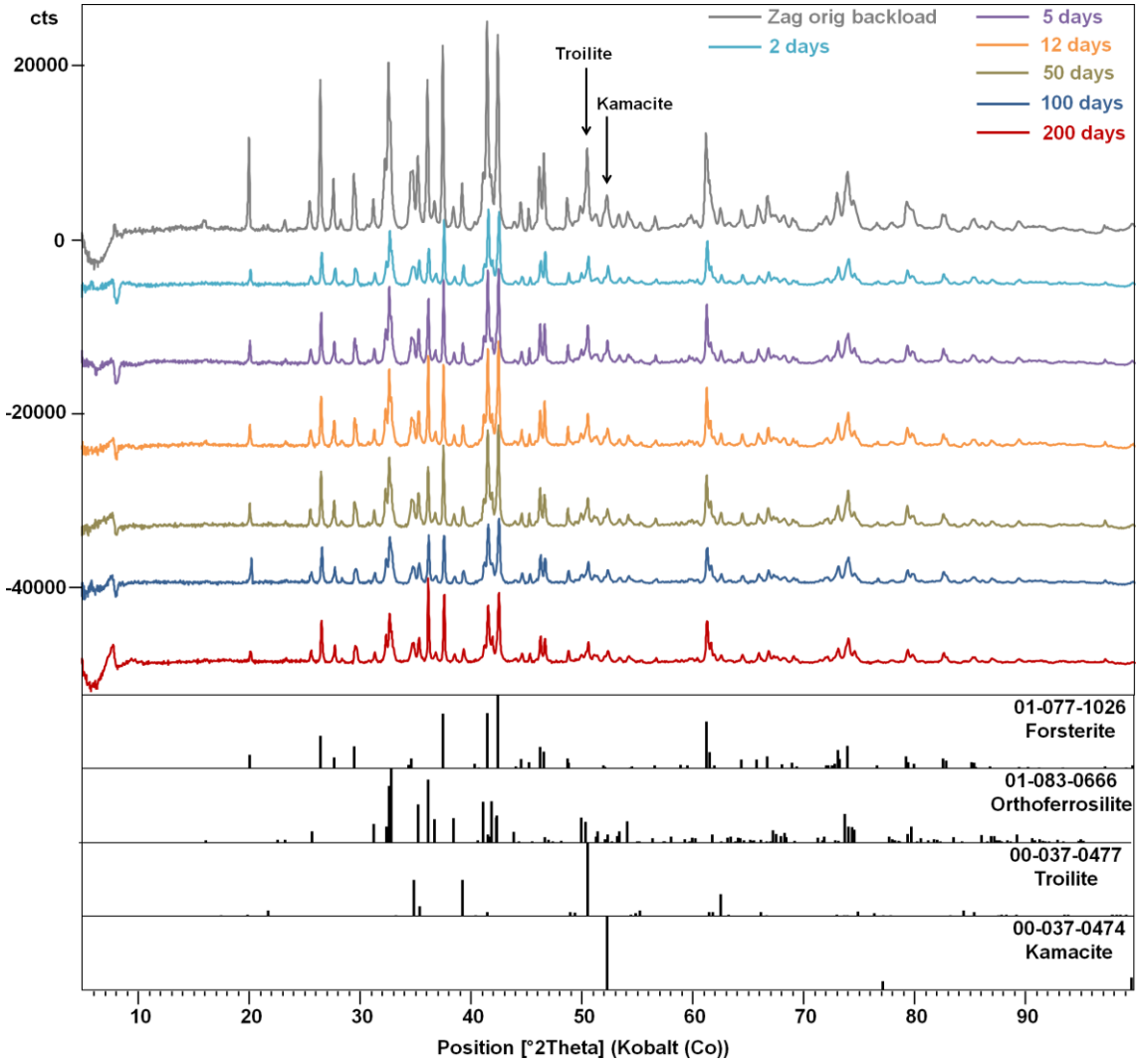

Fig. C3: Diffractograms of Zag powders with increasing alteration time and diffraction lines of matching minerals from PDF files. The Zag original stray preparation diffractogram is not used, because of low quality. The diffractograms are shifted for clarity.

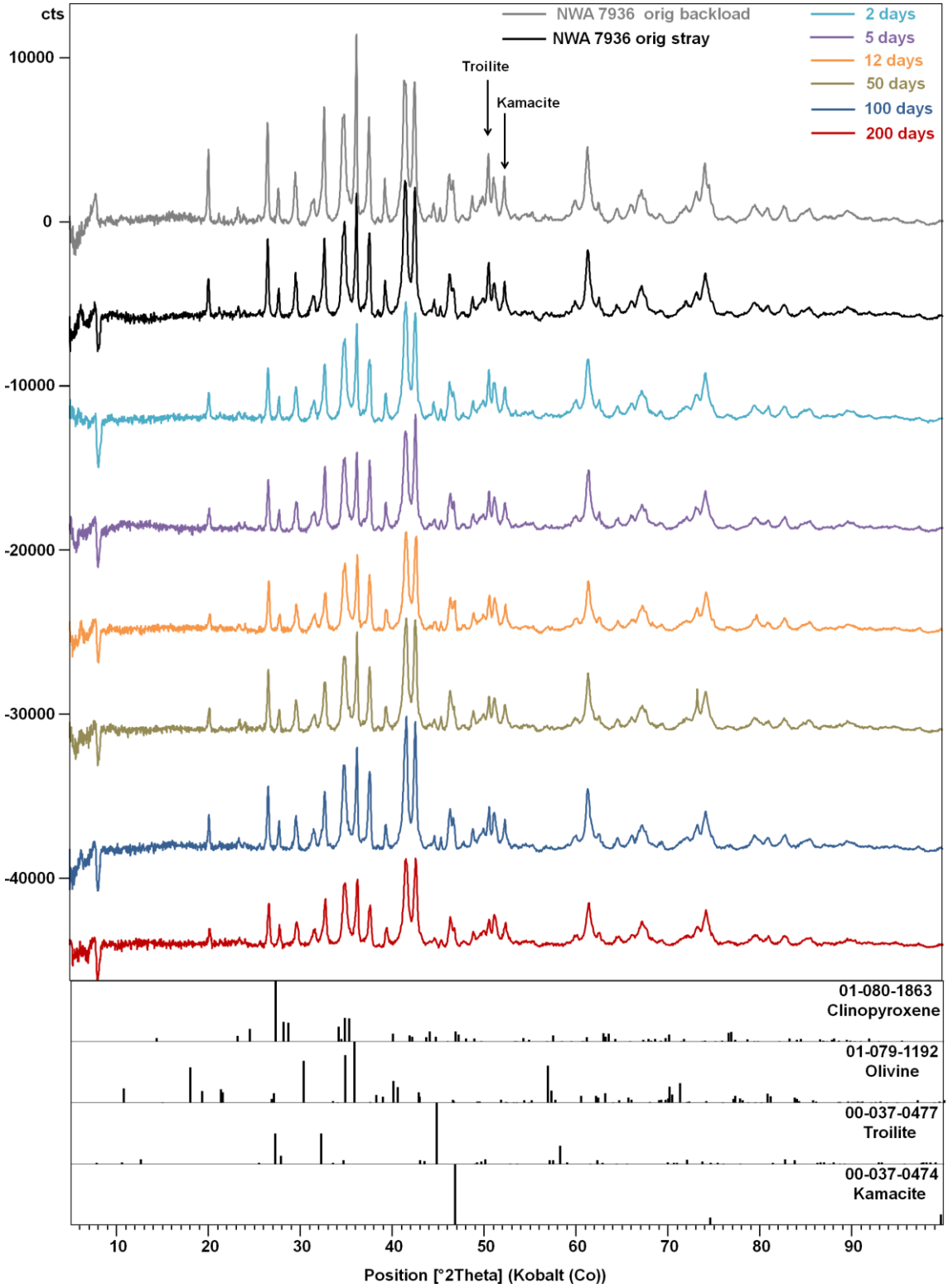

Fig. C4: Diffractograms of NWA 7936 powders with increasing alteration time. The diffractograms are shifted for clarity.

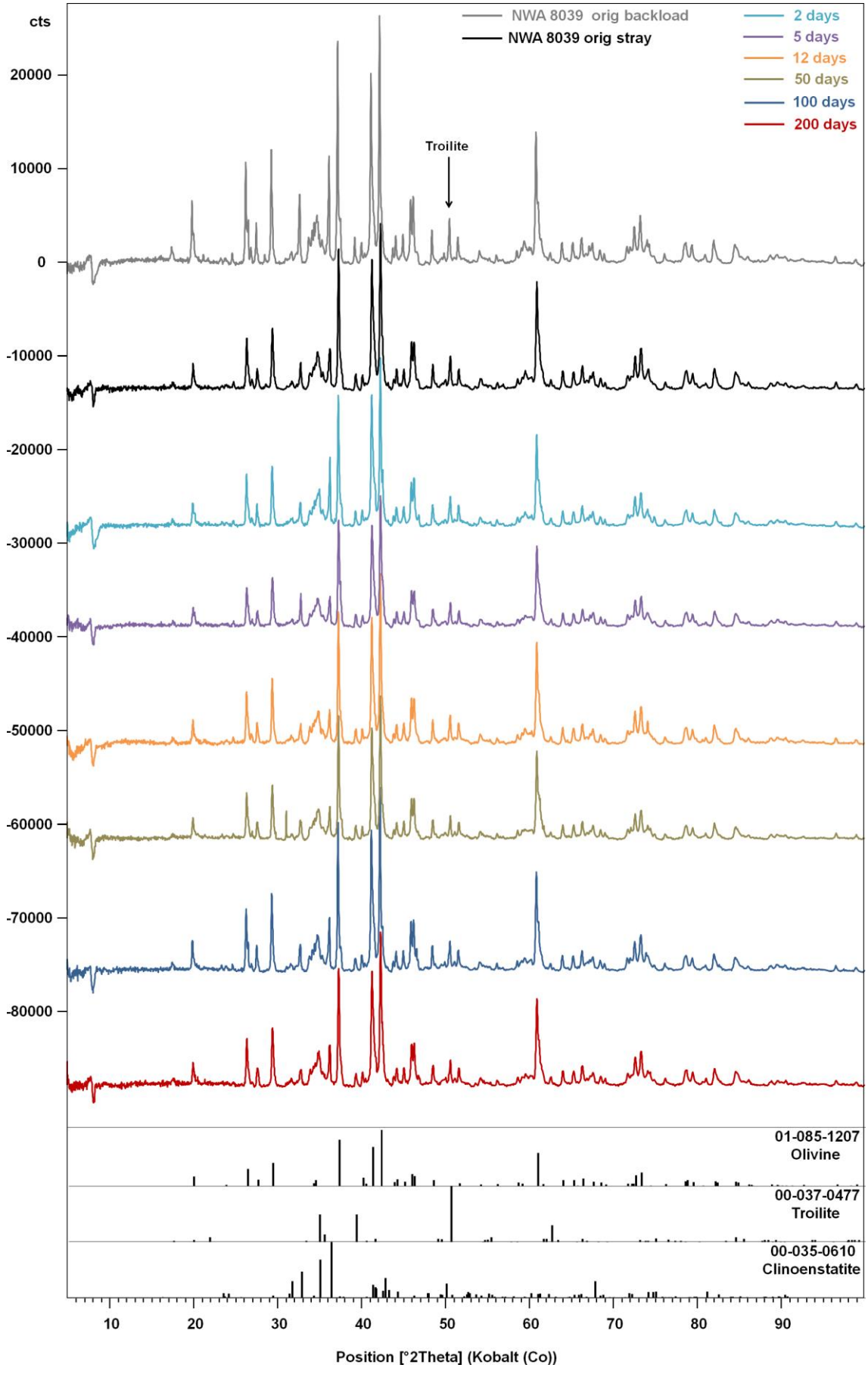

Fig. C5: Diffractograms of NWA 8039 powders with increasing alteration time. The diffractograms are shifted for clarity.

Appendix D: Visible and infrared reflectance spectra

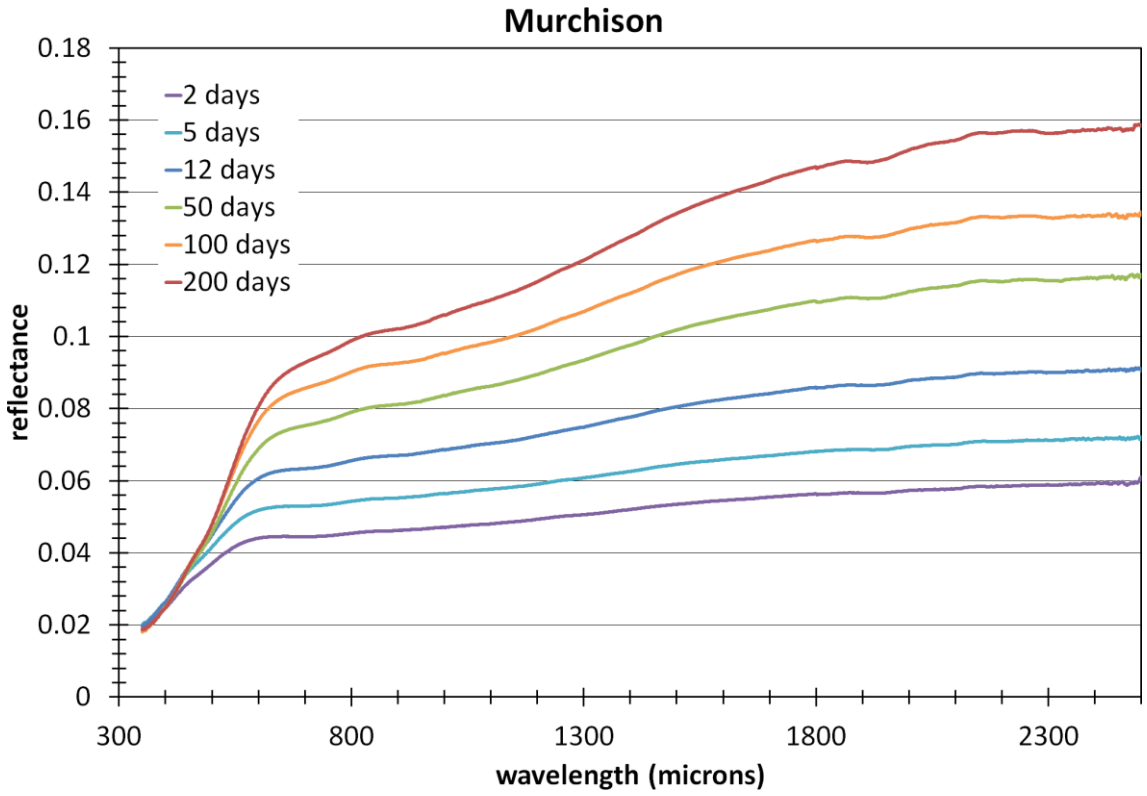

Fig. D1: Reflectance spectra of Murchison for different alteration times.

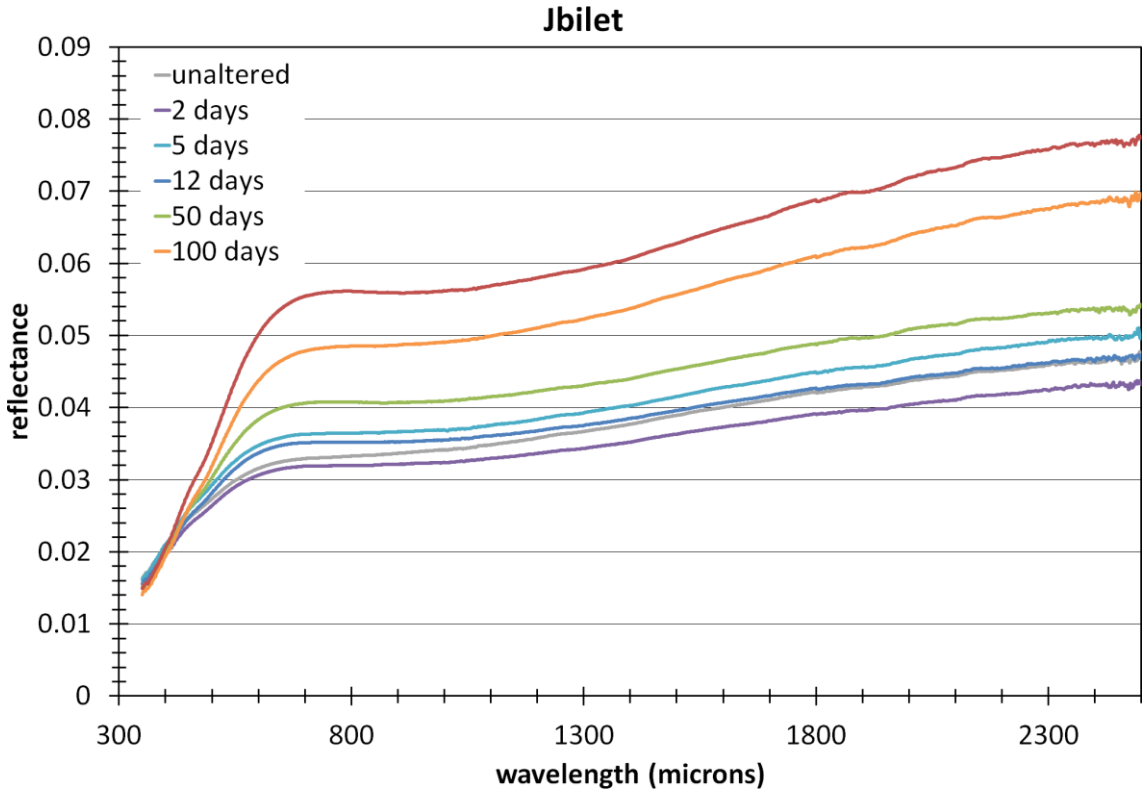

Fig. D2: Reflectance spectra of Jbilet for different alteration times.

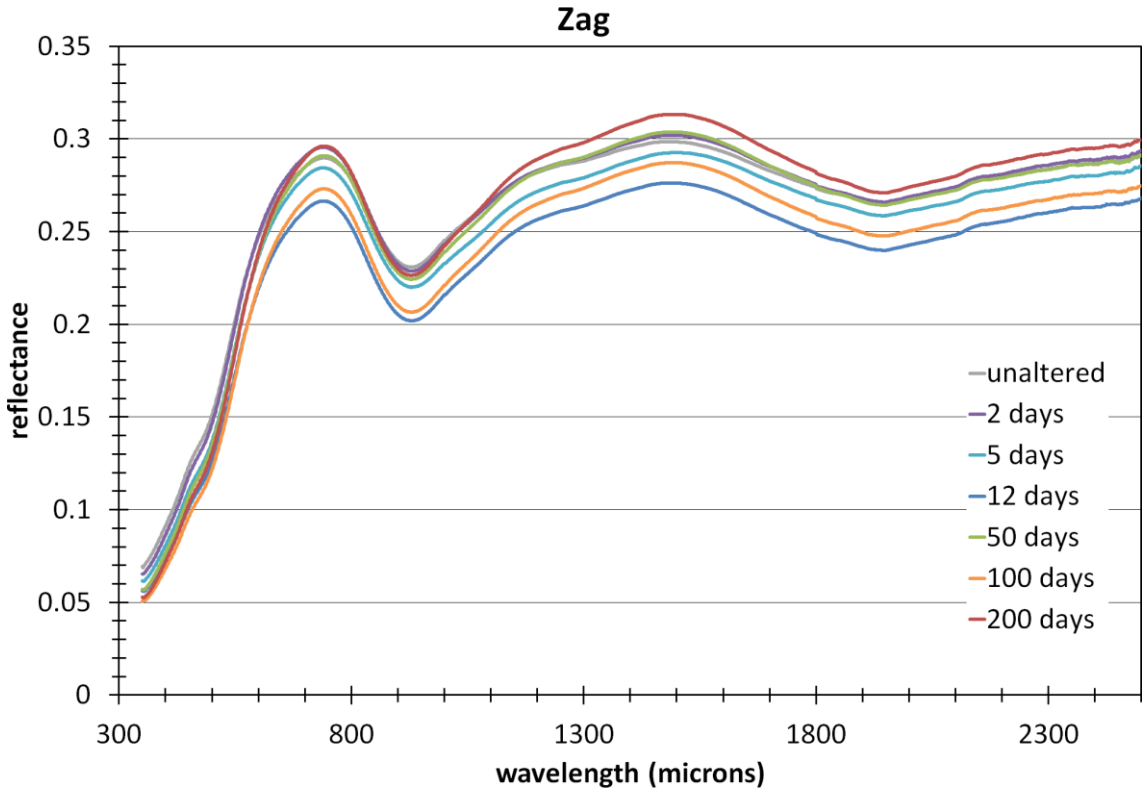

Fig. D3: Reflectance spectra of Zag for different alteration times.

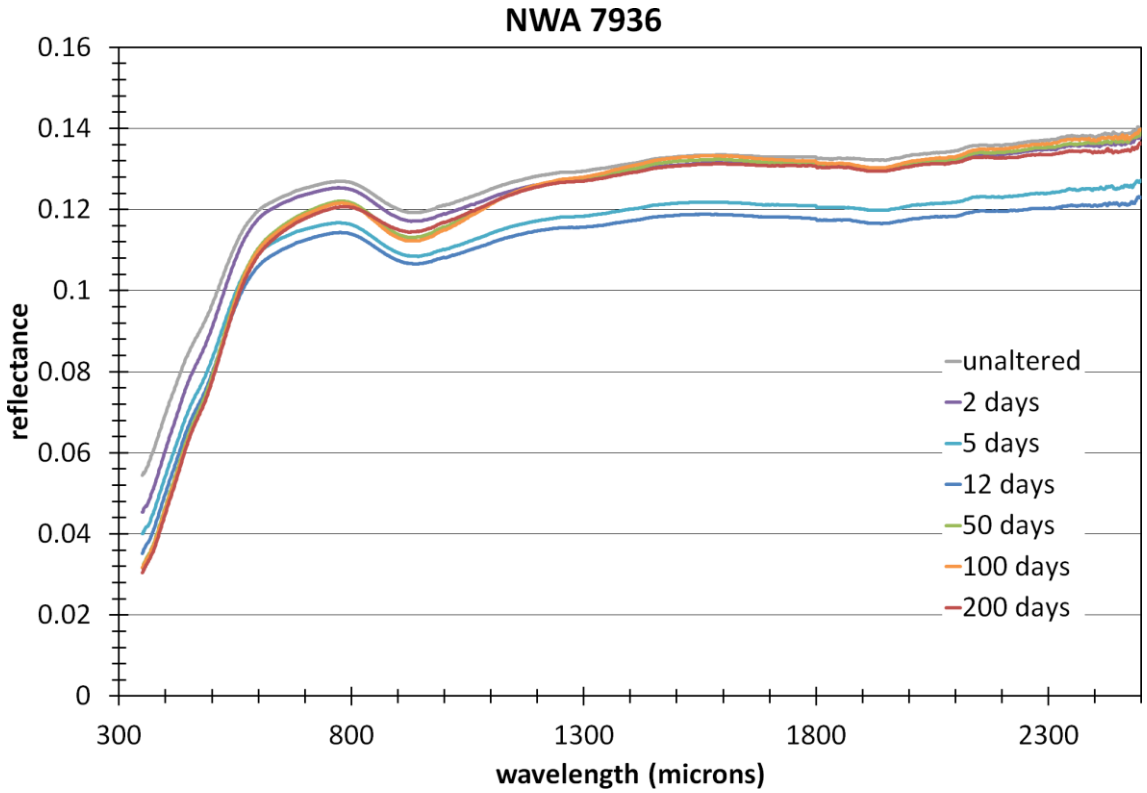

Fig. D4: Reflectance spectra of NWA 7936 for different alteration times.

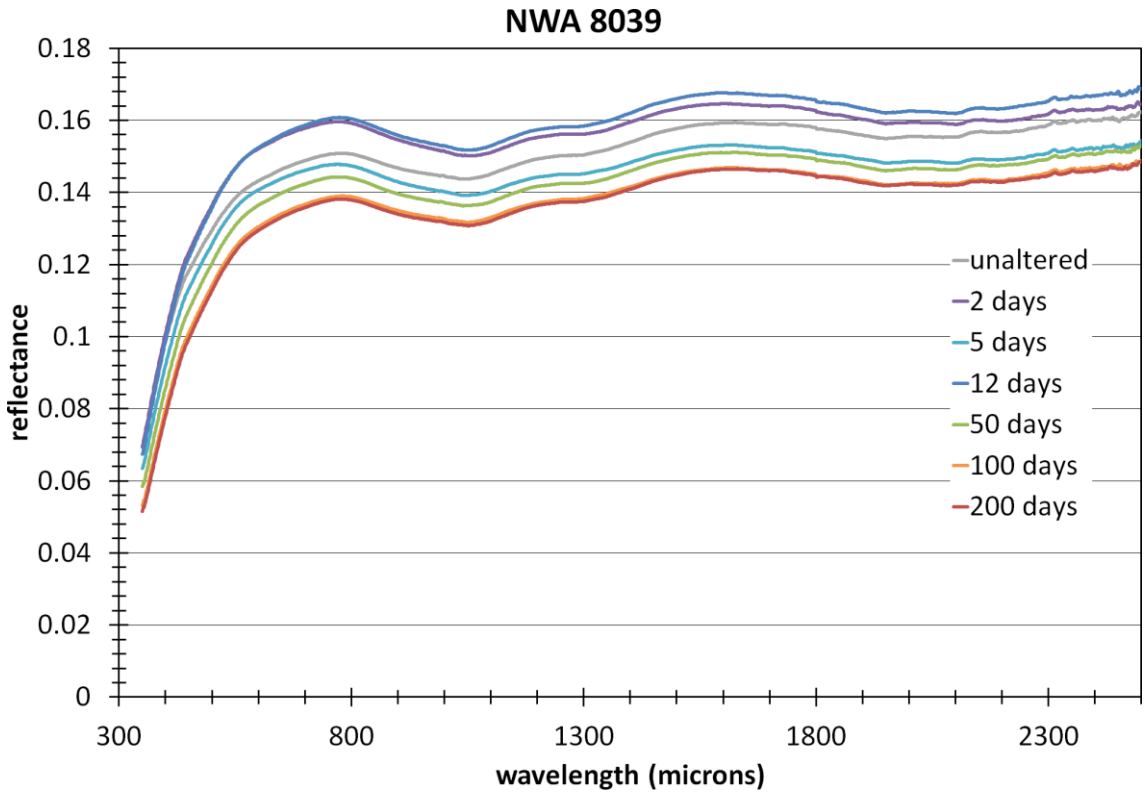

Fig. D5: Reflectance spectra of NWA 8039 for different alteration times.

Appendix E: Input parameter files for FREZCHEM model

```
TITLE: Murchison leachate 200d water case freeze at 500 bars
1, FREEZE(1) OR EVAPORATION(2) OR PRESSURE(3) SCENARIO ? CALLED PATH
BELOW.
2, EQUILIBRIUM(1) OR FRACTIONAL(2) CRYSTALLIZATION?
0, WANT SEAWATER SALINITY(Sp) TO GOVERN THE CALCULATIONS,Y=1, N=0.
0.0, IF YES ABOVE, ENTER SEAWATER PRACTICAL SALINITY(Sp) OR 0.0.
0, WANT SEAWATER CARBONATE SUPERSATURATION TO BE CONSIDERED? Y=1, N=0.
0.0009854, SODIUM(M/KG).
0.0001129, POTASSIUM(M/KG).
0.0023078, CALCIUM(M/KG).
0.0059908, MAGNESIUM(M/KG).
0.00, STRONTIUM(M/KG).
0.00, FERROUS IRON(M/KG).
0.00, FERRIC IRON (M/KG).
0.00, ALUMINUM(M/KG).
0.00, SILICA (M/KG).
0.00, AMMONIUM(M/KG).

FOR FE, AL, SI, AND ALKALINE CHEMISTRIES, DO YOU WANT ACIDITY
IGNORED(1),OR FIXED BY PH(2), OR ACIDITY(3), OR
ALKALINITY(4)? IF YES, THEN ENTER NUM. NOTE THAT OPTIONS 3
AND 4 REQUIRE A FURTHER SPECIFICATION BELOW. OPTIONS 2-4
WILL ADJUST SOLUTION-PHASE CHARGE BALANCE AS AL, FE, OR SI
REACTIONS PRODUCE ACIDITY BY ASSUMING H+ REACTS WITH ROCKS
TO RELEASE NA,K,CA,MG,OR FE(II) IONS. SOME OF THE LATTER
IONS MUST BE PRESENT AS INPUT TO SERVE AS AN ION SINK/SOURCE.
FOR NH3(AQ) + NH4(AQ) CASE, SET OPTION = 2, WITH PH = 10.0.

1, SPECIFY ABOVE ACIDITY OPTION.
7.0, SPECIFY INITIAL PH.
0.000096026, CHLORIDE(M/KG).
0.00, BROMIDE(M/KG).
0.00, PERCHLORATE(M/KG).
0.0083488, SULFATE(M/KG).
0.00, NITRATE(M/KG).
0.00, CARBON ALKALINITY(EQUIVALENTS/KG).
0.0, SULFITE ALKALINITY(EQUIVALENTS/KG).
0.0, SULFIDE ACIDITY(EQUIVALENTS/KG).
0.0, ACIDITY(EQUIVALENTS/KG).
0.00, IF YOU WANT TO SPECIFY HCL(BARS), ENTER VALUE HERE.
0.00, IF YOU WANT TO SPECIFY HNO3(BARS), ENTER VALUE HERE.
0.00, IF YOU WANT TO SPECIFY H2SO4(BARS), ENTER VALUE HERE.
0.00, BORON (M/KG).
0.00, FLUORIDE(M/KG).
500.0, INITIAL TOTAL PRESSURE(BARS).
0.00, INITIAL CO2(BARS).
0.00, ENTER MOLE FRACTION OF CO2, 0=FIXED CO2, 1=PURE CO2.
```

```
0.00, INITIAL O2(BARS).
0.00, INITIAL CH4(BARS).
0.00, ENTER MOLE FRACTION OF CH4, 0=FIXED CH4, 1=PURE CH4.
0.00, CONSIDER A MIXED CO2-CH4 GAS HYDRATE,MIX (YES=1, NO=0)?
0.00, INITIAL NH3(G)(BARS), DO NOT INCLUDE BOTH NH3 INPUTS.
0.00, INITIAL NH3(AQ)(M/KG), DO NOT INCLUDE BOTH NH3 INPUTS.
0.00, INITIAL N2(BARS).
0.00, ENTER MOLE FRACTION OF N2, 0=FIXED N2, 1=PURE N2.
0, CONSIDER A MIXED N2-CH4 GAS HYDRATE,MIX2 (YES=1, NO=0)?
0, CONSIDER A MIXED N2-C02 GAS HYDRATE,MIX3 (YES=1, NO=0)?
0.00, INITIAL C2H6(BARS).
0.00, ENTER MOLE FRACTION OF C2H6, 0=FIXED C2H6, 1=PURE C2H6.
0.00, INITIAL C3H8(BARS).
0.00, ENTER MOLE FRACTION OF C3H8, 0=FIXED C3H8, 1=PURE C3H8.
0, CONSIDER A MIXED C2H6-C3H8 GAS HYDRATE,MIX4 (YES=1, NO=0)?
0, CONSIDER A MIXED C2H6-CH4 GAS HYDRATE,MIX5 (YES=1, NO=0)?
0, CONSIDER A MIXED C3H8-CH4 GAS HYDRATE,MIX6 (YES=1, NO=0)?
0, CONSIDER A MIXED C2H6-N2 GAS HYDRATE,MIX7 (YES=1, NO=0)?
0, CONSIDER A MIXED C3H8-N2 GAS HYDRATE,MIX8 (YES=1, NO=0)?
0, CONSIDER A MIXED C2H6-CO2 GAS HYDRATE,MIX9 (YES=1, NO=0)?
0, CONSIDER A MIXED C3H8-CO2 GAS HYDRATE,MIX10 (YES=1, NO=0)?
0, MOLAR TO MOLAL CONVERSION? YES=1, NO=0.
0.00, IF YES ABOVE, ENTER SALINITY(G)/LITER.
293.0, INITIAL TEMPERATURE(K).
180.0, FINAL TEMPERATURE(K), IF PATH = 1, OTHERWISE, SET = 0.
10.0, TEMPERATURE DECREMENT(K), IF PATH = 1, OTHERWISE, SET = 0.
1000, INITIAL WATER(G), IF PATH = 2, OTHERWISE, SET = 1000.
0, FINAL WATER(G), IF PATH = 2, OTHERWISE, SET = 0.
0, WATER DECREMENT(G), IF PATH = 2, OTHERWISE, SET = 0.
0, FINAL PRESSURE(BARS), IF PATH = 3, OTHERWISE, SET = 0.
0, PRESSURE INCREMENT(BARS), IF PATH = 3, OTHERWISE, SET = 0.
```

TITLE: Murchison leachate 200d NH4-CO2 case freeze

```
1, FREEZE(1) OR EVAPORATION(2) OR PRESSURE(3) SCENARIO ? CALLED PATH
BELOW.
2, EQUILIBRIUM(1) OR FRACTIONAL(2) CRYSTALLIZATION?
0, WANT SEAWATER SALINITY(Sp) TO GOVERN THE CALCULATIONS,Y=1, N=0.
0.0, IF YES ABOVE, ENTER SEAWATER PRACTICAL SALINITY(Sp) OR 0.0.
0, WANT SEAWATER CARBONATE SUPERSATURATION TO BE CONSIDERED? Y=1, N=0.
0.0009854, SODIUM(M/KG).
0.0001129, POTASSIUM(M/KG).
0.0023078, CALCIUM(M/KG).
0.0059908, MAGNESIUM(M/KG).
0.00, STRONTIUM(M/KG).
0.00, FERROUS IRON(M/KG).
0.00, FERRIC IRON (M/KG).
0.00, ALUMINUM(M/KG).
0.00, SILICA (M/KG).
```

```
0.0001, AMMONIUM(M/KG).

FOR FE, AL, SI, AND ALKALINE CHEMISTRIES, DO YOU WANT ACIDITY
IGNORED(1),OR FIXED BY PH(2), OR ACIDITY(3), OR
ALKALINITY(4)? IF YES, THEN ENTER NUM. NOTE THAT OPTIONS 3
AND 4 REQUIRE A FURTHER SPECIFICATION BELOW. OPTIONS 2-4
WILL ADJUST SOLUTION-PHASE CHARGE BALANCE AS AL, FE, OR SI
REACTIONS PRODUCE ACIDITY BY ASSUMING H+ REACTS WITH ROCKS
TO RELEASE NA,K,CA,MG,OR FE(II) IONS. SOME OF THE LATTER
IONS MUST BE PRESENT AS INPUT TO SERVE AS AN ION SINK/SOURCE.
FOR NH3(AQ) + NH4(AQ) CASE, SET OPTION = 2, WITH PH = 10.0.

2, SPECIFY ABOVE ACIDITY OPTION.
10.0, SPECIFY INITIAL PH.
0.000096026, CHLORIDE(M/KG).
0.00, BROMIDE(M/KG).
0.00, PERCHLORATE(M/KG).
0.0083488, SULFATE(M/KG).
0.00, NITRATE(M/KG).
0.002, CARBON ALKALINITY(EQUIVALENTS/KG).
0.0, SULFITE ALKALINITY(EQUIVALENTS/KG).
0.0, SULFIDE ACIDITY(EQUIVALENTS/KG).
0.0, ACIDITY(EQUIVALENTS/KG).
0.00, IF YOU WANT TO SPECIFY HCL(BARS), ENTER VALUE HERE.
0.00, IF YOU WANT TO SPECIFY HNO3(BARS), ENTER VALUE HERE.
0.00, IF YOU WANT TO SPECIFY H2SO4(BARS), ENTER VALUE HERE.
0.00, BORON (M/KG).
0.00, FLUORIDE(M/KG).
500.0, INITIAL TOTAL PRESSURE(BARS).
0.02, INITIAL CO2(BARS).
0.00, ENTER MOLE FRACTION OF CO2, 0=FIXED CO2, 1=PURE CO2.
0.00, INITIAL O2(BARS).
0.00, INITIAL CH4(BARS).
0.00, ENTER MOLE FRACTION OF CH4, 0=FIXED CH4, 1=PURE CH4.
0.00, CONSIDER A MIXED CO2-CH4 GAS HYDRATE,MIX (YES=1, NO=0)?
0.00, INITIAL NH3(G)(BARS), DO NOT INCLUDE BOTH NH3 INPUTS.
0.00, INITIAL NH3(AQ)(M/KG), DO NOT INCLUDE BOTH NH3 INPUTS.
0.00, INITIAL N2(BARS).
0.00, ENTER MOLE FRACTION OF N2, 0=FIXED N2, 1=PURE N2.
0, CONSIDER A MIXED N2-CH4 GAS HYDRATE,MIX2 (YES=1, NO=0)?
0, CONSIDER A MIXED N2-C02 GAS HYDRATE,MIX3 (YES=1, NO=0)?
0.00, INITIAL C2H6(BARS).
0.00, ENTER MOLE FRACTION OF C2H6, 0=FIXED C2H6, 1=PURE C2H6.
0.00, INITIAL C3H8(BARS).
0.00, ENTER MOLE FRACTION OF C3H8, 0=FIXED C3H8, 1=PURE C3H8.
0, CONSIDER A MIXED C2H6-C3H8 GAS HYDRATE,MIX4 (YES=1, NO=0)?
0, CONSIDER A MIXED C2H6-CH4 GAS HYDRATE,MIX5 (YES=1, NO=0)?
0, CONSIDER A MIXED C3H8-CH4 GAS HYDRATE,MIX6 (YES=1, NO=0)?
0, CONSIDER A MIXED C2H6-N2 GAS HYDRATE,MIX7 (YES=1, NO=0)?
0, CONSIDER A MIXED C3H8-N2 GAS HYDRATE,MIX8 (YES=1, NO=0)?
```

```
0, CONSIDER A MIXED C2H6-CO2 GAS HYDRATE,MIX9 (YES=1, NO=0)?
0, CONSIDER A MIXED C3H8-CO2 GAS HYDRATE,MIX10 (YES=1, NO=0)?
0, MOLAR TO MOLAL CONVERSION? YES=1, NO=0.
0.00, IF YES ABOVE, ENTER SALINITY(G)/LITER.
293.0, INITIAL TEMPERATURE(K).
180.0, FINAL TEMPERATURE(K), IF PATH = 1, OTHERWISE, SET = 0.
10.0, TEMPERATURE DECREMENT(K), IF PATH = 1, OTHERWISE, SET = 0.
1000, INITIAL WATER(G), IF PATH = 2, OTHERWISE, SET = 1000.
0, FINAL WATER(G), IF PATH = 2, OTHERWISE, SET = 0.
0, WATER DECREMENT(G), IF PATH = 2, OTHERWISE, SET = 0.
0, FINAL PRESSURE(BARS), IF PATH = 3, OTHERWISE, SET = 0.
0, PRESSURE INCREMENT(BARS), IF PATH = 3, OTHERWISE, SET = 0.
```

TITLE: Murchison leachate 200d evaporation at 0.1 bar 293 K water only case

```
2, FREEZE(1) OR EVAPORATION(2) OR PRESSURE(3) SCENARIO ? CALLED PATH
BELOW.
1, EQUILIBRIUM(1) OR FRACTIONAL(2) CRYSTALLIZATION?
0, WANT SEAWATER SALINITY(Sp) TO GOVERN THE CALCULATIONS,Y=1, N=0.
0.0, IF YES ABOVE, ENTER SEAWATER PRACTICAL SALINITY(Sp) OR 0.0.
0, WANT SEAWATER CARBONATE SUPERSATURATION TO BE CONSIDERED? Y=1, N=0.
0.46791, SODIUM(M/KG).
0.46869, POTASSIUM(M/KG).
0.023269, CALCIUM(M/KG).
0.91533, MAGNESIUM(M/KG).
0.00, STRONTIUM(M/KG).
0.00, FERROUS IRON(M/KG).
0.00, FERRIC IRON (M/KG).
0.00, ALUMINUM(M/KG).
0.00, SILICA (M/KG).
0.00, AMMONIUM(M/KG).

FOR FE, AL, SI, AND ALKALINE CHEMISTRIES, DO YOU WANT ACIDITY
IGNORED(1),OR FIXED BY PH(2), OR ACIDITY(3), OR
ALKALINITY(4)? IF YES, THEN ENTER NUM. NOTE THAT OPTIONS 3
AND 4 REQUIRE A FURTHER SPECIFICATION BELOW. OPTIONS 2-4
WILL ADJUST SOLUTION-PHASE CHARGE BALANCE AS AL, FE, OR SI
REACTIONS PRODUCE ACIDITY BY ASSUMING H+ REACTS WITH ROCKS
TO RELEASE NA,K,CA,MG,OR FE(II) IONS. SOME OF THE LATTER
IONS MUST BE PRESENT AS INPUT TO SERVE AS AN ION SINK/SOURCE.
FOR NH3(AQ) + NH4(AQ) CASE, SET OPTION = 2, WITH PH = 10.0.

2, SPECIFY ABOVE ACIDITY OPTION.
7.0, SPECIFY INITIAL PH.
0.70785, CHLORIDE(M/KG).
0.00, BROMIDE(M/KG).
0.00, PERCHLORATE(M/KG).
1.053, SULFATE(M/KG).
```

```
0.00, NITRATE(M/KG).
0.00, CARBON ALKALINITY(EQUIVALENTS/KG).
0.0, SULFITE ALKALINITY(EQUIVALENTS/KG).
0.0, SULFIDE ACIDITY(EQUIVALENTS/KG).
0.0, ACIDITY(EQUIVALENTS/KG).
0.00, IF YOU WANT TO SPECIFY HCL(BARS), ENTER VALUE HERE.
0.00, IF YOU WANT TO SPECIFY HNO3(BARS), ENTER VALUE HERE.
0.00, IF YOU WANT TO SPECIFY H2SO4(BARS), ENTER VALUE HERE.
0.00, BORON (M/KG).
0.00, FLUORIDE(M/KG).
0.1, INITIAL TOTAL PRESSURE(BARS).
0.00, INITIAL CO2(BARS).
0, ENTER MOLE FRACTION OF CO2, 0=FIXED CO2, 1=PURE CO2.
0.00, INITIAL O2(BARS).
0.00, INITIAL CH4(BARS).
0.00, ENTER MOLE FRACTION OF CH4, 0=FIXED CH4, 1=PURE CH4.
0.00, CONSIDER A MIXED CO2-CH4 GAS HYDRATE,MIX (YES=1, NO=0)?
0.00, INITIAL NH3(G)(BARS), DO NOT INCLUDE BOTH NH3 INPUTS.
0.00, INITIAL NH3(AQ)(M/KG), DO NOT INCLUDE BOTH NH3 INPUTS.
0.00, INITIAL N2(BARS).
0.00, ENTER MOLE FRACTION OF N2, 0=FIXED N2, 1=PURE N2.
0, CONSIDER A MIXED N2-CH4 GAS HYDRATE,MIX2 (YES=1, NO=0)?
0, CONSIDER A MIXED N2-C02 GAS HYDRATE,MIX3 (YES=1, NO=0)?
0.00, INITIAL C2H6(BARS).
0.00, ENTER MOLE FRACTION OF C2H6, 0=FIXED C2H6, 1=PURE C2H6.
0.00, INITIAL C3H8(BARS).
0.00, ENTER MOLE FRACTION OF C3H8, 0=FIXED C3H8, 1=PURE C3H8.
0, CONSIDER A MIXED C2H6-C3H8 GAS HYDRATE,MIX4 (YES=1, NO=0)?
0, CONSIDER A MIXED C2H6-CH4 GAS HYDRATE,MIX5 (YES=1, NO=0)?
0, CONSIDER A MIXED C3H8-CH4 GAS HYDRATE,MIX6 (YES=1, NO=0)?
0, CONSIDER A MIXED C2H6-N2 GAS HYDRATE,MIX7 (YES=1, NO=0)?
0, CONSIDER A MIXED C3H8-N2 GAS HYDRATE,MIX8 (YES=1, NO=0)?
0, CONSIDER A MIXED C2H6-CO2 GAS HYDRATE,MIX9 (YES=1, NO=0)?
0, CONSIDER A MIXED C3H8-CO2 GAS HYDRATE,MIX10 (YES=1, NO=0)?
0, MOLAR TO MOLAL CONVERSION? YES=1, NO=0.
0.00, IF YES ABOVE, ENTER SALINITY(G)/LITER.
293.0, INITIAL TEMPERATURE(K).
0, FINAL TEMPERATURE(K), IF PATH = 1, OTHERWISE, SET = 0.
0, TEMPERATURE DECREMENT(K), IF PATH = 1, OTHERWISE, SET = 0.
1000.0, INITIAL WATER(G), IF PATH = 2, OTHERWISE, SET = 1000.
0.001, FINAL WATER(G), IF PATH = 2, OTHERWISE, SET = 0.
5.0, WATER DECREMENT(G), IF PATH = 2, OTHERWISE, SET = 0.
0, FINAL PRESSURE(BARS), IF PATH = 3, OTHERWISE, SET = 0.
0, PRESSURE INCREMENT(BARS), IF PATH = 3, OTHERWISE, SET = 0.
```

```
TITLE: Murchison leachate 200d evaporation at 0.1 bar 293 K NH4-CO2
case
2, FREEZE(1) OR EVAPORATION(2) OR PRESSURE(3) SCENARIO ? CALLED PATH
BELOW.
1, EQUILIBRIUM(1) OR FRACTIONAL(2) CRYSTALLIZATION?
0, WANT SEAWATER SALINITY(Sp) TO GOVERN THE CALCULATIONS,Y=1, N=0.
0.0, IF YES ABOVE, ENTER SEAWATER PRACTICAL SALINITY(Sp) OR 0.0.
0, WANT SEAWATER CARBONATE SUPERSATURATION TO BE CONSIDERED? Y=1, N=0.
0.42052, SODIUM(M/KG).
0.3632, POTASSIUM(M/KG).
0.023549, CALCIUM(M/KG).
0.83596, MAGNESIUM(M/KG).
0.00, STRONTIUM(M/KG).
0.00, FERROUS IRON(M/KG).
0.00, FERRIC IRON (M/KG).
0.00, ALUMINUM(M/KG).
0.00, SILICA (M/KG).
0.90831, AMMONIUM(M/KG).

FOR FE, AL, SI, AND ALKALINE CHEMISTRIES, DO YOU WANT ACIDITY
IGNORED(1),OR FIXED BY PH(2), OR ACIDITY(3), OR
ALKALINITY(4)? IF YES, THEN ENTER NUM. NOTE THAT OPTIONS 3
AND 4 REQUIRE A FURTHER SPECIFICATION BELOW. OPTIONS 2-4
WILL ADJUST SOLUTION-PHASE CHARGE BALANCE AS AL, FE, OR SI
REACTIONS PRODUCE ACIDITY BY ASSUMING H+ REACTS WITH ROCKS
TO RELEASE NA,K,CA,MG,OR FE(II) IONS. SOME OF THE LATTER
IONS MUST BE PRESENT AS INPUT TO SERVE AS AN ION SINK/SOURCE.
FOR NH3(AQ) + NH4(AQ) CASE, SET OPTION = 2, WITH PH = 10.0.

2, SPECIFY ABOVE ACIDITY OPTION.
6.7, SPECIFY INITIAL PH.
0.87222, CHLORIDE(M/KG).
0.00, BROMIDE(M/KG).
0.00, PERCHLORATE(M/KG).
1.2561, SULFATE(M/KG).
0.00, NITRATE(M/KG).
0.026, CARBON ALKALINITY(EQUIVALENTS/KG).
0.0, SULFITE ALKALINITY(EQUIVALENTS/KG).
0.0, SULFIDE ACIDITY(EQUIVALENTS/KG).
0.0, ACIDITY(EQUIVALENTS/KG).
0.00, IF YOU WANT TO SPECIFY HCL(BARS), ENTER VALUE HERE.
0.00, IF YOU WANT TO SPECIFY HNO3(BARS), ENTER VALUE HERE.
0.00, IF YOU WANT TO SPECIFY H2SO4(BARS), ENTER VALUE HERE.
0.00, BORON (M/KG).
0.00, FLUORIDE(M/KG).
0.1, INITIAL TOTAL PRESSURE(BARS).
0.002, INITIAL CO2(BARS).
0, ENTER MOLE FRACTION OF CO2, 0=FIXED CO2, 1=PURE CO2.
0.00, INITIAL O2(BARS).
0.00, INITIAL CH4(BARS).
```

```
0.00, ENTER MOLE FRACTION OF CH4, 0=FIXED CH4, 1=PURE CH4.
0.00, CONSIDER A MIXED CO2-CH4 GAS HYDRATE,MIX (YES=1, NO=0)?
0.00, INITIAL NH3(G)(BARS), DO NOT INCLUDE BOTH NH3 INPUTS.
0.00, INITIAL NH3(AQ)(M/KG), DO NOT INCLUDE BOTH NH3 INPUTS.
0.00, INITIAL N2(BARS).
0.00, ENTER MOLE FRACTION OF N2, 0=FIXED N2, 1=PURE N2.
0, CONSIDER A MIXED N2-CH4 GAS HYDRATE,MIX2 (YES=1, NO=0)?
0, CONSIDER A MIXED N2-C02 GAS HYDRATE,MIX3 (YES=1, NO=0)?
0.00, INITIAL C2H6(BARS).
0.00, ENTER MOLE FRACTION OF C2H6, 0=FIXED C2H6, 1=PURE C2H6.
0.00, INITIAL C3H8(BARS).
0.00, ENTER MOLE FRACTION OF C3H8, 0=FIXED C3H8, 1=PURE C3H8.
0, CONSIDER A MIXED C2H6-C3H8 GAS HYDRATE,MIX4 (YES=1, NO=0)?
0, CONSIDER A MIXED C2H6-CH4 GAS HYDRATE,MIX5 (YES=1, NO=0)?
0, CONSIDER A MIXED C3H8-CH4 GAS HYDRATE,MIX6 (YES=1, NO=0)?
0, CONSIDER A MIXED C2H6-N2 GAS HYDRATE,MIX7 (YES=1, NO=0)?
0, CONSIDER A MIXED C3H8-N2 GAS HYDRATE,MIX8 (YES=1, NO=0)?
0, CONSIDER A MIXED C2H6-CO2 GAS HYDRATE,MIX9 (YES=1, NO=0)?
0, CONSIDER A MIXED C3H8-CO2 GAS HYDRATE,MIX10 (YES=1, NO=0)?
0, MOLAR TO MOLAL CONVERSION? YES=1, NO=0.
0.00, IF YES ABOVE, ENTER SALINITY(G)/LITER.
293.0, INITIAL TEMPERATURE(K).
0, FINAL TEMPERATURE(K), IF PATH = 1, OTHERWISE, SET = 0.
0, TEMPERATURE DECREMENT(K), IF PATH = 1, OTHERWISE, SET = 0.
1000.0, INITIAL WATER(G), IF PATH = 2, OTHERWISE, SET = 1000.
0.001, FINAL WATER(G), IF PATH = 2, OTHERWISE, SET = 0.
5.0, WATER DECREMENT(G), IF PATH = 2, OTHERWISE, SET = 0.
0, FINAL PRESSURE(BARS), IF PATH = 3, OTHERWISE, SET = 0.
0, PRESSURE INCREMENT(BARS), IF PATH = 3, OTHERWISE, SET = 0.
```

Danksagung

Mein besonderer Dank geht an meinen Doktorvater Herrn Professor Kurt Mengel, insbesondere für den hilfreichen wissenschaftlichen Austausch und dafür, dass er mir immer vertrauensvoll zur Seite stand.

Herrn Professor Hans-Jürgen Gursky danke ich sehr für die Übernahme des Ko-Referats und Herrn Professor Wolfgang Busch für die Übernahme des Vorsitzes.

I am grateful to Professor Ed Cloutis and Professor Matthew Izawa for many years of helpful discussions and collaboration, as well as Dan Applin for shooting the spectra at Ed's lab.

Special thanks go to Andreas Nathues, Carol A. Raymond, and Professor Christopher T. Russell for having had the possibility to write this thesis as a member of the DAWN team. It was a great and extraordinary experience to be involved in this amazing space mission.

Sonja Schuh danke ich für ihre hilfreiche Unterstützung als Koordinatorin der International Max Planck Research School (IMPRS), sowie der IMPRS am Max-. Planck-Institut für Sonnensystemforschung (MPS) für die großzügige Finanzierung der Arbeit. Diesbezüglich danke ich auch Herrn Professor Ulrich R. Christensen für die Gewährung meines Stipendiums und die Beteiligung an meinem Thesis Advisory Committee.

Friederike Funke und Silke Schlenczek danke ich für ihre super motivierte Hilfestellung bei den Laborarbeiten und für die nette Aufnahme in ihr Büro. Thomas Schirmer danke ich für seine wertvollen Tipps zur RDA Auswertung, sowie Saleem Chaudry für seine Hilfe bei der Instandsetzung der Gefriertrocknung.

Frau Steinmetz danke ich sehr für ihre engagierte Hilfe bei der Literaturbeschaffung, sowie auch Ute Seute für die Verwaltungsakte bei der Meteoritenbeschaffung.

Claudia Rudolph und Fee von Saltzwedel gilt großer Dank für ihre herzliche Art und die Hilfe bei organisatorischen Dingen am MPS.

Regina Aznar Cuadrado und Helga Oberländer danke ich für ihre ermutigenden Gespräche und die Organisation des Baby Büros.

Meinen Teamkollegen Irene Büttner, Joachim Ripken, Guneshwar Thangjam Singh und Martin Hoffmann am MPS danke ich für die nette Zusammenarbeit.

Ich danke meinem IMPRS Buddy Stephan Barra für die freundliche und hilfsbereite Begleitung bei meinem Start am MPS.

Another special thanks goes to the members of the IMPRS Coffee Group at MPS, especially Kok Leng Yeo, for the cordial welcome and all the social events we spent together.

Weiterer Dank geht an die Mensa Runde am Institut für Endlagerforschung in Clausthal, insbesondere an Michèle Jungmann und Karl Strauß, für die freundliche Aufnahme und die Erinnerung zur Essenszeit.

Ich bedanke mich auch herzlichst bei allen Freunden und Kollegen, sowie ehemaligen Kollegen des Instituts für Geotechnik und Markscheidewesen der TU Clausthal, die bei meiner Verteidigung dabei waren und daraus ein so familiäres und herzliches Ereignis gemacht haben.

Ich freue mich während dieser Arbeit Nafiseh Masoumzadeh kennengelernt zu haben und bedanke mich für ihre verlässliche Freundschaft.

Nicht zuletzt danke ich meinen Eltern, Schwiegereltern, meinem Bruder Bernd und meiner Schwägerin Regina für ihre Unterstützung auf meinem bisherigen Lebensweg.

Abschließend seien in besonderer Dankbarkeit mein Ehemann Michael und meine Tochter Amélie erwähnt. Danke für Eure große Liebe bei Regen und bei Sonnenschein.